UNIVERSITY OF CRETE

DOCTORAL THESIS

# Exploring Field Theories via the Conformal Bootstrap

*Author:*
Stefanos Robert KOUSVOS

*Supervisor:*
Prof. Theodore TOMARAS

*A thesis submitted in fulfillment of the requirements for the degree of Doctor of Philosophy*

*in the*

Department of Physics

**Examination Committee**

1. Prof. Kiritsis Elias - University of Crete - Physics Department
2. Prof. Niarchos Vasilis - University of Crete - Physics Department
3. Prof. Pavlidou Vasiliki - University of Crete - Physics Department
4. Prof. Rychkov Slava - I.H.E.S. and E.N.S. Paris (France)
5. Dr. Stergiou Andreas - Los Alamos National Laboratory (U.S.A)
6. Prof. Toumbas Nicolaos - University of Cyprus - Physics Department
7. Prof. Tsamis Nicholas - University of Crete - Physics Department

July 1 2021

# Statement of Originality/Foreword

I, Stefanos Robert KOUSVOS, declare that this thesis titled, "Exploring Field Theories via the Conformal Bootstrap" is based on three published articles, namely [62], [63] and [47]. Two of which were authored in collaboration with Andreas Stergiou and one which was authored with Johan Henriksson and Andreas Stergiou. The thesis also contains material from unpublished work in progress such as [64]. Also, many unpublished details from published work have been included, most notably details in Chapter 4 and a number of the Appendices. The numerical computations for the presented plots were either run by myself on the Metropolis cluster at the Crete Center for Quantum Complexity and Nanotechnology or the National Energy Research Scientific Computing Center (NERSC) in the United States, or by Andreas Stergiou on corresponding resources. In addition to the above I confirm that:

- This work was done wholly or mainly while in candidature for a research degree at the University of Crete.
- Where I have consulted the published work of others, this is always clearly attributed.
- Where I have quoted from the work of others, the source is always given.
- I have acknowledged all main sources of help.

Signed: Stefanos Robert Kousvos

Date: July 1 2021

UNIVERSITY OF CRETE

# *Abstract*

School of Sciences and Technology
Department of Physics

Doctor of Philosophy

**Exploring Field Theories via the Conformal Bootstrap**

by Stefanos Robert KOUSVOS

We study conformal field theories of interest due to phenomenological as well as purely theoretical considerations. This is done with the use of consistency conditions. The program of studying (conformal) field theories with the use of self consistency conditions is referred to as "the bootstrap". In the present thesis we will make use of the numerical bootstrap as envisioned in its modern revival. That is, we will impose crossing symmetry on certain correlators and demand unitarity/reflection positivity, from which we will derive constraints on the parameter space. The parameter space is spanned by an in general infinite set of scaling dimensions and OPE coefficients. These determine various observables, such as the critical exponents observed at critical points. With the use of the numerical bootstrap we will provide strong constraints on the space of allowed critical exponents for various universality classes. The constraints in certain circumstances will be in fact so strong that they actually compute the critical exponents. In other words, only small isolated regions of parameter space will be found to be compatible with the imposed consistency conditions. Some examples of theories we will consider are (hyper) cubic $S_n \ltimes {Z_2}^n$, bifundamental $O(m) \times O(n)/Z_2$ and MN $S_n \ltimes O(m)^n$ theories. We will find isolated allowed regions in parameter space for all of these. As a side effect of our analysis we will also work out tensor structures for various global symmetries, which can be useful beyond the numerical bootstrap.


# *Acknowledgements*

First and foremost I would like to thank my parents and grandparents for their continuing support without which this thesis would have not come to fruition. Consequently, I would like to thank my advisor Prof. Theodore Tomaras for his guidance and encouragement both on physics and non-physics matters. I would like to also express my gratitude to Andreas Stergiou who effectively served as my co-advisor throughout the thesis, and for collaboration that led to [62], [63] and [47]. I would also like to thank Johan Henriksson for collaboration on [47]. From November of 2017 until August of 2018 this thesis was supported by a graduate fellowship from ITCP Crete. During the period from January of 2019 until the end of June of 2019, I had the great pleasure of being a visitor at the Institut des Hautes Études Scientifiques (IHES). I would like to thank Slava Rychkov for his hospitality and support during my extended stay there, and making the visit itself possible. I would also like to thank the Institut des Hautes Études Scientifiques (IHES) for their hospitality throughout my stay. This stay was supported by the Simons Foundation grant 488655 (Simons Collaboration on the Nonperturbative Bootstrap) and by Mitsubishi Heavy Industries via an ENS-MHI Chair. As of 23/10/2019 my research work is supported by the Hellenic Foundation for Research and Innovation (HFRI) under the HFRI PhD Fellowship grant (Fellowship Number: 1026), to whom I express my gratitude. I would like to express my gratitude for the computer time allocated on the Metropolis cluster at the Crete Center for Quantum Complexity and Nanotechnology, and on the National Energy Research Scientific Computing Center (NERSC) in the United States. I also thank professors Theodore Tomaras and Vasilis Niarchos for comments on the manuscript.

# Contents

**Statement of Originality/Foreword** iii

**Abstract** v

**Acknowledgements** vii

**1 Introduction** 1

**2 CFT Basics** 7
2.1 Conformal Invariance . . . 7
2.2 The Conformal Algebra . . . 8
2.3 Conformal Transformations On Operators . . . 9
2.4 Correlation Functions . . . 10
2.5 The Operator Product Expansion . . . 11
2.6 Conformal Blocks . . . 13
2.7 The Crossing Equation and Bootstrap Constraints . . . 15

**3 Scalar Field Theories with Cubic Symmetry** 19
3.1 Cubic Theories in $d = 4 - \varepsilon$ Dimensions . . . 19

**4 Tensor Structures in Cubic Theories** 21
4.1 The $\langle\phi\phi\phi\phi\rangle$ correlator . . . 21
4.2 The $\langle XXXX\rangle$ correlator . . . 23
4.3 The $\langle\phi X\phi X\rangle$ correlator . . . 25
4.4 The $\langle\phi\phi XX\rangle$ correlator . . . 26

**5 Bootstrap Constraints** 27
5.1 Crossing Equations . . . 27
Explicit Example . . . 28
5.2 Single Correlator Constraints . . . 29
5.3 $\phi$ - X System of Correlators Constraints . . . 31
5.4 $\phi$ - S System of Correlators Constraints . . . 36

**6 Scalar Field Theories with $O(m) \times O(n)/Z_2$ global symmetry** 41
6.1 Fixed Points in $d = 4 - \varepsilon$ dimensions. . . . 41
6.2 Fixed Points in the Large $n$ limit . . . 43
6.3 Fixed Points in Resummations . . . 43

**7 Tensor Structures in $O(m) \times O(n)/Z_2$ Theories** 45

**8 Bootstrap Constraints** 47
8.1 Crossing Equations . . . 47
8.2 Results . . . 48
8.2.1 Comparing With Perturbation Theory and Regime I . . . 48

8.2.2 $O(2) \times O(3)$ . . . 49

**9 Tensor structures in $G^N \rtimes S_N$ theories** **59**
9.1 The OPE decomposition . . . 59
9.2 Projectors . . . 60
9.3 Examples . . . 61
9.3.1 Hypercubic . . . 61
9.3.2 MN . . . 61
9.3.3 Tetragonal . . . 62
9.4 Applications . . . 62
9.4.1 $\phi$ - $X$ System Islands . . . 62
9.4.2 $\langle ZZZZ \rangle$ Single Correlator Bootstrap . . . 64

**10 Discussion and Future Directions** **71**

**A Generic Projectors of 4-pt Functions** **75**
A.1 $\langle \phi_i \phi_j \phi_k \phi_l \rangle$ and $\langle \phi_i O_{jk} \phi_l O_{mn} \rangle$ Type Projectors . . . 75
A.2 $\langle \phi_i \phi_j O_{kl} O_{mn} \rangle$ Type Projectors . . . 76

**B Six Index Projectors in Cubic Theories** **77**

**C $\phi - X$ crossing equations in generic theories** **79**
C.1 $\langle \phi X \phi X \rangle = \langle \phi X \phi X \rangle$ and $\langle \phi \phi X X \rangle = \langle x \phi \phi X \rangle$ crossing sum rules . . . 79
C.2 $\langle XXXX \rangle = \langle XXXX \rangle$ crossing sum rules . . . 80
C.2.1 The case $N = 3$ . . . 80

**D $O_a$-$S$ System of Correlators Sum Rules** **81**

**E Emergence of $O(2) \times O(n)$ symmetry in physical systems** **83**
E.1 Stacked Triangular Antiferromagnets . . . 83
E.2 Helimagnets . . . 85

**F $\phi_i$-$X_{jk}$ system of correlators in cubic theories** **87**

**G One index MN notation.** **89**

**Bibliography** **91**

# List of Figures

5.1 Exclusion plot for the lowest scaling dimension exchanged operator in the $X$ irrep of the $\phi \times \phi$ OPE. In red are the disallowed values for the scaling dimension $\Delta_X$ (as a function of $\Delta_\phi$), whereas below the line are the allowed ones. The dimension of the operator in the theory of three decoupled Ising models is also marked on the plot. This figure was produced with PyCFTBoot [9] using the parameters $k_{max} = 36$, $l_{max} = 26$, $m_{max} = 6$ and $n_{max} = 9$. Figure reproduced from [62] and [100]. . . . . 30
5.2 Exclusion plot for the lowest scaling dimension exchanged operator in the $X$ irrep of the $\phi \times \phi$ OPE. The number $N$ denotes which hypercubic ($C_N = Z_2^N \rtimes S_N$) model we are talking about. This figure was produced with PyCFTBoot [9] using the parameters $k_{max} = 36$, $l_{max} = 26$, $m_{max} = 6$ and $n_{max} = 9$. . . . . 31
5.3 Exclusion plot for the lowest scaling dimension exchanged operator in the $S$ irrep. In red are the disallowed values for the scaling dimension $\Delta_S$, whereas below the line are the allowed ones. In this plot we impose $\Delta_{X'} \geqslant 3.0$, $\Delta_{\phi'} \geqslant 1.0$ and that $\Delta_X$ saturates Fig 5.1. This figure was produced with PyCFTBoot [9] using the parameters $k_{max} = 32$, $l_{max} = 26$, $m_{max} = 5$ and $n_{max} = 7$. Figure reproduced from [62]. . . . . 32
5.4 Allowed peninsula (in green) for the lowest scaling dimension exchanged operator in the $S$ irrep. In red are the disallowed values for the scaling dimension $\Delta_S$. In this plot we impose $\Delta_{X'} \geqslant 3.0$, $\Delta_{\phi'} \geqslant 1.0$, $\Delta_{S'} \geqslant 3.0$ and that $\Delta_X$ saturates Fig 5.1. This figure was produced with PyCFTBoot [9] using the parameters $k_{max} = 32$, $l_{max} = 26$, $m_{max} = 5$ and $n_{max} = 7$. Figure reproduced from [62]. . . . . 33
5.5 Allowed islands (in green) for the lowest scaling dimension exchanged operator in the $S$ irrep. In red are the disallowed values for the scaling dimension $\Delta_S$. In this plot we impose $\Delta_{X'} \geqslant 3.0$, $\Delta_{\phi'} \geqslant 1.0$ and that $\Delta_X$ saturates Fig 5.1. The islands from biggest to smallest are obtained imposing $\Delta_{S'} \geqslant 3.7$, 3.8 and 3.9 respectively. This figure was produced with PyCFTBoot [9] using the parameters $k_{max} = 32$, $l_{max} = 26$, $m_{max} = 5$ and $n_{max} = 7$. Figure reproduced from [62]. . . . . 34
5.6 Allowed island and remnant of the peninsula (in green) for the lowest scaling dimension exchanged operator in the $S$ irrep. In red are the disallowed values for the scaling dimension $\Delta_S$. In this plot we impose $\Delta_{X'} \geqslant 3.0$, $\Delta_{\phi'} \geqslant 1.0$, $\Delta_{S'} \geqslant 3.8$ and that $\Delta_X$ saturates Fig 5.1. This figure was produced with PyCFTBoot [9] using the parameters $k_{max} = 32$, $l_{max} = 26$, $m_{max} = 5$ and $n_{max} = 7$. Figure reproduced from [62]. . . . . 35

5.7 Allowed strip (in green) for the lowest scaling dimension exchanged operator in the $S$ irrep. In red are the disallowed values for the scaling dimension $\Delta_S$. In this plot we impose $\Delta_{X'} \geqslant 2.8$, $\Delta_{S'} \geqslant 3.0$ and that $\Delta_X$ saturates Fig 5.1. We note that the allowed region truncates on the left, whereas on the right there continues to be an allowed region. Removing the assumption $\Delta_{X'} \geqslant 2.8$ the plot stops truncating on the left. In Fig 5.8 it will become apparent that the two kinks in this plot correspond to the overlap with the peninsula in the mixed $\phi$-$X$ system of the previous section. This figure was produced with PyCFTBoot [9] using the parameters $k_{max} = 36$, $l_{max} = 26$, $m_{max} = 6$ and $n_{max} = 9$. Figure reproduced from [63]. . . . . 37
5.8 Allowed strip (in green) for the lowest scaling dimension exchanged operator in the $S$ irrep. In red are the disallowed values for the scaling dimension $\Delta_S$. In this plot we impose $\Delta_{X'} \geqslant 2.8$, $\Delta_{S'} \geqslant 3.0$ and that $\Delta_X$ saturates Fig 5.1. The assumptions for the peninsula and the island can be found in Fig 5.4 and Fig 5.6 respectively. Figure reproduced from [63]. . . . . 37
5.9 Projection onto the $(\Delta_S, \Delta_Y)$ plane of the isolated allowed region in $(\Delta_\phi, \Delta_S, \Delta_y)$ space (in green). In red are the disallowed values for the scaling dimension $\Delta_S$ as a function of $\Delta_Y$. In this plot we impose $\Delta_{X'} \geqslant 1.4126$, $\Delta_{S'} \geqslant 3.0$, $\Delta_{T_{\mu\nu}} = 3.7$, $\Delta_{T'_{\mu\nu}} \geqslant 4.0$ and $\Delta_{Y'} \geqslant 3.0$. We denote with crosses the positions of the $3D$ Ising CFT and the Platonic theory conjectured in the previous section. The decoupled Ising model appears in our plots since three decoupled Ising models have cubic global symmetry. To see this plug $g_2 = 0$ in 3.1. The position of the Platonic theory is approximate and corresponds to the island of the previous section. This figure was produced with PyCFTBoot [9] using the parameters $k_{max} = 36$, $l_{max} = 26$, $m_{max} = 5$ and $n_{max} = 7$. Figure reproduced from [63]. . . . . 38
5.10 Projection onto the $(\Delta_S, \Delta_\phi)$ plane of the isolated allowed region in $(\Delta_\phi, \Delta_S, \Delta_y)$ space for $\Delta_Y = 0.98575$ (in green). In red are the disallowed values for the scaling dimension $\Delta_S$ as a function of $\Delta_\phi$. In this plot we impose $\Delta_{X'} \geqslant 1.4126$, $\Delta_{S'} \geqslant 3.0$, $\Delta_{T_{\mu\nu}} = 3.7$, $\Delta_{T'_{\mu\nu}} \geqslant 4.0$ and $\Delta_{Y'} \geqslant 3.0$. This figure was produced with PyCFTBoot [9] using the parameters $k_{max} = 36$, $l_{max} = 26$, $m_{max} = 5$ and $n_{max} = 7$. Figure reproduced from [63]. . . . . 39
5.11 Projection onto the $(\Delta_S, \Delta_\phi)$ plane of the isolated allowed region in $(\Delta_\phi, \Delta_S, \Delta_y)$ space for $\Delta_Y = 1.025$ (in green). In red are the disallowed values for the scaling dimension $\Delta_S$ as a function of $\Delta_\phi$. In this plot we impose $\Delta_{X'} \geqslant 1.4126$, $\Delta_{S'} \geqslant 3.0$, $\Delta_{T_{\mu\nu}} = 3.7$, $\Delta_{T'_{\mu\nu}} \geqslant 4.0$ and $\Delta_{Y'} \geqslant 3.0$. This figure was produced with PyCFTBoot [9] using the parameters $k_{max} = 36$, $l_{max} = 26$, $m_{max} = 5$ and $n_{max} = 7$. Figure reproduced from [63]. . . . . 39
5.12 Projection onto the $(\Delta_S, \Delta_\phi)$ plane of the isolated allowed region in $(\Delta_\phi, \Delta_S, \Delta_y)$ space for $\Delta_Y = 1.0$ (in green). In blue we plot the the island with $\Delta_{S'} \geqslant 3.7$ from Fig 5.5 in the previous section. In red are the disallowed values for the scaling dimension $\Delta_S$ as a function of $\Delta_\phi$. In this plot we impose $\Delta_{X'} \geqslant 1.4126$, $\Delta_{S'} \geqslant 3.0$, $\Delta_{T_{\mu\nu}} = 3.7$, $\Delta_{T'_{\mu\nu}} \geqslant 4.0$ and $\Delta_{Y'} \geqslant 3.0$. This figure was produced with PyCFTBoot [9] using the parameters $k_{max} = 36$, $l_{max} = 26$, $m_{max} = 5$ and $n_{max} = 7$. Figure reproduced from [63]. . . . . 40

8.1 Single correlator exclusion plots for the scaling dimension of the first $W$ operator, for $m = 2$ and various values of $n$. The circles on the plot denote the Large $n$ predictions for the dimension of this operator at the anti-chiral fixed point. The box, connected to the circle by a line, represents the Large $n$ predictions for the dimensions of this operator at the chiral fixed point. It is thus clear that the kinks are saturated by the anti-chiral fixed point. The figure was produced using the following parameters in PyCFTBoot [9]: $m_{max} = 8$, $n_{max} = 11$, $l_{max} = 36$ and $k_{max} = 42$. Figure reproduced from [47]. . . . . 49
8.2 Single correlator exclusion plots for the scaling dimension of the first $X$ operator, for $m = 2$ and various values of $n$. The circles on the plot denote the Large $n$ predictions for the dimension of this operator at the anti-chiral fixed point. The box, connected to the circle by a line, represents the Large $n$ predictions for the dimensions of this operator at the chiral fixed point. It is thus clear that the kinks are saturated by the chiral fixed point. The figure was produced using the following parameters in PyCFTBoot [9]: $m_{max} = 8$, $n_{max} = 11$, $l_{max} = 36$ and $k_{max} = 42$. Figure reproduced from [47]. . . . . 50
8.3 Single correlator exclusion plots for the scaling dimension of the first $X$ and $W$ operators respectively, for $m = 2$ and $n = 6$. This case is of particular interest since it sits at the edge of Regime$_1$ in 6.4 from the results of [58]. The figure was produced using the following parameters in PyCFTBoot [9]: $m_{max} = 8$, $n_{max} = 11$, $l_{max} = 36$ and $k_{max} = 42$. Figure reproduced from [47]. . . . . 50
8.4 Islands corresponding to the Chiral and Anti-Chiral fixed points with $m = 2$ and $n = 20$ obtained using the mixed $\phi_{ar}$ - $S$ system of correlators. These islands assume that the first $X$ (for the chiral island) and $W$ (for the anti-chiral island) operators have a scaling dimension that saturates the corresponding single correlator plots Fig 8.2 and Fig 8.1 respectively. We also assume in both that the first $B$ operator has a scaling dimension of $\Delta_B = 2.0$ since it is a conserved vector (remember $B = S \times A$). For the second $B$ operator in both we impose $\Delta_{B'} \geqslant 3.0$. For the second defining operator $\phi'$ we impose $\Delta_{\phi'} \geqslant \Delta_\phi + 0.01$ in both. Lastly, in the Chiral island we impose $\Delta_{S'} \geqslant 3.0$ whereas for the Anti-Chiral island we impose $\Delta'_S \geqslant 1.5$. The figure was produced using the following parameters in PyCFTBoot [9]: $m_{max} = 7$, $n_{max} = 9$, $l_{max} = 30$ and $k_{max} = 40$. Figure reproduced from [47]. . . . . 51

8.5 Islands corresponding to the Chiral and Anti-Chiral fixed points with $m = 2$ and $n = 10$ obtained using the mixed $\phi_{ar}$ - $S$ system of correlators. These islands assume that the first $X$ (for the chiral island) and $W$ (for the anti-chiral island) operators have a scaling dimension that saturates the corresponding single correlator plots Fig 8.2 and Fig 8.1 respectively. We also assume in both that the first $B$ operator has a scaling dimension of $\Delta_B = 2.0$ since it is a conserved vector (remember $B = S \times A$). For the second $B$ operator in both we impose $\Delta_{B'} \geqslant 3.0$. Lastly, in the Chiral fixed point we impose $\Delta_{S'} \geqslant 3.0$ and $\Delta_{\phi'} \geqslant \Delta_\phi + 0.01$ whereas for the Anti-Chiral fixed point we impose $\Delta_{S'} \geqslant 1.6$ and $\Delta_{\phi'} \geqslant 1.6$. We note that there seems to be some minor deviation between the island and the Large $n$ prediction in the Chiral case, however this is not very worrying since $n = 10$ is quite far from $n \to \infty$. The figure was produced using the following parameters in PyCFTBoot [9]: $m_{max} = 7$, $n_{max} = 9$, $l_{max} = 30$ and $k_{max} = 40$. Figure reproduced from [47]. . . . . 52

8.6 Island corresponding to the Chiral fixed point with $m = 2$ and $n = 6$ obtained using the mixed $\phi_{ar}$ - $S$ system of correlators. This island assumes that the first $X$ operator has a scaling dimension that saturates the corresponding single correlator plot Fig 8.3. We also assume that the first $B$ operator has a scaling dimension of $\Delta_B = 2.0$ since it is a conserved vector (remember $B = S \times A$). For the second $B$ operator we impose $\Delta_{B'} \geqslant 3.0$. Lastly, we impose $\Delta_{S'} \geqslant 3.0$ and $\Delta_{\phi'} \geqslant \Delta_\phi + 0.01$. We note that there seems to be some tension between the island and the six loop resummed $\varepsilon$-expansion results of [58]. The figure was produced using the following parameters in PyCFTBoot [9]: $m_{max} = 7$, $n_{max} = 9$, $l_{max} = 30$ and $k_{max} = 40$. Figure reproduced from [47]. . . . . 53

8.7 Single correlator exclusion plot for the scaling dimension of the first $W$ operator for $m = 2$ and $n = 3$. The figure was produced using the following parameters in PyCFTBoot [9]: $m_{max} = 8$, $n_{max} = 11$, $l_{max} = 36$ and $k_{max} = 42$. Figure reproduced from [47]. . . . . 55

8.8 Single correlator exclusion plot for the scaling dimension of the first $W$ operator for $m = 2$ and $n = 3$. The same as in Fig 8.7 but with least square fits adapted to the left and right of the plot in order to indicate that even though it is not very pronounced, there does seems to be a well defined change of slope. The figure was produced using the following parameters in PyCFTBoot [9]: $m_{max} = 8$, $n_{max} = 11$, $l_{max} = 36$ and $k_{max} = 42$. . . . . 55

8.9 Island corresponding to the Chiral fixed point with $m = 2$ and $n = 3$ obtained using the mixed $\phi_{ar}$ - $S$ system of correlators. This island assumes that the first $W$ operator has a scaling dimension that saturates the corresponding single correlator plot Fig 8.7. We also assume that the first $B$ operator has a scaling dimension of $\Delta_B = 2.0$ since it is a conserved vector (remember $B = S \times A$). For the second $B$ operator we impose $\Delta_{B'} \geqslant 2.4$. Lastly, we impose $\Delta_{S'} \geqslant 2.0$ and $\Delta_{\phi'} \geqslant 1.5$. We note that we have checked that the island remains even if we impose $\Delta_{S'} \geqslant 3.0$ which corresponds to it being a stable fixed point in the language of RG. We once again stress that this island is unrelated to the Chiral islands of the $\varepsilon$ expansion but they have the same name in the literature since the coupling $v$ in 6.2 is positive for both types of fixed points. The figure was produced using the following parameters in PyCFTBoot [9]: $m_{max} = 7$, $n_{max} = 9$, $l_{max} = 30$ and $k_{max} = 40$. Figure reproduced from [47]. . . . . 56

8.10 Single correlator exclusion plot for the scaling dimension of the first $Z$ operator for $m = 2$ and $n = 3$. The figure was produced using the following parameters in PyCFTBoot [9]: $m_{max} = 8$, $n_{max} = 11$, $l_{max} = 36$ and $k_{max} = 42$. Figure reproduced from [47]. . . . . 56

8.11 Island corresponding to the Collinear fixed point with $m = 2$ and $n = 3$ obtained using the mixed $\phi_{ar}$ - $S$ system of correlators. This island assumes that the first $Z$ operator has a scaling dimension that saturates the corresponding single correlator plot Fig 8.10. We also assume that the first $B$ operator has a scaling dimension of $\Delta_B = 2.0$ since it is a conserved vector (remember $B = S \times A$). For the second $B$ operator we impose $\Delta_{B'} \geqslant 2.5$. Lastly, we impose $\Delta_{S'} \geqslant 3.0$ and $\Delta_{\phi'} \geqslant \Delta_{\phi} + 0.01$. The figure was produced using the following parameters in PyCFTBoot [9]: $m_{max} = 7$, $n_{max} = 9$, $l_{max} = 30$ and $k_{max} = 40$. Figure reproduced from [47]. . . . . 57

9.1 Single correlator exclusion plot for the scaling dimension of the first $X$ operator for $M = 2$ and $N = 3$. Points above the line are disallowed. The figure was produced using the following parameters in qboot [41]: $\Lambda = 45$, $l = (0 - 50, 55, 56, 59, 60, 64, 65, 69, 70, 74, 75, 79, 80, 84, 85, 89, 90)$ and $\nu_{max} = 20$. . . . . 63

9.2 MN = 2, 3 island corresponding to the fixed point saturating Fig 9.1 obtained using the mixed $\phi_i^a$ - $X^{bc}$ system of correlators. The island assumes that the second $S$, $X$ and $A$ operators have scaling dimensions that satisfy $\Delta \geqslant 3.0$. The first $X$ operator is assumed to have a scaling dimension that saturates Fig 9.1, also the first $A$ operator satisfies $\Delta_A = 2.0$ since it is the conserved vector of $O(M)$. Lastly, we impose $\Delta_{\phi'} \geqslant 1.0$ for the second operator in the defining representation. The figure was produced using the following parameters in qboot [41]: $\Lambda = 27$, $l = (0 - 50, 55, 56, 59, 60, 64, 65, 69, 70, 74, 75, 79, 80, 84, 85, 89, 90)$ and $\nu_{max} = 25$. . . . . 64

9.3 MN = 2, 3 island corresponding to the fixed point saturating Fig 9.1 obtained using the mixed $\phi_i^a$ - $X^{bc}$ system of correlators. The island assumes that the second $S$, $X$ and $A$ operators have scaling dimensions that satisfy $\Delta_{S'} \geqslant 3.5$, $\Delta_{X'} \geqslant 3.0$ and $\Delta_{A'} \geqslant 3.9$ respectively. The first $X$ operator is assumed to have a scaling dimension that saturates Fig 9.1, also the first $A$ operator satisfies $\Delta_A = 2.0$ since it is the conserved vector of $O(M)$. Lastly, we impose $\Delta_{\phi'} \geqslant 1.5$ for the second operator in the defining representation. The figure was produced using the following parameters in qboot [41]: $\Lambda = 20$, $l = (0-50, 55, 56, 59, 60, 64, 65, 69, 70, 74, 75, 79, 80, 84, 85, 89, 90)$ and $\nu_{max} = 25$. . . . . 65

9.4 $\phi$ - $X$ mixed correlator system exclusion plot for the scaling dimension of the first $X$ operator for $M = 2$ and $N = 2$. Points above the line are disallowed. The figure was produced using the following parameters in qboot [41]: $\Lambda = 45$, $l = (0-50, 55, 56, 59, 60, 64, 65, 69, 70, 74, 75, 79, 80, 84, 85, 89, 90)$ and $\nu_{max} = 20$. Note that in contrast with Fig 9.1, here we use the full $\phi$ - $X$ system of correlators since it contains less sum rules, and thus is numerically less costly, than the $N = 3$ one. . . . . 66

9.5 MN = 2, 2 island corresponding to the fixed point saturating Fig 9.4 obtained using the mixed $\phi_i^a$ - $X^{bc}$ system of correlators. The island assumes that the second $S$, $X$ and $A$ operators have scaling dimensions that satisfy $\Delta \geqslant 3.0$. The first $X$ operator is assumed to have a scaling dimension that saturates Fig 9.1, also the first $A$ operator satisfies $\Delta_A = 2.0$ since it is the conserved vector of $O(M)$. Lastly, we impose $\Delta_{\phi'} \geqslant 1.0$ for the second operator in the defining representation. The figure was produced using the following parameters in qboot [41]: $\Lambda = 35$, $l = (0-50, 55, 56, 59, 60, 64, 65, 69, 70, 74, 75, 79, 80, 84, 85, 89, 90)$ and $\nu_{max} = 25$. . . . . 67

9.6 Single correlator exclusion plot for the scaling dimension of the first $SY$ (note that $SY = Y$) operator for $M = 100$ and $N = 2$ appearing in the $Z \times Z$ OPE. Points above the line are disallowed. The figure was produced using the following parameters in qboot [41]: $\Lambda = 20$, $l = (0-50, 55, 56, 59, 60, 64, 65, 69, 70, 74, 75, 79, 80, 84, 85, 89, 90)$ and $\nu_{max} = 25$. . . . . 69

# List of Tables

8.1 $O(2) \times O(3)$ "chiral" critical exponents. Reproduced from [47]. . . . . 55
8.2 $O(2) \times O(3)$ "antichiral/collinear" critical exponents. Reproduced from [47]. . . . . 57

# List of Abbreviations

| | |
|---|---|
| **irrep** | **i**rreducible **rep**resentation |
| **OPE** | **O**perator **P**roduct **E**xpansion |
| **CFT** | **C**onformal **F**ield **T**heory |
| **RG** | **R**enormalization **G**roup |
| **4-pt** | **F**our **P**oint (Correlation Function) |
| **3-pt** | **T**hree **P**oint (Correlation Function) |
| **2-pt** | **T**wo **P**oint (Correlation Function) |
| **External Operator** | An operator appearing on the left hand side of an OPE |
| **Exchanged Operator** | An operator appearing on the right hand side of an OPE |
| **Defining Representation** | This will be shorthand for the "obvious" representation. [1] |
| **RHS** | **R**ight **H**and **S**ide |

[1] For example in $O(N)$ it will be the vector representation, and in $S_N$ it will be the representation with dimension $N-1$ that is traceless.

# Chapter 1

# Introduction

The goal of this thesis will be to study conformal field theories (CFTs) relevant to physically interesting critical phenomena and phase transitions. Critical phenomena are usually discovered[1] as fixed points of Renormalization Group (RG) flows [84]. Consequently, if one assumes that the scale invariance at the fixed points is enhanced to conformal invariance one can study the critical phenomena by studying their corresponding CFT. Physical observables are then related to specific quantities in the CFT. These quantities are the scaling dimensions and the operator product expansion (OPE) coefficients. Another motivation will be a curiosity about the nature of various debated fixed points that arise in some implementations of the RG, but not others. Naturally one then asks if these fixed points are physical or spurious, a question that gets complicated since each form of RG makes its own concessions. For example, the standard $d = d_c - \varepsilon$ expansion [107] [106] around the upper critical dimension of a system has a convenient control parameter, $\varepsilon$ itself, but is perturbative and needs resummations in order to make meaningful predictions in physically interesting scenarios. Hence, the discrepancy between different implementations of RG could be due to the differing concessions between implementations, and not necessarily of the fixed point in question.

It is natural to try and study the above questions using a radically different approach, free of the concessions of other methods. This approach will be the modern (numerical) conformal bootstrap [90]. The numerical bootstrap has the benefit of being non perturbative, hence results will never depend on an expansion parameter and its convergence properties, or lack thereof. Even compared to non-perturbative methods, such as Monte Carlo simulations, the boostrap has its benefits. For example, it is equally easy to run the bootstrap algorithm in any space-time dimensionality, whereas Monte Carlo scales very badly. Another example, is that Monte Carlo requires extrapolation to infinite volume whereas the boostrap doesn't. Also, the bootstrap takes directly into account conformal symmetry. Lastly, and probably most importantly, the bootstrap provides rigorous results in the sense that if it excludes a point in parameter space then this point will never become allowed if we increase our numerical precision[2].

In the bootstrap approach one uses self consistency conditions in order to narrow down the parameter space. This approach has been tremendously successful since

[1] At least on the theoretical side. Although, one should also mention that critical phenomena have also been discovered using lattice techniques, see e.g. [83] and the discussion in the introduction of [91].

[2] This statement is subject to an asterisk. The statement holds true assuming one includes a sufficient amount of spins for "exchanged" operators in the operator product expansion. The success of the bootstrap in practice is due to the fact that this number of sufficient spins is reasonable, such as e.g. 50 spins. See page 19 in [97].

in various circumstances one can find small isolated islands in parameter space that are consistent with the imposed conditions. Hence, if a CFT is conjectured to live in this island, we have then by definition calculated the corresponding parameters of this theory (with an error bar that corresponds to the size of the island). Then, increasing the number of constraints, by e.g. using stronger numerics, one can make the island smaller[3], and hence the determination of the parameters in the theory more precise. The first success of this methodology was the 3D critical Ising Model [59]. This method led to the most precise determination of the critical exponents in the 3D Ising Model to date [61]. Similarly, the critical exponents where also computed with very high precision in the (3D) $O(2)$ and $O(3)$ critical theories [22] [21]. Interestingly, in the case of [22] it solved a discrepancy between Monte Carlo [46][45] and experiment [69], indicating that Monte Carlo was correct[4]. Another virtue of the numerical conformal bootstrap is that even before one tries to isolate a theory of interest into an island, quite often the theory already lies on the edge of parameter space creating a kink in the so called exclusion plots. These kinks are often used as indicators for the location of theories in parameter space. Although, it should be mentioned that theories do not need, nor do they in practice, always lie on the edge of parameter space. It is nevertheless quite a common occurrence. For a comprehensive list of references up to 2018-2019 we point the reader to [87]. For a pedagogic introduction to the numerical bootstrap see [20].

With the exception of the $O(N)$ family of models, the space of three dimensional CFTs that are interesting due to critical phenomena is under-explored. Although numerous calculations have been done in the context of the $\varepsilon$ expansion, many questions remain unanswered. Critical points beyond the $O(N)$ family are ubiquitous in statistical and condensed matter physics. One class of examples is due to structural phase transitions. In these phase transitions the order parameter can be the expectation value of the displacement of some given particles on the lattice from their high temperature equilibrium position. Hence, assuming one may create a lattice system with a certain symmetry and make it undergo a continuous phase transition, this would then correspond to a fixed point in e.g. a scalar field theory where the scalar (i.e. the order parameter) has as a global symmetry the symmetry of the lattice. For a review on structural phase transitions see [24] and [15], regarding the Landau theory see [104]. A second class of examples includes models with an emergent global symmetry different from the microscopic one. Two popular examples of this phenomenon are phase transitions in stacked triangular anti-ferromagnets and helimagnets, which at the microscopic level have an $O(n)$ global symmetry. In the case of stacked triangular anti-ferromagnets, an enhanced $O(2) \times O(n)/Z_2$ symmetry arises due to the specific shape of the lattice. Whereas, in the helimagnet example an enhanced $O(2) \times O(n)/Z_2$ symmetry arises due to the competition between nearest neighbour and next nearest neighbour interactions. The interested reader may find more details in E. Also, in addition to the above examples, one can imagine fixed points that are not able to be captured by e.g. the $\varepsilon$ expansion, or any other technique. Nevertheless, these fixed points may be equally physically and/or theoretically interesting.

With these issues in mind we believe it is a worthwhile task to try and broaden our knowledge regarding the space of CFTs in three dimensions using the numerical

[3] We mention that there are also other ways of shrinking an island beyond using stronger numerics.
[4] This is important given that the experiment was performed in earth orbit.

conformal bootstrap. Ideally we would like to be able to perform precision studies such as the ones in [22] and [21]. In practice many complications can arise. The most common problem is that all known multi scalar theories bootstrapped to date have a singlet sector exclusion bound which is saturated by a kink due to an $O(N)$ model for some value of $N$. This happens because all the aforementioned theories have a global symmetry that is a subgroup of $O(N)$. Hence, the $O(N)$ kink "hides" the theory we are interested in studying. This can in some cases be circumvented if the theory we are interested in has a kink that saturates some other sector. We will see that this is the case in the $O(m) \times O(n)/Z_2$ multi-scalar theories. Conversely, the cubic theory of the $\epsilon$-expansion does not seem to saturate any bound. Even omitting the above issues, subgroups of $O(N)$ tend to have a more complicated group theory structure, which in practice means that knowledge of more operators is needed to fully determine the low lying spectrum of these theories. Take as an example the hyper-cubic theories, which are some of the simplest deformations of an $O(N)$ model. For cubic theories ($N = 3$) if we include all low lying operators as external operators in our algorithm we obtain 64 sum rules, this can be checked with [42]. Whereas in [21], which is the most advanced study to date, the authors had 28 sum rules. Thus, even though one can in principle directly apply the methodology of [22] and [21], which are the strongest results to date, the computational cost can quickly become very large[5]. Recently, though, there have been advances in performing higher dimensional scans in parameter space. Perhaps most notably in [92], where the authors developed a method for systematically finding allowed points in parameter space, a task that can become highly non-trivial in higher dimensional scans. These advances should alleviate some of the issues mentioned above.

In the main part of this thesis we will study multi scalar CFTs with cubic and $O(m) \times O(n)/Z_2$ global symmetry. These sections will be based on the results from [62], [63] and [47]. Towards the end of the thesis we will discuss theories with $G^N \rtimes S_N$ global symmetry, for $G$ arbitrary. This is based on work in progress [64]. In our study of theories with cubic global symmetry we will not see signs of the cubic theory of the $\varepsilon$ expansion. Nevertheless, we will find evidence of a new CFT which we will dub "Platonic". This name was chosen since, at least at the level of perturbative field theory, in $d = 4 - \varepsilon$ dimensions it is the only possible three flavour multi-scalar theory with the symmetry of a Platonic solid[6]. Of course, this name does not preclude the possibility that the fixed point may actually be of purely non perturbative nature. Interestingly, this conjectured CFT has critical exponents that agree very well with certain experiments for critical phenomena in perovskites. We will isolate the Platonic theory in an island using two different methods. The first method consists of isolating it using the fact that it seems to saturate the exclusion plot in a specific sector. Whereas the second way we isolate it, is by performing a 3D scan of parameter space over the scaling dimensions of three low lying operators. This second method gives a bigger, hence less constraining, island. The upshot is that it drops the assumption of exclusion bound saturation (i.e. we do not necessarily require the theory to live at the kink). This paves the way towards shrinking this island using the new state of the art technology from [92]. Another interesting observation is that there exist more kinks if one moves to larger values of the scaling dimension of the first defining scalar $\phi$. We leave an investigation of these for future work. Lastly, it is worth noting that cubic fixed points beyond those of the $\varepsilon$ expansion have been

[5] Always assuming that one wishes to consider a carbon copy implementation.
[6] See [62].

reported in the literature [29] but they were discarded as spurious. We de not know what relation, if any, our conjectured theory has to those. We will discuss these fixed points beyond the $\varepsilon$ expansion when we study the $O(m) \times O(n)/Z_2$ theories, where these fixed points have been the object of many debates.

Consequently, we proceed to study $O(m) \times O(n)/Z_2$ theories for $m = 2$ and various values of $n$. These theories are interesting since they are believed to describe phase transitions in helimagnets and frustrated antiferromagnets among other systems. They are also interesting for purely theoretical reasons. This is because people have studied fixed points beyond the $\varepsilon$ expansion in them extensively (for references see the main text). These fixed points are found by first resumming the perturbative beta functions (directly in 3D) and then looking for fixed points. Doing this, from a specific order of loops and above, one finds new fixed points. These fixed points have been reported by various authors to be spurious. Hence, our analysis of $O(m) \times O(n)/Z_2$ is separated in to two ideological sections. In the first we compare to the ordinary and widely accepted fixed points (large $n$, $\varepsilon$ expansion) to numerical bootstrap data. In the second we look for potential evidence of the debated fixed points. For the large $n$ fixed points we find excellent agreement of the numerics with analytic predictions. With regards to the $\epsilon$ expansion, we find our results are in some tension with the perturbative data. Concerning the debated fixed points found in resummations, we find two islands that may correspond to them, assuming they are not spurious, although this is something that cannot be conclusively confirmed since the perturbative predictions have large deviations between themselves making it hard to compare.

Lastly, before ending the thesis we present some results from work in porgress [64]. This work concerns theories with $G^N \rtimes S_N$ global symmetry. As an example we apply these results to theories with $G = O(M)$ and obtain some islands in parameter space.

The thesis is organized as follows. In Chapter 2 we provide a lightning fast (elementary) introduction to CFT and the conformal bootstrap. Readers familiar with both subjects may entirely skip it. Readers familiar with CFT but unfamiliar with the conformal bootstrap can directly read Section 2.7. Consequently, in Chapter 3, we set the stage for fixed points with hyper-cubic symmetry within the context of a brief discussion. In Chapter 4 we work out all the tensor structures we will need for cubic theories. A lot of the details in Chapter 4 will carry over to other groups as well. Given that it is rather technical, the reader interested directly in the bootstrap results may skip this chapter entirely. We thus proceed to Chapter 5 where we present the results of the numerical analysis for systems with cubic symmetry. In Chapter 6 and Chapter 7 we review the fixed points from the literature pertaining to $O(m) \times O(n)/Z_2$ theories and write down the relevant tensor structures. With this in hand we present the numerical results relevant to $O(m) \times O(n)/Z_2$ theories in Chapter 8. We also give a glimpse of results from work in progress regarding theories with $S_N \ltimes G^N$ global symmetry in Chapter 9, where $G$ may be any group. Lastly, we conclude with an overview of the established results and some future directions we would like to pursue in Chapter 10. It should be noted that the main text is supplemented with various appendices where several details are worked out or discussed. Also, the thesis contains a number of details that did not appear in [62] [63] and [47], hence may be of use to the reader interested in reproducing some of the technical details.

An important note is that we will be considering the spacetime dimensionality to be equal to three throughout the thesis. Also, we will use a notation for 4-pt functions $\langle O_1 O_2 O_3 O_4 \rangle$, by which we imply that they are calculated by taking the OPE between $O_1$ and $O_2$, and the OPE between $O_3$ and $O_4$. Hence, $\langle O_1(x_1) O_2(x_2) O_3(x_3) O_4(x_4) \rangle$ and e.g. $\langle O_3(x_3) O_2(x_2) O_1(x_1) O_4(x_4) \rangle$ are in general expressed in two different, but equivalent, infinite sums over exchanged operators.

# Chapter 2

# CFT Basics

## 2.1 Conformal Invariance

In the present chapter we review some basic knowledge about CFT that will be needed later to fully understand our results. Two references the present author found particularly useful are [89] and [94][1], our analysis will mostly follow these references. We note that the chapter is written to accommodate readers unfamiliar with CFT, thus those already comfortable with the subject may skip it.

Our starting point will be to define what we mean when we say "conformal transformations", these are transformations that change the metric in the following way[2]

$$g_{\mu\nu} \to g'_{\mu\nu} = c(x) g_{\mu\nu} \tag{2.1}$$

Let us now parametrize the transformations in the following infinitesimal form

$$x^\mu \to x'^\mu = x^\mu + \epsilon^\mu(x) \tag{2.2}$$

and plug this expression into

$$ds^2 = g_{\mu\nu} dx^\mu dx^\mu \to g_{\mu\nu} d(x^\mu + \epsilon^\mu) d(x^\nu + \epsilon^\nu) \tag{2.3}$$

for 2.1 to hold we must satisfy

$$g_{\mu\nu}\left(\frac{dx^\mu}{dx^\rho} + \frac{d\epsilon^\mu}{dx^\rho}\right)\left(\frac{dx^\nu}{dx^\sigma} + \frac{d\epsilon^\nu}{dx^\sigma}\right) dx^\rho dx^\sigma = c(x) g_{\rho\sigma} dx^\rho dx^\sigma \tag{2.4}$$

remembering that $g_{\mu\nu} = \delta_{\mu\nu}$ this implies

$$\partial_\rho \epsilon^\sigma + \partial_\sigma \epsilon^\rho = (c(x) - 1) g_{\rho\sigma} = (c(x) - 1)\delta_{\rho\sigma} \tag{2.5}$$

this equation has four solutions in $d > 2$. Two for $c(x) = 1$ and two for $c(x) \neq 1$. These are

[1] Also, I thank Andreas Stergiou for sending some of his unpublished notes.

[2] We will only talk about conformal transformations in flat space. Thus we choose $g_{\mu\nu} = \delta_{\mu\nu}$ (Euclidean space). Note that we will freely switch between upper and lower indices since they are equivalent. Repeated indices are summed over unless stated otherwise.

$$\begin{aligned} \epsilon^\mu &= \alpha^\mu = const \\ \epsilon^\mu &= \alpha^{[\nu\mu]}x^\nu \\ \epsilon^\mu &= \alpha x^\mu \\ \epsilon^\mu &= 2(a^\nu x^\nu)x^\mu - x^2 a^\mu \end{aligned} \tag{2.6}$$

where $\alpha$ either represents an infinitesimal constant, vector or tensor accordingly. The first element in 2.6 represents a translation, the second a rotation, the third a dilatation and the fourth a special conformal transformation. Special conformal transformations are composed of an inversion ($x^\mu \to \frac{x^\mu}{x^2}$) followed by a translation followed up by another inversion. This will be useful to remember later. We consider special conformal transformations, instead of inversions which look simpler, since inversions do not have an infinitesimal form.

One comment is that if we set $d = 2$, then defining $z = x_1 + ix_2$ and $\bar{z} = x_1 - ix_2$ would allow us to write $ds^2 = dzd\bar{z}$. In this case it is apparent that any analytic transformation $z \to f(z)$ and $\bar{z} \to f(\bar{z})$ would be a conformal transformation. Then the set of all conformal transformations would not be limited to those in 2.6. Instead, we would have an infinite amount, corresponding to all the powers of $z$. We will not comment further on this since $2D$ CFT is a massive an incredibly rich subject in and of itself. See for example [33].

## 2.2 The Conformal Algebra

To write down the conformal algebra we first need the generators of the conformal transformations in 2.6. One way to read the generators off of 2.6 is by using the Baker-Campbell-Hausdorff formula

$$e^{-A}Be^A = B + [B, A] + \frac{1}{2!}[[B, A], A] + ... \tag{2.7}$$

If we take e.g. $A \sim -i\alpha^\mu P^\mu$ where $P^\mu$ is the momentum generator, and $B \sim x^\nu$, then on the right hand side by definition we should find $x'^\nu$.

$$\begin{aligned} e^{ia^\mu P^\mu}x^\nu e^{-ia^\mu P^\mu} &= x^\nu + [x^\nu, -i\alpha^\mu P^\mu] + O(a^2) \\ = x^\nu - i\alpha^\mu x^\nu P^\mu + i\alpha^\mu P^\mu x^\nu + i\alpha^\mu x^\nu P^\mu + O(a^2) \\ &= x^\nu + i\alpha^\mu P^\mu x^\nu + O(a^2) \end{aligned} \tag{2.8}$$

thus we find that if $P^\mu = -i\partial_\mu$ we indeed get $e^{ia^\mu P^\mu}x^\nu e^{-ia^\mu P^\mu} = x'^\nu = x^\nu + \alpha^\nu$. Note that we implicitly think of the commutator as acting on a function on its right. Using this methodology one may read off the remaining generators

$$\begin{aligned} P^\mu &= -i\partial_\mu \\ L_{\mu\nu} &= i(x^\mu\partial_\nu - x^\nu\partial_\mu) \\ D &= -ix^\mu\partial_\mu \\ K_\mu &= -i(2x^\mu x^\nu\partial_\nu - x^2\partial_\nu) \end{aligned} \tag{2.9}$$

Knowing all the generators we may now write down their algebra

$$\begin{aligned}
[D, P_\mu] &= iP_\mu \\
[D, K_\mu] &= -iK_\mu \\
[K_\mu, P_\nu] &= 2i(\delta_{\mu\nu}D - L_{\mu\nu}) \\
[K_\rho, L_{\mu\nu}] &= i(\delta_{\rho\mu}K_\nu - \delta_{\rho\nu}K_\mu) \\
[P_\rho, L_{\mu\nu}] &= i(\delta_{\rho\mu}P_\nu - \delta_{\rho\nu}P_\mu) \\
[L_{\mu\nu}, L_{\rho\sigma}] &= i(\delta_{\nu\rho}L_{\mu\sigma} + \delta_{\mu\sigma}L_{\nu\rho} - \delta_{\mu\rho}L_{\nu\sigma} - \delta_{\nu\sigma}L_{\mu\rho}) \\
[L_{\mu\nu}, D] &= 0
\end{aligned} \tag{2.10}$$

the last line tells us that dilatations do not change the spin, and conversely that rotations do not change the scaling dimension[3]. Hence, operators may be labelled by their spin and scaling dimension.

## 2.3 Conformal Transformations On Operators

The next important step is to determine how the generators act on operators. Our main interest is going to be in so called "primary" operators. These are operators that cannot be written as derivatives of other operators. These operators transform as $O(x) \to O'(x') = b(x)^{-\Delta}R(x) \cdot O(x)$, where we have left space-time indices implicit. For example in the case of a spin-1 operator we would have $O_\mu(x) \to O'_\mu(x') = R_{\mu\nu}(x)b(x)^{-\Delta}O_\nu(x)$. The quantity $\Delta$ is called the scaling dimension, whereas the quantity "$R(x)$" depends on the spin of the field. For scalars $R(x) \sim 1$ whereas for spin-1 $R(x) \sim R_{\mu\nu}(x)$ is a rotation matrix. The factor $b(x)$ prevents the fields from being writable as the derivative of some other field. Note that from 2.1 conformal transformations can be thought of (locally) as a product of rotations and dilatations, this agrees with the above discussion.

We will derive the transformation laws of operators by defining how they transform at the origin, and then translating them to a generic position $x$. For a more in depth discussion on this topic see [33]. Remember that:

$$\begin{aligned}
f(z - x) &= f(z) - x \cdot \nabla f(z) + \frac{1}{2!}(x \cdot \nabla)^2 f(z) + ... \\
&= e^{-ix^\mu P_\mu} f(z)
\end{aligned} \tag{2.11}$$

Next we assume $L_{\mu\nu}O(0) = S_{\mu\nu}O(0)$, $DO(0) = -i\Delta O(0)$ and $K_\mu O(0) = k_\mu O(0)$ where $S_{\mu\nu}$ is some matrix that obeys the same commutation relations as $L_{\mu\nu}$. In addition, $\Delta$ is called the scaling dimension. We will eventually set $k_\mu$ to zero, hence we avoid naming it. We then have

$$\begin{aligned}
L_{\mu\nu}O(x) = e^{+ix^\mu P_\mu}L_{\mu\nu}O(0) &= e^{+ix^\mu P_\mu}S_{\mu\nu}e^{-ix^\mu P_\mu}e^{+ix^\mu P_\mu}O(0) \\
&= (S_{\mu\nu} - x_\mu P_\nu - x_\nu P_\mu)O(x)
\end{aligned} \tag{2.12}$$

where to get the second line we have used the Baker-Campbell-Hausdorff formula 2.7. Similarly we get

[3] Which is the eigenvalue under $D$.

$$\begin{aligned} P_\mu &= -i\partial_\mu O(x) \\ DO(x) &= (-i\Delta + x^\mu P_\mu)O(x) \\ K_\mu O(x) &= (k_\mu - 2ix_\mu\Delta - 2x^\nu S_{\mu\nu} + 2x_\mu x^\nu P_\nu - x^2 P_\mu)O(x) \end{aligned} \tag{2.13}$$

Thus we have the action of all generators on operators. The reason that we fixed $DO(0) = -i\Delta O(0)$ with $\Delta$ a constant is due to the commutation relation $[L_{\mu\nu}, D] = 0$. Consequently, the commutation relation $[\Delta, k_\mu] = k_\mu$ sets $k_\mu = 0$ since $\Delta$ is proportional to the identity. Hence, we have $K_\mu O(0) = 0$, this is the definition of what we will call a conformal primary operator. From which it follows that $O(0)$ cannot be written as the derivative of another operator since then (assume spin 0 for simplicity) $K_\mu O(0) = K_\mu P_\nu O'(0) = (P_\nu K_\mu + 2\delta_{\mu\nu}\Delta)O'(0) \neq 0$.

An interesting observation, see [94], is that we could have derived the preceding equations by using the transformation law

$$\phi(x) \to \phi(x') = b(x)^{-\Delta}\phi(x) \tag{2.14}$$

written for scalars in favor of simplicity of demonstration. Where we have $b(x) = 1 + \partial_\mu \epsilon_\mu$ with $\epsilon_\mu$ defined in 2.6.

## 2.4 Correlation Functions

We will now show that using conformal transformations one can fix 2-pt and 3-pt functions (for simplicity containing only scalars) up to some constants, called the conformal data, which consist of scaling dimensions and OPE coefficients.

Firstly, from dilatations we have

$$\langle O(\lambda x)\rangle = \lambda^{-\Delta}\langle O(x)\rangle \tag{2.15}$$

this implies

$$\langle O(x)\rangle = 0 \tag{2.16}$$

since if it were equal to a non zero constant, this constant would change under dilatations. Next, we consider 2-pt functions, using translations and rotations they can be fixed to the following form

$$\langle A(x)B(y)\rangle = c_{AB} f(|x-y|) \tag{2.17}$$

where $f$ is an arbitrary function and $c_{AB}$ is a constant that depends on which two operators we are considering. Using dilatations this is further fixed to

$$\langle A(x)B(y)\rangle = c_{AB}\frac{1}{|x-y|^{\Delta_A+\Delta_B}} \tag{2.18}$$

which is indeed invariant under $O(\lambda x) \to O(x') = \lambda^{-\Delta_O} O(x)$ and $x \to x' = \lambda x$. Consequently, the 2-pt function is further fixed to be non zero only between identical operators i.e. $c_{AB} = c\delta_{AB}$. To see this we need to use special conformal transformations. We have

$$K_\mu \langle A(x)B(y)\rangle = 0 = \langle (K_\mu A(x))B(y)\rangle + \langle A(x)(K_\mu B(y))\rangle \tag{2.19}$$

and using 2.18 and 2.13 we obtain

$$K_\mu \langle A(x)B(y)\rangle \sim c_{AB}(\Delta_A - \Delta_B) = 0 \tag{2.20}$$

Finally, note that we can rescale the operators in order to absorb the factor of $c$. This leads to the final expression for the 2-pt function

$$\langle O(x)O(y)\rangle = \frac{1}{|x-y|^{2\Delta}} \tag{2.21}$$

The last $n$-point function that is completely fixed by conformal symmetry is the 3-pt function. Use of translations, rotations and dilatations fixes it to the form

$$\langle A(x)B(y)C(z)\rangle = \sum \frac{c_{ABC}}{|x-y|^a |y-z|^b |z-x|^c} \tag{2.22}$$

where $a$, $b$ and $c$ are defined by the relation $a+b+c = \Delta_A + \Delta_B + \Delta_C$. The sum should be thought of as running over all possible values of $(a, b, c)$ and the constant $c_{ABC}$ will be called an OPE coefficient[4]. The naming of the constant will become clear in the next section. Using special conformal transformations we can reduce the possible combinations $(a, b, c)$ down to a single one. This is $a = \Delta_A + \Delta_B - \Delta_C$, $b = \Delta_B + \Delta_C - \Delta_A$ and $c = \Delta_C + \Delta_A - \Delta_B$. See for example [88].

The above were written for scalar fields in favour of simplicity. Nevertheless we note that they can also be worked out in the case of spinning fields.

## 2.5 The Operator Product Expansion

In this section we will motivate the notion of the operator product expansion (OPE). Using initially the free scalar field theory, and then a generic interacting scalar field theory, we show why one expects the product of two fields, each at a different position, to be expressible in a sum over various operators. We will see that in the free theory this sum is over a finite number of operators, whereas once we add interactions the sum contains an infinite amount of operators. Our demonstration will be for a Hamiltonian theory which is perturbatively accessible, nevertheless the notion of the OPE is completely general and independent of either. For a demonstration of the perturbative uses of the OPE see [18], for motivation of the OPE using only CFT properties see [94]. Note that we will brush all subtle issues, such as convergence, under the carpet, since our goal is to merely motivate the existence of the expansion.

Let us first consider the following 3-pt functions

[4] Under the assumption that the 2-pt function is normalized as in 2.21.

$$\begin{aligned}&\langle\phi(x)\phi(0)\phi^2(y)\rangle\\&\langle\phi(x)\phi(0)\phi^4(y)\rangle\\&\langle\phi(x)\phi(0)\phi^6(y)\rangle\\&\dots\end{aligned} \tag{2.23}$$

these are computable by Wick contractions in the free theory. Only the first is non-zero. Also, we know the following two point function:

$$\langle\phi(x)\phi(0)\rangle = \frac{1}{x^{2\Delta_\phi}} \tag{2.24}$$

We observe that the expressions for the correlators in 2.23 calculated by Wick contractions, could instead be reproduced in the $x \to 0$ limit if we had assumed

$$\phi(x) \times \phi(0) \sim \frac{1}{x^{2\Delta_\phi}} + \phi^2(0) \tag{2.25}$$

The symbol $\sim$ implies that 2.25 holds specifically when inserted in correlators. The first term on the RHS reproduces the two point function, whereas the second term is needed to reproduce the first line of 2.23 in the limit $x \to 0$. Lastly, since the three point function $\langle\phi\phi\phi^a\rangle$ is zero in the free theory if $a > 2$, the OPE coefficients corresponding to exchanged $\phi^a$ operators (with $a > 2$) in the $(\phi \times \phi)$ OPE are zero. For simplicity we have not explicitly written out the contributions of operators containing derivatives. Thus, we see that for free fields the OPE truncates at a specific operator, which of course depends on which operators we take the OPE between.

Now let us consider an interacting case, for demonstration purposes assume our Hamiltonian is deformed with a quartic scalar term $H = H_0 + g\phi^4$, where $H_0$ is the free part. In this case

$$\begin{aligned}\langle\phi(x)\phi(0)\phi^2(y)\rangle &\sim \langle\phi(x)\phi(0)\phi^2(y)\rangle_f - g\int d^dz\langle\phi^4(z)\phi(x)\phi(0)\phi^2(y)\rangle_f + O(g^2)\\\langle\phi(x)\phi(0)\phi^4(y)\rangle &\sim \langle\phi(x)\phi(0)\phi^4(y)\rangle_f - g\int d^dz\langle\phi^4(z)\phi(x)\phi(0)\phi^4(y)\rangle_f + O(g^2)\\\langle\phi(x)\phi(0)\phi^6(y)\rangle &\sim \langle\phi(x)\phi(0)\phi^6(y)\rangle_f - g\int d^dz\langle\phi^4(z)\phi(x)\phi(0)\phi^6(y)\rangle_f + O(g^2)\\&\dots\end{aligned} \tag{2.26}$$

where the left hand side is evaluated in the full theory, and the terms on the right hand side are evaluated in the free theory. The minus sign is due to the expansion of $e^{-\int d^dz(H_0+g\phi^4)}$ around $g \to 0$, where we have also set the usual factor $\beta = 1$ in $e^{-\beta\mathcal{H}}$. From 2.26 it is now straightforward to see that the OPE of $\phi$ with itself should now contain an infinite amount of terms, and the terms that did not appear in 2.25 should have OPE coefficients that start at $O(g)$ or above.

For the rest of this thesis operators that appear on the left hand side of the OPE will be called "external" operators, and operators that appear on the right hand side of the OPE will be called "exchanged" operators.

## 2.6 Conformal Blocks

The computation of four point functions is done by expressing them in an (in general) infinite series of other functions, called conformal blocks. This can be done in principle by taking the OPE twice in order to reduce the four point function to an (in general) infinite sum of two point functions. Conformal blocks are convenient since each one of them contains the contribution of a primary and all its descendents to the four point function. Another way of computing the conformal blocks is via the conformal Casimir. The Casimir is an operator made up of generators, that commutes with all generators. Hence descendents, which are expressible as a primary acted upon by various powers of the momentum generator, all have the same eigenvalue under the Casimir as the primary. This leads to a differential equation one can solve to find the conformal blocks. For this approach see [35], see also [34]. In practice, in the numerical bootstrap what is used to compute the blocks are Zamolodchikov recursion relations[5], see e.g. [60], [59] or [85] as well as the recent numerical implementation [39]. Below we provide a brief sketch of how this works.

The first tool we will need is the operator-state correspondence. This tells us that an operator inserted at the origin acting on the vacuum, for all intents and purposes, is equivalent to a state with the same scaling dimension and spin. We have e.g.

$$DO(0)|0\rangle = -i\Delta O(0)|0\rangle \tag{2.27}$$

from 2.13. Thus we can make the identification $O(0)|0\rangle = |\Delta\rangle$. The second tool we will need is referred to as radial quantization. This is the practice of foliating our space in slices of fixed radii. We write our metric schematically as

$$ds^2 = dr^2 + r^2 d\boldsymbol{\theta}^2 \tag{2.28}$$

in $d = 2$ $\boldsymbol{\theta}$ is an angle, in higher dimensions it is a more complicated metric element we will not need to specify. Consequently, we change coordinates $\tau \to logr$ in order to obtain

$$ds^2 = e^{2\tau}(d\tau^2 + d\boldsymbol{\theta}^2) \tag{2.29}$$

In this choice of foliation the evolution operator is $U = e^{iD\tau}$. Note that since the generator $D$ has a factor of $i$ in it, the exponent is real. We would like to learn what conjugation looks like in radial quantization. This can be done by considering the evolution of an operator in Minkowski space and then continuing to Euclidean space[6]. We start with [20]

$$O(t) = e^{iHt - iPx} O(0) e^{-iHt + iPx} \tag{2.30}$$

where $O(t)$ is some Hermitian operator. Continuing $t$ to $t = -i\tau$ we get

$$O(\tau) = e^{H\tau - iPx} O(0) e^{-H\tau + iPx} \tag{2.31}$$

[5] For the original papers see [109] and [108]

[6] We are not going to touch on the delicate issue of the assumptions required for continuations between the two to exist.

hence for the equation to continue to make sense we must have $O(\tau)^\dagger = O(-\tau)$. In other words, under conjugation we have $r \to 1/r$ since $\tau = logr$. Now remember that the generator of special conformal transformations is a composition of an inversion a translation and another inversion. Denoting an inversion as $I$ we have

$$K_\mu = IP_\mu I = IP_\mu I^{-1} = P_\mu^\dagger \tag{2.32}$$

where we used that the inverse of an inversion is an inversion. Equation 2.32 is very important since it tells us that $P_\mu$ and $K_\mu$ can be thought of as raising and lowering operators of the scaling dimension respectively.

We are now ready to motivate the recursion relation for conformal blocks. First, from the above, note that a field $O(x)$ that is a descendent and a primary at the same time is a null state

$$\langle\Delta|\Delta\rangle = \langle\Delta|P_\mu|\Delta-1\rangle = (\langle\Delta|\overleftarrow{K_\mu})|\Delta-1\rangle = 0 \tag{2.33}$$

where we used that $K_\mu$ gives zero when acting on a primary state, and that it is the conjugate of $P_\mu$. Next let us consider the four point function expanded in a complete set of states

$$\langle OOOO\rangle = \sum_{\bar{O}} \frac{\langle OO|\bar{O}\rangle\langle\bar{O}|OO\rangle}{\langle\bar{O}|\bar{O}\rangle} \sim \sum_{\bar{O}'} \lambda^2_{OO\bar{O}'} g_{\Delta_{\bar{O}'},l} \tag{2.34}$$

where $g_{\Delta_{\bar{O}'},l}$ is the conformal block, which encodes information about a primary $\bar{O}'$ and all its descendants. Note that in 2.34 the first sum on the right hand side runs over all exchanged operators, whereas the second sum only over primaries (descendants have been implicitly grouped with their corresponding primaries). In 2.34 we have made use of

$$1 = \sum_{\bar{O}} \frac{|\bar{O}\rangle\langle\bar{O}|}{\langle\bar{O}|\bar{O}\rangle} \tag{2.35}$$

thus if $\langle\bar{O}|\bar{O}\rangle$ has a zero, then 2.34 has a pole. This happens whenever some $\bar{O}$ is simultaneously a primary and a descendent[7]. Then, at some value of the scaling dimension $\Delta_{\bar{O}} = \Delta^\star_{\bar{O}}$ the expression 2.35 will have a pole $\frac{1}{\Delta_{\bar{O}} - \Delta^\star_{\bar{O}}}$ due to a descendent at some level $n$. Note that the norm of all descendents of the null state will have a zero at the same position, thus the pole factors out. But this sum over a primary and all its descendents is a conformal block, thus we conclude that the residue of the pole will be another conformal block with spin and scaling dimension that of the descendent that becomes null.

$$g_{\Delta,l} = f_{\Delta,l} + \sum_{poles} \frac{c}{\Delta - \Delta^\star} g_{\Delta^\star+n,l^\star} \tag{2.36}$$

Where we have denoted by $f_{\Delta,l}$ a function that does not have poles in $\Delta$, but a singularity that behaves as $r^\Delta$, $r$ is a coordinate that is not important for now given that it will be taken to be $r < 1$. Also $c$ stands for a set of coefficients which are also computable, as is the set of $\Delta^\star$s that gives us the positions of the poles. Iterating

[7] We have not discussed unitarity bounds, see e.g. the discussion in [20]. These bounds, which are lower bounds on the scaling dimensions of operators $\Delta_O > \Delta_{min}$ as a function of the operator's spin, must always be satisfied in unitary theories. The poles in 2.34 always appear for values of the scaling dimensions at or below the unitarity bounds, hence will not cause us any problems.

this equation numerically one computes conformal blocks to a desired accuracy. For more details we refer the reader to [60].

## 2.7 The Crossing Equation and Bootstrap Constraints

We now have all the tools needed to discuss the crossing equation and its constraints. For simplicity we will start with four identical scalars that carry no index under global symmetry. We shall explain later how this generalizes to different fields transforming in arbitrary representations of arbitrary global symmetry.

To start we write the OPE in following general form

$$O(x)O(0) \sim \sum_{O'} c_{OO}^{O'} x^{\mu_1} ... x^{\mu_l} O'_{\mu_1 \mu_2 ... \mu_l} \tag{2.37}$$

and then reorganize it as

$$O(x)O(y) \sim \sum_{O'} c_{OO}^{O'} P(x-y, \partial_y) O'(y) \tag{2.38}$$

where the function $P(x-y, \partial_y)$ is used to schematically organize the OPE in terms of primaries. Note that we could actually compute the explicit form of this function, see e.g. [94], but it will not be particularly useful for our purposes. Now, we may compute a 4-pt function by taking the OPE twice in the following way

$$\begin{aligned} &\langle O(x_1)O(x_2)O(x_3)O(x_4)\rangle \\ &= \sum_{O'} c_{OO}^{O'} c_{OO}^{O'} P(x_1-x_2, \partial_{x_2}) P(x_3-x_4, \partial_{x_4}) \langle O'(x_2)O'(x_4)\rangle \end{aligned} \tag{2.39}$$

which is recast as

$$\begin{aligned} &\langle O(x_1)O(x_2)O(x_3)O(x_4)\rangle \\ &= \sum_{O'} (c_{OO}^{O'})^2 \frac{1}{|x_{12}|^{2\Delta_O} |x_{34}|^{2\Delta_O}} g_{\Delta_{O'},l}(u,v) \end{aligned} \tag{2.40}$$

by puling out a factor of the coordinates that has the expected transformation properties under conformal transformations and isolating the invariant part in a separate function $g_{\Delta_{O'},l}(u,v)$ which is the conformal block. The variables $u$ and $v$ are conformally invariant combinations of the coordinates at which the external operators are inserted at, and are given by

$$u = \frac{x_{12}^2 x_{34}^2}{x_{13}^2 x_{24}^2}, v = \frac{x_{14}^2 x_{23}^2}{x_{13}^2 x_{24}^2} \tag{2.41}$$

For later convenience note that we can also define another set of variables $z$ and $\bar{z}$ via $u = z\bar{z}$ and $v = (1-z)(1-\bar{z})$. Notice that the above choice of taking the OPE between two specific operators is not the only choice, we could have taken the OPE between two other operators. More explicitly, instead of taking the OPE of the first with the second and then the third with the fourth, and finally computing the resulting two point function, we could have taken the OPE of the first with the fourth and

the second with the third. Both choices are equivalent[8], hence should be equal, thus we obtain

$$\begin{aligned}&\sum_{O'}(c_{OO}^{O'})^2\frac{1}{|x_{14}|^{2\Delta_O}|x_{23}|^{2\Delta_O}}g_{\Delta_{O'},l}(v,u)\\=&\sum_{O'}(c_{OO}^{O'})^2\frac{1}{|x_{12}|^{2\Delta_O}|x_{34}|^{2\Delta_O}}g_{\Delta_{O'},l}(u,v)\end{aligned}\tag{2.42}$$

which can be re-written as

$$0=\sum_{O'}(c_{OO}^{O'})^2F^{\Delta_O}_{\Delta_{O'},l}\tag{2.43}$$

by defining the so called convolved conformal blocks

$$F^{\Delta_O}_{\Delta_{O'},l}=u^{-\Delta_O}g_{\Delta_{O'},l}(u,v)-v^{-\Delta_O}g_{\Delta_{O'},l}(v,u)\tag{2.44}$$

2.43 is referred to as a sum rule. As we will see later the number of sum rules that result from a given crossing equation depends on the number of irreducible representations of the global symmetry that appear on the right hand side of the OPE. Any CFT must satisfy its corresponding sum rules, this provides constraints on the CFT data. In addition to the sum rules, unitary CFTs must satisfy so called unitarity bounds. These are

$$\Delta\geqslant\frac{d-2}{2}\tag{2.45}$$

for spin-0 operators, and

$$\Delta\geqslant d-2+l\tag{2.46}$$

for spin-$l$ operators with $l\geqslant 1$, where $d$ is the dimensionality. Unitarity also implies that the OPE coefficients should be real numbers, for a proof of this and a discussion of unitarity bounds see [20].

We now have all the ingredients needed to demonstrate how the bootstrap algorithm works. Recast 2.43 as

$$0=\sum_{O'\neq 1}(c_{OO}^{O'})^2F^{\Delta_O}_{\Delta_{O'},l}+F^{\Delta_O}_{0,0}\tag{2.47}$$

where we have explicitly separated the contribution of the unit operator. Assume we can find a functional $a$ such that:

$$a(F^{\Delta_O}_{0,0})=1\tag{2.48}$$

and

$$a(F^{\Delta_O}_{\Delta_{O'},l})\geqslant 0\tag{2.49}$$

for each $\Delta_{O'}$. Then, rewriting the previous sum rule we get

$$\sum_{O'}(c_{OO}^{O'})^2a(F^{\Delta_O}_{\Delta_{O'},l})=-a(F^{\Delta_O}_{0,0})=-1\tag{2.50}$$

[8]Under the assumption that the operators are placed at positions $x_1$, $x_2$, $x_3$ and $x_4$ chosen such that all aforementioned OPEs converge.

noting that squares of real numbers are positive numbers we realize that we have arrived at a contradiction, since we have $(positive) = (negative)$. Thus, the set scaling dimensions and OPE coefficients we had plugged in to 2.43 does not correspond to a self consistent conformal field theory, and hence is excluded from parameter space.

We note that the functional is usually parametrized as $a = \sum_{m,n} a_{mn}\partial_z^m \partial_{\bar{z}}^n|_{z=\bar{z}=1/2}$ with $z$ and $\bar{z}$ defined as under 2.41. Even though this is the standard choice one may choose a functional however they like[9]. The simplest bootstrap algorithm now proceeds as follows

1) Require that all operators in the theory satisfy their corresponding unitarity bound.

2) Choose a specific operator and demand that its scaling dimension starts above the the unitarity bound, $\Delta > \Delta_{unitarity} + x$, for some value of $x > 0$

3) See if you can find a functional of the form specified above. If yes, then that choice of $x$ does not correspond to a unitary self consistent CFT and thus you have placed an upper bound on the scaling dimension of this operator $\Delta < \Delta_{unitarity} + x$. If you cannot find a functional, raise the value of $x$ until you can.

The above procedure, when done to find the optimal value of $x$, will produce what we will call exclusion plots. These are most often plots of the maximum allowed scaling dimension of some operator as a function of the scaling dimension of some external operator. Note also that the above is the simplest version of the bootstrap algorithm, one can move as many operators as they want away from the unitarity bound.

Alternatively, one can perform an algorithm in order to maximize (or minimize) an OPE coefficient. Take 2.47 and in addition to to the unit operator, isolate the operator whose OPE coefficient we are interested in constraining, and call it $O_A$

$$0 = \sum_{O' \neq 1, O_A} (c_{OO}^{O'})^2 F^{\Delta_O}_{\Delta_{O'},l} + F^{\Delta_O}_{0,0} + (c_{OO}^{O_A})^2 F^{\Delta_O}_{\Delta_{O_A},l_{O_A}} \tag{2.51}$$

this time we will search for a functional satisfying

$$a(F^{\Delta_O}_{\Delta_{O'},l}) \geqslant 0 \tag{2.52}$$

for all $O \neq 1, O_A$ , and

$$a(F^{\Delta_O}_{\Delta_{O_A},l_{O_A}}) = 1 \tag{2.53}$$

Recasting the sum rule 2.51 as follows we get an inequality

$$(c_{OO}^{O_A})^2 = -\sum_{O'} (c_{OO}^{O'})^2 a(F^{\Delta_O}_{\Delta_{O'},l}) - a(F^{\Delta_O}_{0,0}) \leqslant -a(F^{\Delta_O}_{0,0}) \tag{2.54}$$

in order to get the inequality we used the fact that $(c_{OO}^{O'})^2 a(F_{\Delta_{O'},l})$ is positive. Minimizing $-a(F^{\Delta_O}_{0,0})$ we may find an upper bound on the OPE coefficient of $O_A$. Conversely if we had chosen

$$a(F^{\Delta_O}_{\Delta_{O_A},l_{O_A}}) = -1 \tag{2.55}$$

[9] See e.g. [19], where the authors sample different points rather than just $z = \bar{z} = 1/2$.

we would get a lower bound on the OPE coefficient. These procedures for finding a functional under certain constraints are performed by the specialized software SDPB [97], [65]. Also, to write the sum rules that result from crossing symmetry in a form understandable to SDPB, the present author has so far used the following software [9] [41]. Note also that a software called Autoboot exists, which calculates the sum rules for a given group automatically [42].

Note that SDPB solves semi-definite programming problems. This is needed since if we move away from single correlator bootstrap examples, such as the one described above, instead of sum rules consisting of functions we now have sum rules consisting of matrices of functions. Hence, we now need a functional that when acting on a sum rule gives positive semi-definite matrices. If we name these matrices $M$, they must satisfy $\lambda^\tau M\lambda \geqslant 0$ for any $\lambda$. Where $\lambda$ is a column vector consisting of real numbers (corresponding to the OPE coefficients). With this in mind the generalization of the steps outlined above is straightforward to work out.

# Chapter 3

# Scalar Field Theories with Cubic Symmetry

## 3.1 Cubic Theories in $d = 4 - \varepsilon$ Dimensions

It will be instructive to review some basic knowledge about scalar field theories with (hyper) cubic ($C_N = {Z_2}^N \rtimes S_N$)[1] $C_3 = {Z_2}^3 \rtimes S_3$[2] symmetry in $d = 4 - \varepsilon$ dimensions. Their Hamiltonian density can be written in two equivalent forms[3], related by a coupling constant redefinition:

$$\mathcal{H} = g_1(\phi_1^4 + \phi_2^4 + \phi_3^4) + g_2(\phi_1^2\phi_2^2 + \phi_2^2\phi_3^2 + \phi_3^2\phi_1^2) \tag{3.1}$$

and

$$\mathcal{H} = g_1'(\phi_1^2 + \phi_2^2 + \phi_3^2)^2 + g_2'(\phi_1^4 + \phi_2^4 + \phi_3^4) \tag{3.2}$$

Note that in 3.1 and 3.2 we have at most four powers of $\phi$ appearing, since any more would be irrelevant in $d < 4$, in the renormalization group sense of the word. Although incredibly simple, 3.1 and 3.2 tell us a lot. The first equation tells us that the cubic theory can be viewed as a deformation of three decoupled Ising models. See for example [57], which considered this viewpoint in conformal perturbation theory [18]. The second equation equation tells us that the cubic theory can be viewed as a deformation of the $O(3)$ model, see for example the discussion in the "Future directions" section of [21], where the authors use conformal perturbation theory arguments to show that the scaling dimension of the lowest dimension scalar singlet ($\Delta_S$) should satisfy (roughly) $\Delta_S^{C_3} - \Delta_S^{O(3)} \sim 0.0001$. Note that this proximity of the scaling dimensions in the $O(3)$ and $C_3$ theories is not something obvious a priori in the traditional $\varepsilon$ expansion, in which all theories are studied as a deformation of the free theory. Of course, after resummations are performed, one indeed observes the proximity of scaling dimensions between the two models. For the state of the art $\varepsilon$ expansion results see [1].

Let us write 3.1 in a more generic form, valid for an arbitrary amount of scalars instead of three

$$\mathcal{H} = g_1'\delta_{ij}\delta_{kl}\phi_i\phi_j\phi_k\phi_l + g_2'\delta_{ijkl}\phi_i\phi_j\phi_k\phi_l \tag{3.3}$$

[1] This is just the symmetry of $N$ copies of the Ising model, either coupled or not.

[2] The symbol $\rtimes$ implies that ${Z_2}^3$ is a normal subgroup of $C_3$ but $S_3$ is not. In other words, an element of ${Z_2}^3$ conjugated by $S_3$ is still an element of ${Z_2}^3$. Whereas the reverse statement is not true. One may convince themselves by explicitly checking the action of $S_3$ and ${Z_2}^3$ on $\phi_i = (\phi_1, \phi_2, \phi_3)$

[3] We write only the interaction part and omit the kinetic and mass terms.

where summation of indices is implied, and $\delta_{ijkl}$ is non-zero only when all indices are identical. From this rewriting we learn that, compared to $O(N)$ theories, hypercubic theories ($C_N = Z_2^N \rtimes S_N$) have an additional four-index invariant tensor $\delta_{ijkl}$. This observation will be very useful in Chapter 4 where we will build 4-pt projectors from invariant tensors of the global symmetry.

Our qualitative discussion so far makes it apparent that, in $d = 4 - \varepsilon$, a multi-scalar theory with hypercubic symmetry has at least four fixed points: Gaussian Fixed Point - Free Theory (both couplings zero), $O(N)$ Fixed Point ($g_2' = 0$ in 3.2), ($N$ Identical) Ising Fixed Point(s) ($g_2 = 0$ in 3.1), Hypercubic Fixed Point (both couplings non-zero). This picture is indeed confirmed by a standard perturbative calculation [110]. No additional fixed points are found in the standard $\varepsilon$ expansion. However, additional fixed points can be found if one performs resummations first, and then looks for zeroes of the beta function[4] [29]. These additional fixed points are a controversial topic in the literature, we will return to them when we talk about $O(m) \times O(n)$ theories in Chapter 6, where they have received significant attention. Some recent relevant literature includes [51] [95] [79] [78] [6] [10] [96] [23] [13] [1], for older references we point to [84] and references therein. For the Large $N$ limit see [2], or more recently [14]

[4] Usually one does the converse.

# Chapter 4

# Tensor Structures in Cubic Theories

## 4.1 The $\langle\phi\phi\phi\phi\rangle$ correlator

The first step in deriving the sum rules required for the numerical investigation of a model in the bootstrap, is to determine the tensor structures[1] that appear in 4-pt functions when decomposed onto irreducible representations. We note that recently the procedure of deriving sum rules from a given crossing equation was automated for a large number of groups [42]. Nevertheless, it will be instructive to determine the tensor structures since they can provide us with intuition for several things. For example, explicit knowledge of the tensor structures can tell us what an operator looks like in the weak coupling limit[2]. Knowledge of the tensor structures can also point out dualities between crossing equations. By this we mean that crossing equations containing operators from different symmetry groups and different representations give exactly the same (or equivalent) sum rules. This is something that needs to be taken into account when studying theories in the numerical bootstrap in order to know what theories we expect to appear in our plots. As an example, 4-pt functions containing four $\phi_i$ operators or four $\bar{\phi}_i$ operators transforming in the defining representation of $O(2)$ or $Z_2 \times S_3$ respectively, have the same sum rules. Tensor structures of global symmetries are also useful in the analytic bootstrap where they determine the crossing matrix, such as in [48] [47] [4] [49] [5] [31] [32]. Lastly, a lot of our calculations will be useful for groups not currently supported in [42]. This will be the case in Chapter 9.

The first correlator of interest will be

$$\langle\phi_i\phi_j\phi_k\phi_l\rangle \tag{4.1}$$

where the four operators transform in the defining representation of the cubic group. We will decompose this onto irreps of $C_3 = Z_2^3 \rtimes S_3$. To determine the tensor structure corresponding to each representation it will suffice to know that $C_3$ is a subgroup of $O(3)$. When reducing the symmetry from $O(3)$ to $C_3$, the traceless symmetric representation of $O(3)$ decomposes into two irreducible representations of $C_3$ which we call $X$ and $Y$. For further details on the group theory of $C_3$, in the context of physics, see [6]. We will also work out the general case for $G^N \rtimes S_N$, where $G$ is any group, in Chapter 9. The OPE of two operators transforming in the vector representation of $O(3)$ is schematically

[1] For the rest of this work, unless stated otherwise, the term "tensor structure" will refer to a tensor structure of a global symmetry.

[2] In most cases for us this will be the $\varepsilon \to 0$ limit in $d = 4 - \varepsilon$.

$$\phi_i \times \phi_j \sim \delta_{ij} S + T_{ij} + A_{ij} \tag{4.2}$$

where $\delta_{ij}$ is the Kronecker delta, and S, T, and A are respectively the Singlet, Traceless Symmetric and Antisymmetric representations. To break the symmetry down to $C_3$ we decompose $T$ into $X$ and $Y$ ($S$ and $A$ are unchanged). We thus obtain

$$\phi_i \times \phi_j \sim \delta_{ij} S + X_{ij} + Y_{ij} + A_{ij} \tag{4.3}$$

We can use this expression to write the four point function as

$$\langle \phi_i \phi_j \phi_k \phi_l \rangle \sim \delta_{ij}\delta_{kl} \langle SS \rangle + \langle X_{ij} X_{kl} \rangle + \langle Y_{ij} Y_{kl} \rangle + \langle A_{ij} A_{kl} \rangle \tag{4.4}$$

where we took the OPE between the first two and last two operators in the four point function respectively. It is now trivial to read off the four point tensor structure of the "S" representation: $P^S_{ijkl} \sim \delta_{ij}\delta_{kl}$[3]. Also, since the contribution from the "A" representation is identical to that of $O(3)$, we have $P^A_{ijkl} \sim \delta_{ik}\delta_{jl} - \delta_{il}\delta_{jk}$.

All that remains is to calculate the projectors corresponding to the representations $X$ and $Y$. First we note that $X_{ij}$ is composed of the diagonal elements of $T_{ij}$, while $Y_{ij}$ is composed of the remaining non diagonal elements:

$$T_{ij} = \begin{pmatrix} X_{11} & Y_{12} & Y_{13} \\ Y_{21} & X_{22} & Y_{23} \\ Y_{31} & Y_{32} & X_{33} \end{pmatrix} \tag{4.5}$$

It is easy to check explicitly that under $C_3$ the elements $Y$ and $X$ in 4.5 do not mix. We also note that the grouping of elements into diagonal and non-diagonal holds for hypercubic theories in general (i.e. not just for $N = 3$). Thus, keeping in mind that the cubic group also has $\delta_{ijkl}$ as an invariant tensor[4] and demanding that the tensor structures for the $X$ and $Y$ representations are orthogonal to each other, as well as diagonal/non-diagonal respectively we obtain

$$\begin{aligned} P^X_{ijkl} &= \delta_{ijkl} - \frac{1}{3}\delta_{ij}\delta_{kl} \\ P^Y_{ijkl} &= \frac{1}{2}(\delta_{ik}\delta_{jl} + \delta_{il}\delta_{jk} - 2\delta_{ijkl}) \end{aligned} \tag{4.6}$$

and, indeed

$$P^X_{ijkl} + P^Y_{ijkl} = \frac{1}{2}(\delta_{ik}\delta_{jl} + \delta_{il}\delta_{jk} - \frac{2}{3}\delta_{ij}\delta_{kl}) = P^T_{ijkl} \tag{4.7}$$

In conclusion, knowing that $C_3$ is a subgroup of $O(3)$, and that $C_3$ has an additional invariant tensor, $\delta_{ijkl}$, we were able to explicitly construct the 4-pt tensor structures.

[3] The letter "P" was chosen to hint that, when appropriately normalized, the tensor structures are projectors. By slight abuse of terminology we will use these names interchangeably, even if the tensor structures are not appropriately normalized.

[4] In other words $\delta_{ijkl}\phi_i\phi_j\phi_k\phi_k = \phi_1^4 + \phi_2^4 + \phi_3^4$ is an invariant.

## 4.2 The $\langle XXXX \rangle$ correlator

The 4-pt correlator involving four fields in the $X$ representation can be simplified considerably as follows[5]. First note that from 4.5 we have

$$\Sigma_{i=j} X_{ij} = X_{11} + X_{22} + X_{33} = 0 \tag{4.8}$$

also, we can rewrite $X_{ij}$ in a more convenient form

$$X_{ij} = \Sigma_m \delta_{im} \delta_{jm} \tilde{X}_m \tag{4.9}$$

which can also be inverted to

$$\tilde{X}_m = \Sigma_{i,j} \delta_{im} \delta_{jm} X_{ij} \tag{4.10}$$

Both 4.9 and 4.10 are simply a redefinition: $X_{11} = \tilde{X}_1$, $X_{22} = \tilde{X}_2$ and $X_{33} = \tilde{X}_3$. But, three fields which are acted on by permutations and satisfy $\tilde{X}_1 + \tilde{X}_2 + \tilde{X}_3 = 0$ furnish the defining representation of $S_3$[6], the permutation group of three objects. The OPE between two operators in the defining representation of $S_N$ can be found in [50]. They obtain, as adapted to our current notation, and dropping the tildes for convenience

$$X_a \times X_b \sim P_{ab} S + (P_{ab} - \frac{1}{N})(X_a + X_b) + \bar{S}_{ab} + T_{ab} \tag{4.11}$$

with $P_{ab} = \delta_{ab} - \frac{1}{N}$. Where the last two representations are anti-symmetric and symmetric in their indices respectively. The representations have dimensions ($dim S$, $dim V$, $dim \bar{S}$, $dim T$) = (1, $N-1$, $\frac{1}{2}(N-1)(N-2)$, $\frac{1}{2}N(N-3)$), thus for $N = 3$ the symmetric representation drops out.

One needs to be careful when proceeding with summations including the tensor $P_{ab}$. For example, lets take the sum over the index $a$ in 4.11, the left side is zero identically. Lets us check that the same holds true for the second term on the right hand side

$$\Sigma_a (P_{ab} - \frac{1}{N})(X_a + X_b) = (P_{1b} X_1 + P_{2b} X_2 + P_{3b} X_3) + (P_{1b} X_b + P_{2b} X_b + P_{3b} X_b - X_b) \tag{4.12}$$

note that in 4.12 there is no implicit summation. Plugging in the definition of $P_{ab}$ we have

$$\Sigma_a (P_{ab} - \frac{1}{N})(X_a + X_b) = (\Sigma_a \delta_{ab} X_a) + (\Sigma_a \delta_{ab} X_b - 2X_b) = 0 \tag{4.13}$$

We now focus on the tensor structures of the 4-pt function $\langle X_a X_b X_c X_d \rangle$. These can be found by decomposing it onto the irreducible representations that appear in 4.11 by taking the OPE between the first two and last two operators in the correlator. For this we report the results in [50]

[5] Interestingly, as we will see in Chapter 9, this works for any group $G^N \rtimes S_N$ with $G$ arbitrary. This happens since the operator $X$ is always a singlet of $G$.

[6] Note that all the arguments of this section can be repeated verbatim for arbitrary $N$.

$$\langle X_a X_b \rangle \sim P_{ab} \tag{4.14}$$

$$\langle \bar{S}_{ab} \bar{S}_{cd} \rangle \sim P_{a[c} P_{d]b} \tag{4.15}$$

and

$$\langle T_{ab} T_{cd} \rangle \sim P_{abcd} \tag{4.16}$$

having defined

$$P_{abcd} = \delta_{a\neq b}\delta_{c\neq d}\left(\delta_{ac}\delta_{bd} + \delta_{ad}\delta_{bc} - \frac{1}{N-2}(\delta_{ac} + \delta_{ad} + \delta_{bc} + \delta_{bd}) + \frac{1}{(N-1)(N-2)}\right) \tag{4.17}$$

The last step is to illustrate how to go from the $S_N$ indices back to the $C_N = Z_2^N \rtimes S_N$ indices. We do this explicitly for the $X_{ij}$ $X_{kl}$ two point function which is the simplest case and report the results for the rest. From 4.9 we have

$$\langle X_{ij} X_{kl} \rangle \sim \Sigma_a \Sigma_b \delta_{ia}\delta_{ja}\delta_{kb}\delta_{lb} \langle X_a X_b \rangle \tag{4.18}$$

next we plug in $\langle X_a X_b \rangle \sim P_{ab}$ and get

$$\langle X_{ij} X_{kl} \rangle \sim \Sigma_a \Sigma_b \delta_{ia}\delta_{ja}\delta_{kb}\delta_{lb}(\delta_{ab} - \frac{1}{N}) = \delta_{ijkl} - \frac{1}{N}\delta_{ij}\delta_{kl} \tag{4.19}$$

which is precisely 4.6. This methodology leads to the following set of tensor structures for a 4-pt function involving four operators in the $X$ representation (for $N = 3$) $\langle X_{ij} X_{kl} X_{mn} X_{pq} \rangle$

$$P^S_{ijklmnpq} = \left(\delta_{ijkl} - \frac{1}{3}\delta_{ij}\delta_{kl}\right)\left(\delta_{mnpq} - \frac{1}{3}\delta_{mn}\delta_{pq}\right) \tag{4.20}$$

$$P\bar{S}_{ijklmnpq} = -\delta_{ijmn}\delta_{klpq} + \frac{1}{3}(\delta_{ij}\delta_{mn}\delta_{klpq} + \delta_{kl}\delta_{mn}\delta_{ijmn}) - (mn \leftrightarrow pq) \tag{4.21}$$

$$\begin{aligned} P^X_{ijklmnpq} = &-\delta_{ijkl}\delta_{mnpq} + \delta_{ijmn}\delta_{klpq} + \delta_{ijpq}\delta_{klmn} \\ &+\frac{1}{3}(\delta_{ij}\delta_{kl}\delta_{mnpq} + \delta_{mn}\delta_{pq}\delta_{ijkl}) \\ &-\frac{1}{3}(\delta_{ij}\delta_{mn}\delta_{klpq} + \delta_{kl}\delta_{pq}\delta_{ijmn}) \\ &-\frac{1}{3}(\delta_{ij}\delta_{pq}\delta_{mnkl} + \delta_{kl}\delta_{mn}\delta_{ijpq}) \\ &+\frac{1}{9}\delta_{ij}\delta_{kl}\delta_{mn}\delta_{pq} \end{aligned} \tag{4.22}$$

where we have used the identity[7]

[7] Note that in the $N = 2$ case there is a similar identity for $\delta_{ijklmn}$: $\delta_{ijklmn} = \frac{1}{2}(\delta_{ij}\delta_{klmn} + \delta_{kl}\delta_{ijmn} + \delta_{mn}\delta_{ijkl}) - \frac{1}{2}\delta_{ij}\delta_{kl}\delta_{mn}$.

$$\begin{aligned}\delta_{ijklmnpq} = \frac{1}{3}(\delta_{ij}\delta_{klmnpq} + \delta_{kl}\delta_{ijmnpq} + \delta_{mn}\delta_{ijklpq} + \delta_{pq}\delta_{ijklmn}) \\ \frac{1}{6}(\delta_{ijkl}\delta_{mnpq} + \delta_{ijmn}\delta_{klpq} + \delta_{ijpq}\delta_{klmn}) - \frac{1}{6}(\delta_{ij}\delta_{mn}\delta_{klpq} + \delta_{kl}\delta_{pq}\delta_{ijmn}) \\ -\frac{1}{6}(\delta_{ij}\delta_{pq}\delta_{klmn} + \delta_{kl}\delta_{mn}\delta_{ijpq}) + \frac{1}{6}\delta_{ij}\delta_{kl}\delta_{mn}\delta_{pq}\end{aligned} \tag{4.23}$$

which holds specifically for $N = 3$. We stress that the above projectors 4.20 4.21 and 4.22 are written specifically for $N = 3$. Nevertheless, in Appendix C.2 we report the sum rules for any value of $N$ which originally appeared in [93] and [100] in the context of hyper tetrahedral theories ($S_N \times Z_2$).

## 4.3 The $\langle \phi X \phi X \rangle$ correlator

First, let us reiterate that throughout this thesis when writing a 4-pt function it will be implied that we take the OPE between the first two and last two operators respectively. Thus, $\langle \phi_i X_{jk} \phi_l X_{mn} \rangle$ and $\langle \phi_i \phi_l X_{jk} X_{mn} \rangle$ will have different decompositions in terms of sums of conformal blocks, given that in general different irreducible representations will appear as exchanged operators when taking the different OPEs.

For the correlator in question we need to consider the OPE $\phi_i \times X_{jk}$. Note that since the representation of $\phi_i$ has dimension[8] 3 and that of $X_{jk}$ has dimension 2, the dimensions of the representations appearing on the right hand side of the OPE have to add up to 6. In addition to this, we have

$$\langle \phi_i \phi_j X_{kl} \rangle = \langle \phi_i X_{kl} \phi_j \rangle \tag{4.24}$$

which in our notation is the statement that the 3-pt function can be calculated by taking the OPE in two different but equivalent ways. This enforces that $\phi_l$ must appear in the $\phi_i \times X_{jk}$ OPE, since $X_{kl}$ appears in the $\phi_i \times \phi_j$ OPE. The tensor structure with which it appears can be found by multiplying both sides of the OPE with $\phi_{l'}$ and taking the expectation value

$$\langle (\phi_i \times X_{jk}) \phi_{l'} \rangle = T_{jkil} \langle \phi_l \phi_{l'} \rangle \tag{4.25}$$

this fixes $T_{jkil} = P^X_{jkil}$ , where $P^X_{jkil}$ is defined in 4.16. Now what remains on the right hand side of the OPE must have dimensions that add up to three. We have

$$\phi_i \times X_{jk} \sim P^X_{jkil} \phi_l + ... \tag{4.26}$$

where it is understood that $\phi$ schematically stands for all possible operators in that representation along with their appropriate OPE coefficients. With this in mind we can invert 4.26

$$\phi_l \sim P^X_{jkil} \phi_i X_{jk} \tag{4.27}$$

thus plugging in explicit values we get

[8] Not to be confused with scaling dimension.

$$\begin{aligned}\phi_1 \sim P^X_{jki1}\phi_i X_{jk} \sim \phi_1 X_{11} \sim \phi_1(X_{22}+X_{33})\\ \phi_2 \sim ... \sim \phi_2(X_{11}+X_{33})\\ \phi_3 \sim ... \sim \phi_3(X_{11}+X_{22})\end{aligned} \tag{4.28}$$

where we have made use of 4.6 and 4.8. In 4.26 we have two possibilities: ($i=j=k$) or ($i\neq j$ and $i\neq k$ and $j=k$). Lets consider the second possibility, e.g.

$$\phi_1 X_{22} = \frac{1}{2}\phi_1(X_{22}+X_{33}) + \frac{1}{2}\phi_1(X_{22}-X_{33}) \tag{4.29}$$

we now see that the second term is simply an element of an antisymmetric representation $A$ which indeed has dimension 3. The elements $A \sim (\ \phi_1(X_{22}-X_{33})\ ,\ \phi_2(X_{33}-X_{11})\ ,\ \phi_3(X_{11}-X_{22})\ )$ are antisymmetric under permutation of the indices. The first term is simply an element of the defining representation as can be seen from 4.28.

Knowledge of 4.29 suffices to find the tensor structure corresponding to $A$, see Appendix B

$$P^A_{ijklmn} = -3\delta_{ijklmn} + 2\delta_{il}\delta_{jkmn} + (\delta_{jk}\delta_{ilmn} + \delta_{mn}\delta_{ijkl}) - \delta_{il}\delta_{jk}\delta_{mn} \tag{4.30}$$

also, by plugging 4.26 into the four point function twice we get

$$P^X_{ijklmn} = \delta_{ijklmn} - \frac{1}{3}(\delta_{jk}\delta_{ilmn} + \delta_{mn}\delta_{ijkl}) + \frac{1}{9}\delta_{il}\delta_{jk}\delta_{mn} \tag{4.31}$$

Notice that so far we have not really cared about the normalization of the tensor structures. This is because in general a rescaling of the tensor structure with a positive number is equivalent to rescaling the OPE coefficients, which need only be real for our bootstrap algorithm. The exception to this is 4.31, which must be normalized as we present it in order for the OPE coefficient equality $\lambda_{\phi\phi X} = \lambda_{\phi X\phi}$ to hold.

## 4.4 The $\langle\phi\phi XX\rangle$ correlator

The last correlator we wish to consider is $\langle\phi_i\phi_j X_{kl} X_{mn}\rangle$. The required OPEs are 4.11 and 4.3. These OPEs have in common the singlet representation $S$ and the representation $X$ as exchanged operators. The tensor structure corresponding to an exchange of a scalar singlet is

$$P^S_{ijklmn} = \delta_{ij}(\delta_{klmn} - \frac{1}{3}\delta_{ij}\delta_{mn}) \tag{4.32}$$

whereas the one corresponding to the exchange of an operator in the $X$ representation is

$$P^X_{ijklmn} = \delta_{ijklmn} - \frac{1}{3}(\delta_{ij}\delta_{klmn} + \delta_{kl}\delta_{ijmn} + \delta_{mn}\delta_{ijkl}) + \frac{2}{9}\delta_{ij}\delta_{kl}\delta_{mn} \tag{4.33}$$

which can be calculated using 4.9 and 4.11. For the generic $N$ expressions replace $1/3$ in 4.32 with $1/N$ and $1/3$ in 4.33 with $1/N$ as well as $2/9$ with $2/N^2$.

# Chapter 5

# Bootstrap Constraints

Having worked out all the possible tensor structures that can appear in the 4-pt functions of interest one may work out the crossing equation sum rules. These sum rules lead to constraints that the CFT data appearing in these equations must satisfy.

## 5.1 Crossing Equations

First let us consider the most arbitrary 4-pt function containing four scalars. For this subsection we will follow the analysis in [59]. We have

$$\mathcal{G}_{abcd}\left(x_1, x_2, x_3, x_4\right) = \left\langle O_a\left(x_1\right) O_b\left(x_2\right) O_c\left(x_3\right) O_d\left(x_4\right)\right\rangle \tag{5.1}$$

Note that even though all the $O$ operators are scalars, they need not be in the same representation of the global symmetry. Thus, for the time being, the indices ($a$, $b$, $c$, $d$) should be thought as labeling each different operator, and not specific global symmetry indices. We will soon demonstrate the correspondence between the two with explicit examples, which should clear any confusion.

Separating contributions according to properties under conformal symmetry, 5.1 can be simplified as

$$\mathcal{G}_{abcd}\left(x_1, x_2, x_3, x_4\right) = \frac{1}{x_{12}^{\Delta_a+\Delta_b} x_{34}^{\Delta_c+\Delta_d}} \left(\frac{x_{24}}{x_{14}}\right)^{\Delta_{ab}} \left(\frac{x_{14}}{x_{13}}\right)^{\Delta_{cd}} G_{abcd}\left(u, v\right) \tag{5.2}$$

where we have made the following definitions: $\Delta_{ab} = \Delta_a - \Delta_b$ with $\Delta_a$ the corresponding scaling dimension of the operator indexed by $a$, also $u = \frac{x_{12}^2 x_{34}^2}{x_{13}^2 x_{24}^2}$, $v = \frac{x_{23}^2 x_{14}^2}{x_{13}^2 x_{24}^2}$ are the two conformaly invariant combinations of the points ($x_1$, $x_2$, $x_3$, $x_4$), lastly $x_{12} = x_1 - x_2$. Swapping the operator indexed by $a$ with the one indexed by $c$ we obtain the crossing equation

$$v^{\frac{\Delta_b+\Delta_c}{2}} G_{abcd} = u^{\frac{\Delta_a+\Delta_b}{2}} G_{cbad} \tag{5.3}$$

we emphasize that 5.3 is simply the statement that 5.1 can be calculated by taking the OPEs between the operators in the 4-pt function in two different, but equivalent, ways. Note that the OPE that results from swapping the operator indexed by $a$ with the one indexed by $b$ or $d$ either does not contain any additional information or does not converge (see e.g. [90] and the discussion in [87]). One can now use the conformal block decomposition

$$G_{abcd} = \sum_O \lambda_{abO}\lambda_{cdO} g^{\Delta_{ab},\Delta_{cd}}_{\Delta_O,l}(u,v) \tag{5.4}$$

to obtain

$$\sum_O \left(\lambda_{abO}\lambda_{cdO} v^{\frac{\Delta_b+\Delta_c}{2}} g^{\Delta_{ab},\Delta_{cd}}_{\Delta_O,l}(u,v) - \lambda_{cbO}\lambda_{adO} v^{\frac{\Delta_a+\Delta_b}{2}} g^{\Delta_{bc},\Delta_{ad}}_{\Delta_O,l}(v,u)\right) = 0 \tag{5.5}$$

where $g$ is the conformal block and the sum runs over all possible operators $O$ that are exchanged in each respective OPE. Lastly, by $\lambda$ we denote the OPE coefficients, which in the above equations should also be multiplied implicitly by the corresponding tensor structure. We will illustrate momentarily what we mean by this. The last step will be to define what is sometimes referred to as the convolved conformal block

$$F^{ab,cd}_{\pm,\Delta_O,l}(u,v) \equiv v^{\frac{\Delta_c+\Delta_b}{2}} g^{\Delta_{ab},\Delta_{cd}}_{\Delta_O,l}(u,v) \pm u^{\frac{\Delta_c+\Delta_b}{2}} g^{\Delta_{ab},\Delta_{cd}}_{\Delta_O,l}(v,u) \tag{5.6}$$

and with this we arrive at our desired final form

$$\sum_O \left(\lambda_{abO}\lambda_{cdO} F^{ab,cd}_{\mp,\Delta_O,l}(u,v) \pm \lambda_{cbO}\lambda_{adO} F^{cb,ad}_{\mp,\Delta_O,l}(u,v)\right) = 0 \tag{5.7}$$

**Explicit Example**

Let us consider the case where ($O_a$, $O_b$, $O_c$, $O_d$) = ($\phi_i$, $\phi_j$, $\phi_k$, $\phi_l$), i.e. we take four identical operators in the defining representation of the cubic group. In this case

$$\lambda_{abO_R}\lambda_{cdO_R} = \lambda_{\phi\phi O_R}\lambda_{\phi\phi O_R} P^R_{ijkl} \tag{5.8}$$

where $R$ denotes the irreducible representation under which the exchanged operator $O$ transforms in (remember $\phi_i \times \phi_j \sim \sum_R \lambda_{\phi\phi O_R} O^R_{ij}$). We have calculated the quantities $P^R$ for four identical scalars in Section 4.1

$$\begin{aligned} P^S_{ijkl} &= \frac{1}{3}\delta_{ij}\delta_{kl} \\ P^A_{ijkl} &= -\frac{1}{2}\delta_{ik}\delta_{jl} - \delta_{il}\delta_{jk} \\ P^X_{ijkl} &= \delta_{ijkl} - \frac{1}{3}\delta_{ij}\delta_{kl} \\ P^Y_{ijkl} &= \frac{1}{2}(\delta_{ik}\delta_{jl} + \delta_{il}\delta_{jk} - 2\delta_{ijkl}) \end{aligned} \tag{5.9}$$

We may now plug 5.9 back in to 5.7, what we find is that four independent combinations of tensors appear, multiplying different terms. These combinations are

$$\begin{aligned} T^1_{ijkl} &= \delta_{ik}\delta_{jl} \\ T^2_{ijkl} &= \delta_{ijkl} \\ T^3_{ijkl} &= \delta_{ij}\delta_{kl} + \delta_{il}\delta_{jk} \\ T^4_{ijkl} &= \delta_{ij}\delta_{kl} - \delta_{il}\delta_{jk} \end{aligned} \tag{5.10}$$

using these we recast 5.7 schematically as

$$T^1_{ijkl}F^1 + T^2_{ijkl}F^2 + T^3_{ijkl}F^3 + T^4_{ijkl}F^4 = 0 \tag{5.11}$$

where the $F$ symbol stands for sums of convolved conformal blocks. Setting each sum of convolved conformal blocks to zero independently we obtain

$$\begin{aligned}
\sum_{Y^+} \lambda^2_{O_Y} F^-_{\Delta,\ell} + \sum_{A^-} \lambda^2_{O_A} F^-_{\Delta,\ell} &= 0\,, \\
\tfrac{1}{3}\sum_{S^+} \lambda^2_{O_S} F^-_{\Delta,\ell} - \tfrac{2}{3}\sum_{X^+} \lambda^2_{O_X} F^-_{\Delta,\ell} + \sum_{Y^+} \lambda^2_{O_Y} F^-_{\Delta,\ell} - \sum_{A^-} \lambda^2_{O_A} F^-_{\Delta,\ell} &= 0\,, \\
\tfrac{1}{3}\sum_{S^+} \lambda^2_{O_S} F^+_{\Delta,\ell} - \tfrac{2}{3}\sum_{X^+} \lambda^2_{O_X} F^+_{\Delta,\ell} - \sum_{Y^+} \lambda^2_{O_Y} F^+_{\Delta,\ell} + \sum_{A^-} \lambda^2_{O_A} F^+_{\Delta,\ell} &= 0\,, \\
\tfrac{1}{3}\sum_{S^+} \lambda^2_{O_S} F^-_{\Delta,\ell} + \tfrac{4}{3}\sum_{X^+} \lambda^2_{O_X} F^-_{\Delta,\ell} &= 0\,,
\end{aligned} \tag{5.12}$$

where we have suppressed various indices in favor of simplicity of presentation and moved the $\pm$ subscripts to superscripts on the functions $F_{\Delta,\ell}$. These sum rules were first studied with the numerical bootstrap in [93] and [100]. An important comment is that since in the bootstrap algorithm we look for a functional which is positive (semi-definite) when acting on each individual term of the sum rule[1], we may rescale the OPE coefficients by arbitrary positive numbers without affecting our results. Also, we may freely add and subtract the lines in 5.12 without changing our results. To see this, note that we could have alternatively derived the sum rules by contracting 5.11 with various tensors in order to get rid of the indices. This would produce different sum rules, which would be linear combinations of those in 5.12.

## 5.2 Single Correlator Constraints

The first and simplest correlator equation to probe for self consistency is composed of four defining operators of the global symmetry $\phi_i$. This is

$$\langle \phi_i \phi_j \phi_k \phi_l \rangle = \langle \phi_k \phi_j \phi_i \phi_l \rangle \tag{5.13}$$

where it is implicitly assumed by our notation that we take the OPE between the first two and last two operators in each correlator. In the previous section we outlined explicitly how to derive the four resulting sum rules, one for each irrep in the $\phi \times \phi$ OPE, from the crossing equation 5.13. To get our first non-trivial constraints on OPE data from the crossing equation, we choose an operator in one of the irreps and change its lower bound from the unitarity bound to a value of our choice. If for the given value of our choice we can find a functional that is positive (semi-definite) on each term, then our choice of lower bound is excluded. Finding the highest value the lower bound may take, for a given $\Delta_\phi$, we can make so called exclusion plots. In other words, we assume $\Delta_R \geqslant \Delta_{min}$ and try to maximize $\Delta_{min}$. This in turn gives us the maximum value of $\Delta_R$. For the cubic theory, the single correlator system was first studied in [93] and [100]. The most interesting plot is the exclusion plot in the $X$ sector.

What makes Fig 5.1 interesting is the observation that around roughly $\Delta_\phi \sim 0.518$

[1] Each term corresponds to the contribution of different exchanged primary operator.

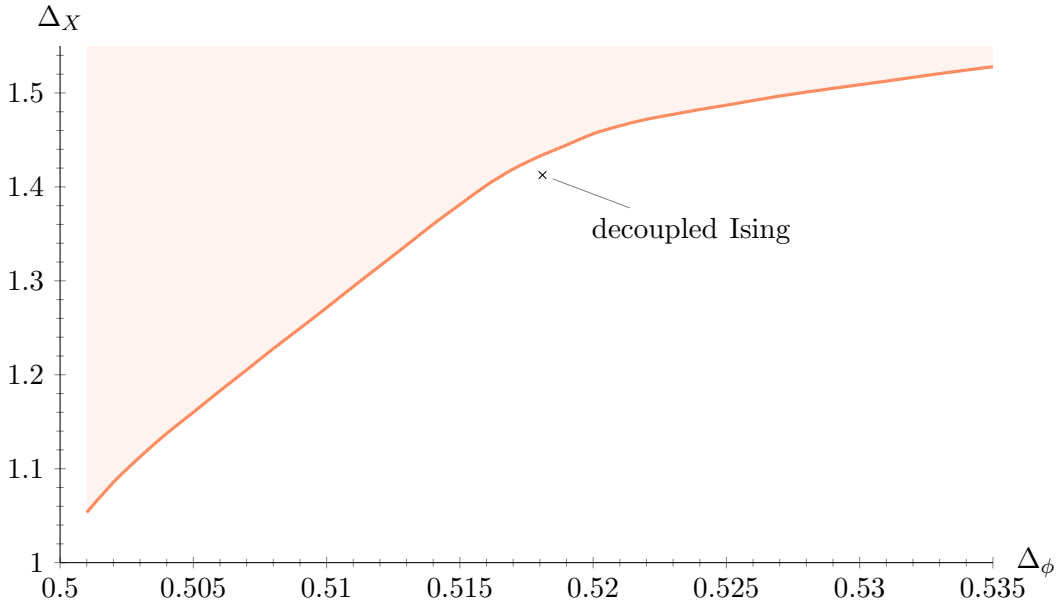


FIGURE 5.1: Exclusion plot for the lowest scaling dimension exchanged operator in the $X$ irrep of the $\phi \times \phi$ OPE. In red are the disallowed values for the scaling dimension $\Delta_X$ (as a function of $\Delta_\phi$), whereas below the line are the allowed ones. The dimension of the operator in the theory of three decoupled Ising models is also marked on the plot. This figure was produced with PyCFTBoot [9] using the parameters $k_{max} = 36$, $l_{max} = 26$, $m_{max} = 6$ and $n_{max} = 9$. Figure reproduced from [62] and [100].

there is change of slope[2]. These changes of slope have been observed to be in heavy correspondence with the positions of physically interesting CFTs in the literature. The prototypical examples are the Ising, $O(2)$, and $O(3)$ CFTs which have had their CFT data calculated to record precision following this observation. See [61], [22], and [21] respectively. The rest of the sectors do not present us with additional information as we will explain.

In addition to the change of slope observed above, which occurs for $\Delta_\phi$ close to the unitarity bound ($\Delta_\phi = 0.5$), there also exist additional changes of slope in the $X$ sector for larger values of $\Delta_\phi$. This is illustrated in Fig 5.2 for various values of $N$ in the hypercubic group $C_N = {Z_2}^N \rtimes S_N$, where we remind that $N = 3$ specifically is the cubic case. The observed change of slope becomes more pronounced as we increase $N$. This is qualitatively very similar to results that appeared in [93]. In [93] they study the group $Z_2 \times S_N$ which overlaps with the hypercubic group in the specific case of $Z_2 \times S_4 \sim {Z_2}^3 \rtimes S_3$. The changes of slope in that work appear in the same sector as in our work (i.e. the defining representation of $S_N$, which we remind $X_{ij}$ transforms in).

Lastly, a few comments are in hand about the $Y$, $A$ and $S$ sectors. Specifically, the $Y$ and $A$ sectors do not present any interesting features, see e.g. [100]. Whereas in the case of the $S$ sector, there are kinks, but they are saturated by the $O(N)$ CFTs. This happens for the following reason: the bootstrap cannot exclude the possibility that

[2] If this change of slope were sharper, we might also call it a "kink" as is standard in the literature.

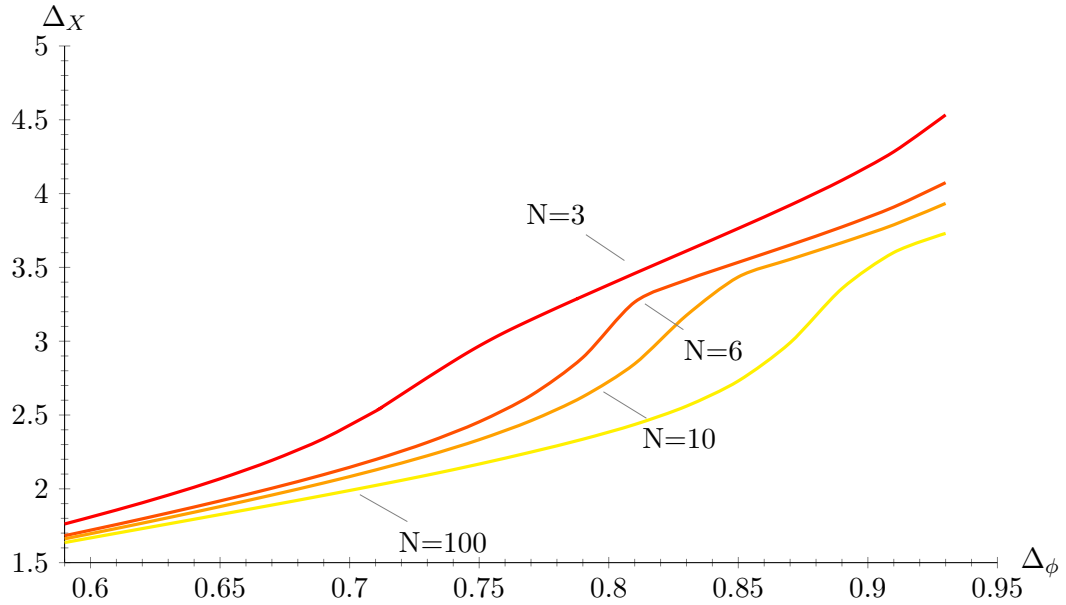


FIGURE 5.2: Exclusion plot for the lowest scaling dimension exchanged operator in the $X$ irrep of the $\phi \times \phi$ OPE. The number $N$ denotes which hypercubic ($C_N = Z_2^N \rtimes S_N$) model we are talking about. This figure was produced with PyCFTBoot [9] using the parameters $k_{max} = 36$, $l_{max} = 26$, $m_{max} = 6$ and $n_{max} = 9$.

$\Delta_X = \Delta_Y$. This choice of scaling dimensions is part of a perfectly normal solution to the crossing equation, namely the $O(3)$ solution. One can indeed check that plugging $\Delta_X = \Delta_Y$ into 5.12 the number of independent sum rules reduces from four to three, and they are equivalent to those in [60]. For a more general understanding of this phenomenon see [67] and [66]. Hence, since the bootstrap cannot exclude the enhancement of symmetry to $O(N)$, it doesn't. This leads to the saturation of the singlet sector hypercubic plots by the $O(N)$ CFTs. Hence, in the singlet sector any theory with cubic symmetry is "hidden" underneath the bound saturated by the $O(3)$ theory.

## 5.3 $\phi$ - X System of Correlators Constraints

The focus of this and the next section will be to investigate whether or not the change of slope, henceforth "kink" for brevity, in Fig 5.1 is due to the saturation of the bound by some CFT. One strong hint for the existence of a CFT near the kink would be if we can isolate it in a closed region (island) in parameter space by using additional assumptions. These additional assumptions in our case will be to place lower bounds on the dimensions of various operators above the unitarity bound. The sum rules resulting from the crossing equations $\langle\phi\phi XX\rangle = \langle X\phi\phi X\rangle$ and $\langle\phi X\phi X\rangle = \langle\phi X\phi X\rangle$ can be found in Appendix C. The sum rules from the full $\phi$ - $X$ system as they appeared in [62] are reported for completeness in Appendix F.

All plots in this subsection are produced using the $\phi$ - $X$ correlator system which consists of the following equations (and their resulting sum rules) $\langle\phi_i\phi_j\phi_k\phi_l\rangle = \langle\phi_k\phi_j\phi_i\phi_l\rangle$, $\langle\phi_i X_{jk}\phi_l X_{mn}\rangle = \langle\phi_l X_{jk}\phi_i X_{mn}\rangle$, $\langle\phi_i\phi_j X_{kl} X_{mn}\rangle = \langle X_{kl}\phi_i\phi_j X_{mn}\rangle$ and $\langle X_{ij} X_{kl} X_{mn} X_{op}\rangle = \langle X_{mn} X_{kl} X_{ij} X_{op}\rangle$. For all the plots of this subsection we use the same set of parameters in PyCFTBoot [9], namely $k_{max} = 32$, $l_{max} = 26$, $m_{max} = 5$ and $n_{max} = 7$. In

addition to the above, we take the dimension of the operator in the $X$ irrep with the lowest scaling dimension to saturate Fig 5.1. The reasoning behind this is to investigate the properties of whatever theory may or may not saturate the bound. The saturation of the $X$ bound is also a handy way to exclude the $O(3)$ model from our parameter space.

In Fig 5.3 we assume the $X$ operator with the second lowest scaling dimension satisfies $\Delta_{X'} \geqslant 3.0$ and the operator with the second lowest scaling dimension in the same representation as $\phi_i$ satisfies $\Delta_{\phi'} \geqslant 1.0$[3]. We observe a pronounced peak in the space of allowed values for the first scalar singlet. This peak in Fig 5.3 is located precisely at the position (with respect to $\Delta_\phi$) of the kink in the $X$ sector bound.

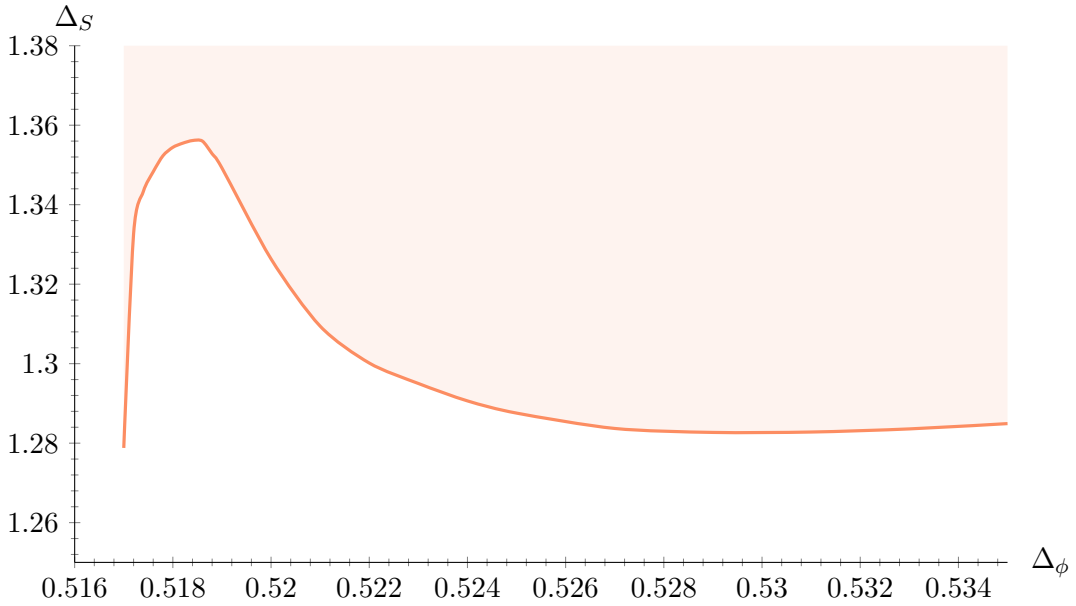


FIGURE 5.3: Exclusion plot for the lowest scaling dimension exchanged operator in the $S$ irrep. In red are the disallowed values for the scaling dimension $\Delta_S$, whereas below the line are the allowed ones. In this plot we impose $\Delta_{X'} \geqslant 3.0$, $\Delta_{\phi'} \geqslant 1.0$ and that $\Delta_X$ saturates Fig 5.1. This figure was produced with PyCFTBoot [9] using the parameters $k_{max} = 32$, $l_{max} = 26$, $m_{max} = 5$ and $n_{max} = 7$. Figure reproduced from [62].

A useful comment at this point is that our assumptions can, in some sense, be motivated using the extremal functional method [37] [38] (see also [98], specifically the discussion in Appendix A). This method gives an approximation to the spectrum of a given CFT which can then be used as input in the numerical bootstrap. The drawback of the method is that it does not provide rigorous bounds, but only estimates of solutions to a crossing equation.

It is now interesting to see what happens to Fig 5.3 if we supplement it with further assumptions. In Fig 5.4 we assume, in addition to $\Delta_{X'} \geqslant 3.0$ and $\Delta_{\phi'} \geqslant 1.0$, that $\Delta_{S'} \geqslant 3.0$. We now obtain a peninsula of allowed parameter space located in a sea of disallowed parameter space.

[3] We use primes to denote the next to leading operator, with respect to scaling dimension, in each irrep.

We would like to reduce the peninsula in Fig 5.4 to an isolated island of allowed parameter space. This would then lead to determinations for the scaling dimensions of the operators that live in this region of parameter space, which we plan to associate with a CFT. Doing this we also effectively calculate the experimentally measurable critical exponents of the associated theory. The reduction of the peninsula to an island is indeed achieved assuming $\Delta_{S'} \geqslant 3.7$. In Fig 5.5 we demonstrate the resulting island for $\Delta_{S'} \geqslant 3.7$, $\Delta_{S'} \geqslant 3.8$ and $\Delta_{S'} \geqslant 3.9$ respectively. If we further raise the lower bound on $\Delta_{S'}$ the island abruptly disappears. This indicates that there should be an operator close to the aforementioned values, which when excluded, excludes the theory. This picture is corroborated by the extremal functional method, which also indicated the existence of an operator $S'$ with a scaling dimension near $\Delta_{S'} \sim 3.7 - 3.9$. This means that the conjectured CFT that lives in the island is stable, in the renormalization group sense of the word. This has experimental significance, since it indicates that an experimentalist would need to tune only one parameter to reach the fixed point/phase transition. This parameter could e.g. be the temperature (which is proportional to the mass in field theory $m^2 \sim T - T_C$). In Fig 5.6 we show for $\Delta_{S'} \geqslant 3.8$, how the island detaches from the peninsula. What is interesting to note, is that this happens in a qualitatively very similar way as in the $3D$ Ising model [59]. We will give the name "Platonic" to the CFT conjectured to live in Fig 5.5.

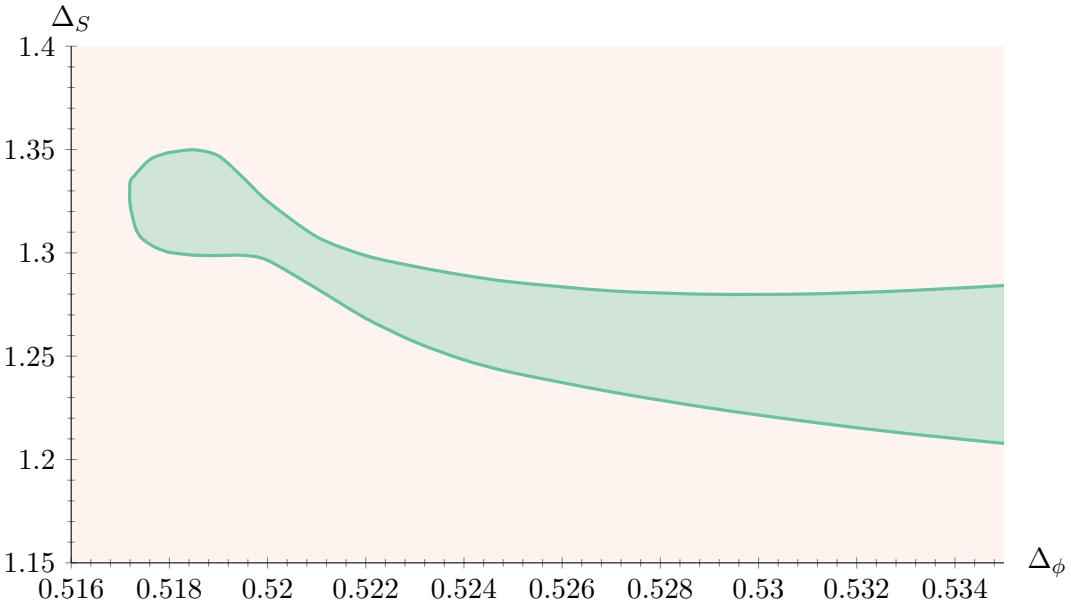


FIGURE 5.4: Allowed peninsula (in green) for the lowest scaling dimension exchanged operator in the $S$ irrep. In red are the disallowed values for the scaling dimension $\Delta_S$. In this plot we impose $\Delta_{X'} \geqslant 3.0$, $\Delta_{\phi'} \geqslant 1.0$, $\Delta_{S'} \geqslant 3.0$ and that $\Delta_X$ saturates Fig 5.1. This figure was produced with PyCFTBoot [9] using the parameters $k_{max} = 32$, $l_{max} = 26$, $m_{max} = 5$ and $n_{max} = 7$. Figure reproduced from [62].

From Fig 5.5 we obtain a determination for the scaling dimensions and the corresponding critical exponents in the conjectured CFT. Note that from our discussion

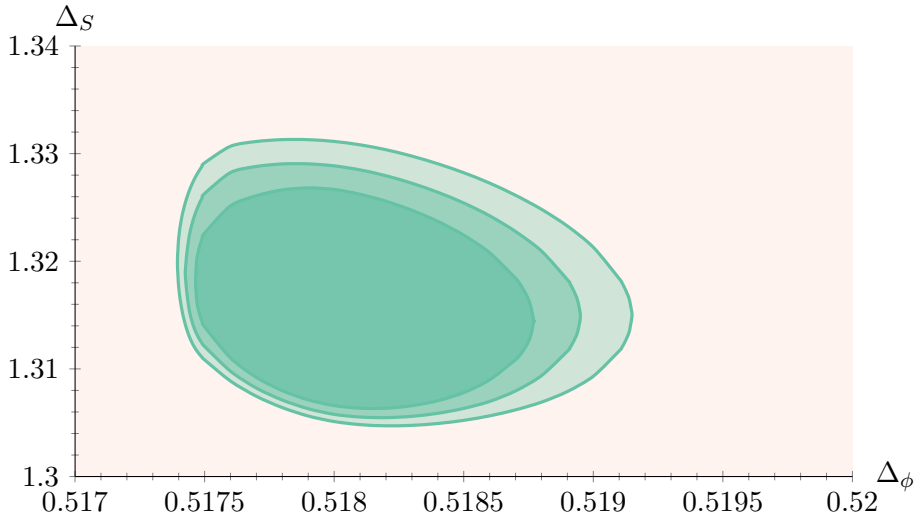


FIGURE 5.5: Allowed islands (in green) for the lowest scaling dimension exchanged operator in the $S$ irrep. In red are the disallowed values for the scaling dimension $\Delta_S$. In this plot we impose $\Delta_{X'} \geqslant 3.0$, $\Delta_{\phi'} \geqslant 1.0$ and that $\Delta_X$ saturates Fig 5.1. The islands from biggest to smallest are obtained imposing $\Delta_{S'} \geqslant 3.7$, 3.8 and 3.9 respectively. This figure was produced with PyCFTBoot [9] using the parameters $k_{max} = 32$, $l_{max} = 26$, $m_{max} = 5$ and $n_{max} = 7$. Figure reproduced from [62].

in Chapter 3, that the island in Fig 5.5 is not due to the cubic theory of the $\varepsilon$ expansion. As mentioned there, the cubic theory of the $\varepsilon$ expansion has scaling dimensions very close to those of the $O(3)$ model, which for example has $\Delta_S = 1.59488(81)$ [21]. The operator dimensions and corresponding critical exponents we have are

$$\begin{aligned} \Delta_\phi &= 0.518 \pm 0.001 \\ \Delta_S &= 1.317 \pm 0.012 \end{aligned} \tag{5.14}$$

and

$$\begin{aligned} \beta &= 0.308 \pm 0.002 \\ \nu &= 0.594 \pm 0.004 \\ \gamma &= 1.167 \pm 0.008 \\ \delta &= 4.792 \pm 0.011 \end{aligned} \tag{5.15}$$

where the error bars in the scaling dimensions correspond to the size of the island, and the critical exponents are given by the relations $\beta = \Delta_\phi/(d - \Delta_S)$, $\nu = 1/(d - \Delta_S)$, $\gamma = (d - 2\Delta_\phi)/(d - \Delta_S)$ and $\delta = (d - \Delta_\phi)/\Delta_\phi$ (remember that $d = 3$ in our case). The first three critical exponents correspond to the order parameter, the correlation length, and the susceptibility respectively[4]. Experimental determinations for critical exponents in systems with cubic symmetry, but not of the type of

[4]The fourth exponent $\delta$ describes the dependence of the order parameter on the source field, see e.g. [18]. Note that this exponent is defined directly at criticality.

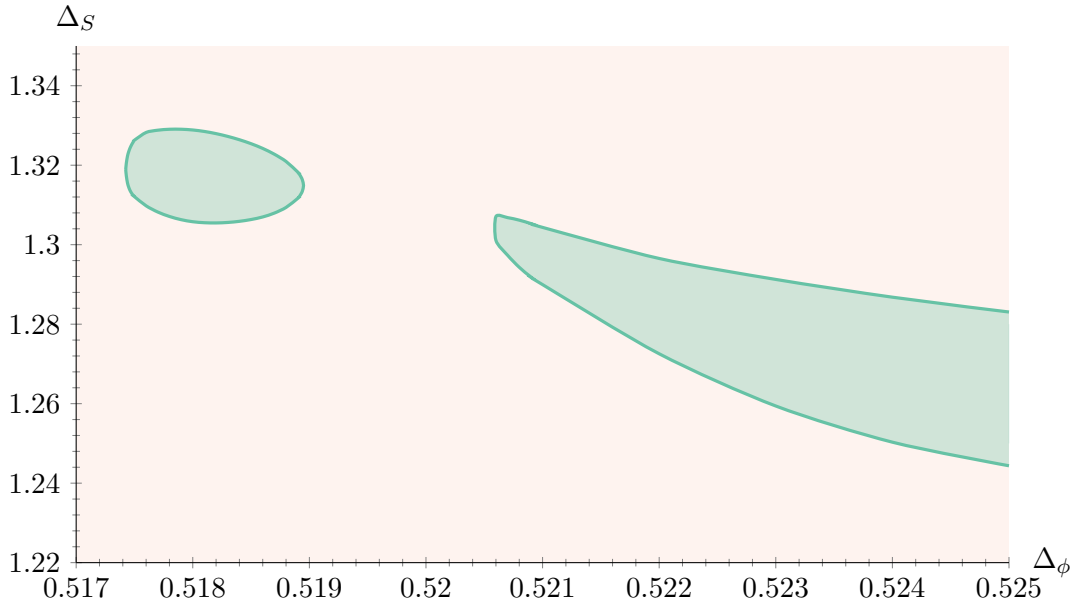


FIGURE 5.6: Allowed island and remnant of the peninsula (in green) for the lowest scaling dimension exchanged operator in the $S$ irrep. In red are the disallowed values for the scaling dimension $\Delta_S$. In this plot we impose $\Delta_{X'} \geqslant 3.0$, $\Delta_{\phi'} \geqslant 1.0$, $\Delta_{S'} \geqslant 3.8$ and that $\Delta_X$ saturates Fig 5.1. This figure was produced with PyCFTBoot [9] using the parameters $k_{max} = 32$, $l_{max} = 26$, $m_{max} = 5$ and $n_{max} = 7$. Figure reproduced from [62].

the $\varepsilon$ expansion, give [74] [105]

$$\begin{aligned} \beta &= 0.33 \pm 0.02 \\ \nu &= 0.63 \pm 0.07 \end{aligned} \tag{5.16}$$

or more recently (for systems on an orthorhombic lattice) [11]

$$\begin{aligned} \beta &= 0.306 \pm 0.002 \\ \gamma &= 1.185 \pm 0.013 \\ \delta &= 4.857 \pm 0.030 \end{aligned} \tag{5.17}$$

and

$$\begin{aligned} \beta &= 0.312 \pm 0.011 \\ \gamma &= 1.167 \pm 0.008 \\ \delta &= 4.792 \pm 0.011 \end{aligned} \tag{5.18}$$

The papers [74] and [105] study structural phase transitions $SrTiO_3$. The symmetry of the material above the critical temperature is cubic. The order parameter in this case is the expectation value of the position of some particle on the lattice. Whereas in [11] they study LYPMO and LEPMO[5] which have an orthorhombic lattice. To make a statement about the symmetry of the field theory that describes the (LYPMO and LEPMO) transition in the continuum limit, we would ideally like to know the

[5] Or more explicitly $La_{0.47}Y_{0.2}Pb_{0.33}MnO_3$ and $La_{0.47}Eu_{0.2}Pb_{0.33}MnO_3$.

initial microscopic Hamiltonian. The interested reader may look at Appendix E for more information on how symmetries in the continuum limit arise. With the information the present author is currently aware of, we do not know the symmetry of the field theory describing these experiments. Nevertheless, our results match the experimental measurements better than any other candidate field theory (Ising, $O(2)$, $O(3)$). In these experiments the phase transition is magnetic (paramagnetic to ferromagnetic). Hence the order parameter in this case would be the expectation value of some continuum spin field.

An important note is that in [3] it was proposed that the exponents of [74] [105] where actually due to the Ising universality class. This was explained to happen due to strains of the crystal which introduced a preferred direction to the system. This effectively reduces the three component order parameter to a two or one component order parameter depending on the sign of the applied stresses. This in turn implies either Ising or $O(2)$ critical exponents.

## 5.4 $\phi$ - S System of Correlators Constraints

Having discovered an island in parameter space in the previous section, we would like to further probe its properties. Firstly, we would like to relax the assumption that the first $X$ operator saturates Fig 5.1. Furthermore, we would like to see whether the model captured by the bootstrap is a short or long range model. This is important to check since long range models can also appear in the bootstrap, see e.g. [8] for a study of the long range Ising model. Lastly, the approach of this section should make it easier to systematically improve our determinations of critical exponents in the future, which should hopefully in turn motivate further experimental studies.

The system of crossing equations we will study is $\langle\phi_i\phi_j\phi_k\phi_l\rangle = \langle\phi_k\phi_j\phi_i\phi_l\rangle$, $\langle\phi_i S\phi_j S\rangle = \langle\phi_j S\phi_i S\rangle$, $\langle\phi_i\phi_j SS\rangle = \langle S\phi_i\phi_j S\rangle$ and $\langle SSSS\rangle = \langle SSSS\rangle$. These can be found in Appendix D. We will also make use of the single correlator equation $\langle\phi_i\phi_j\phi_k\phi_l\rangle = \langle\phi_k\phi_j\phi_i\phi_l\rangle$ for some specific plots. For all plots in this section, except Fig 5.7, we use the PyCFTBoot [9] parameters $k_{max} = 36$, $l_{max} = 26$, $m_{max} = 5$ and $n_{max} = 7$. Whereas, for Fig 5.7 we use $k_{max} = 36$, $l_{max} = 26$, $m_{max} = 6$ and $n_{max} = 9$

First, we demonstrate Fig 5.7 which is produced using the single correlator system. For this plot we make the assumptions that $\Delta_X$ saturates the bound in Fig 5.1, $\Delta_{X'} \geqslant 2.8$, $\Delta_{T_{mn}} = 3$, $\Delta_{T'_{mn}} \geqslant 4.0$ and $\Delta_{S'} \geqslant 3.0$. Where $T'_{mn}$ is the operator with the next highest scaling dimension in the representation of the stress tensor, i.e. the second spin-2 singlet. Also, in Fig 5.8 we overlap Fig 5.7 with Fig 5.4 and Fig 5.6 of the previous section to demonstrate their compatibility.

Next, we move to the $\phi$ - $S$ mixed correlator system. In all the following plots: Fig 5.9, Fig 5.10, Fig 5.11 and Fig 5.12 we use the assumptions $\Delta_X \geqslant 1.4126$[6], $\Delta_{T_{\mu\nu}} = 3.0$, $\Delta_{T'_{\mu\nu}} \geqslant 4.0$, $\Delta_{Y'} \geqslant 3.0$, $\Delta_{\phi'} \geqslant 1.5$ and scan over the scaling dimensions $\Delta_\phi$, $\Delta_S$ and $\Delta_Y$. What we have essentially done, is trade in the assumption that we saturate Fig 5.1 with the need to perform a scan over $\Delta_Y$. In other words, we have turned a $2D$ scan of parameter space $(\Delta_\phi, \Delta_S)$ into a $3D$ one $(\Delta_\phi, \Delta_S, \Delta_Y)$. The upshot of this approach

[6] This is simply the assumption $\Delta_X \geqslant \Delta_{X_{Ising}}$ , which is imposed since $\Delta_X \to \Delta_{X_{Ising}}$ (from above) only in the limit $N \to \infty$. See Fig 2 in [100].

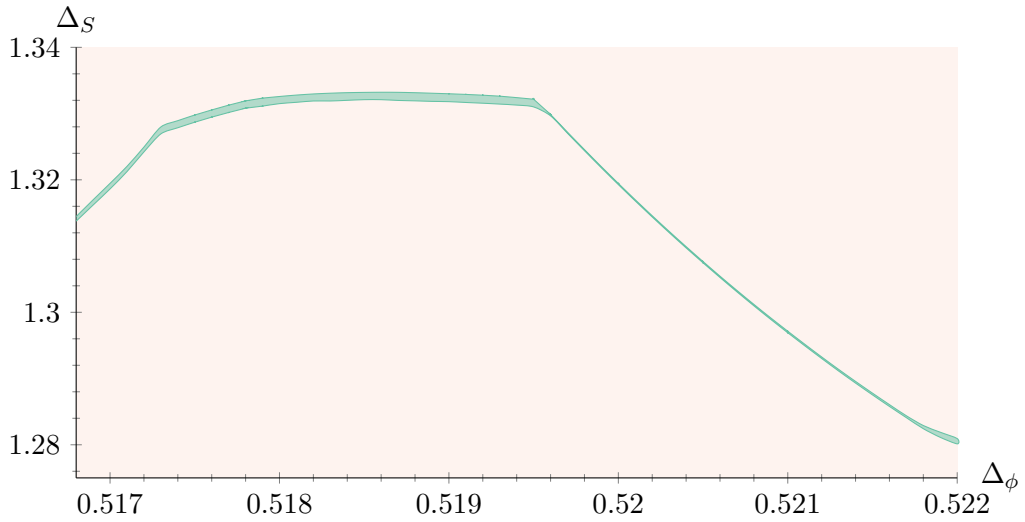


FIGURE 5.7: Allowed strip (in green) for the lowest scaling dimension exchanged operator in the $S$ irrep. In red are the disallowed values for the scaling dimension $\Delta_S$. In this plot we impose $\Delta_{X'} \geqslant 2.8$, $\Delta_{S'} \geqslant 3.0$ and that $\Delta_X$ saturates Fig 5.1. We note that the allowed region truncates on the left, whereas on the right there continues to be an allowed region. Removing the assumption $\Delta_{X'} \geqslant 2.8$ the plot stops truncating on the left. In Fig 5.8 it will become apparent that the two kinks in this plot correspond to the overlap with the peninsula in the mixed $\phi$-$X$ system of the previous section. This figure was produced with PyCFTBoot [9] using the parameters $k_{max} = 36$, $l_{max} = 26$, $m_{max} = 6$ and $n_{max} = 9$. Figure reproduced from [63].

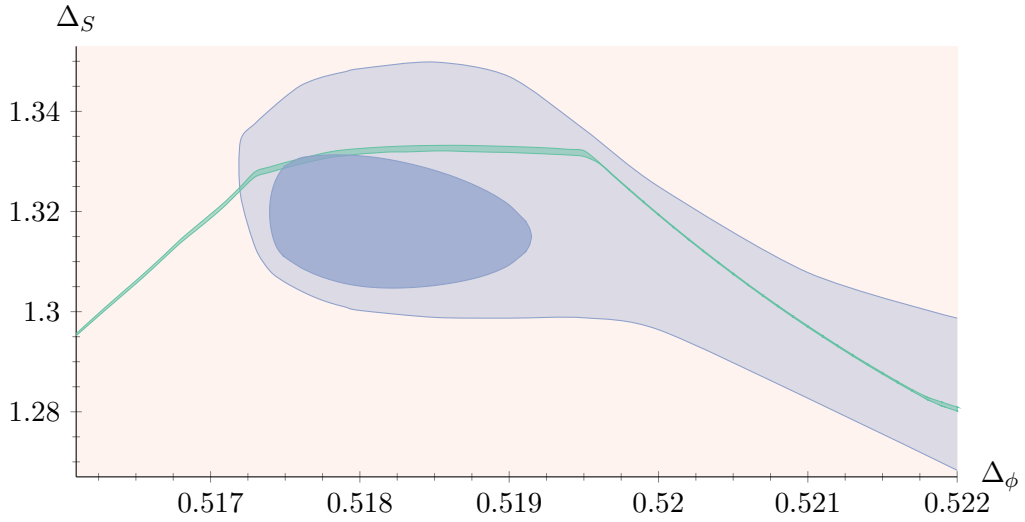


FIGURE 5.8: Allowed strip (in green) for the lowest scaling dimension exchanged operator in the $S$ irrep. In red are the disallowed values for the scaling dimension $\Delta_S$. In this plot we impose $\Delta_{X'} \geqslant 2.8$, $\Delta_{S'} \geqslant 3.0$ and that $\Delta_X$ saturates Fig 5.1. The assumptions for the peninsula and the island can be found in Fig 5.4 and Fig 5.6 respectively. Figure reproduced from [63].

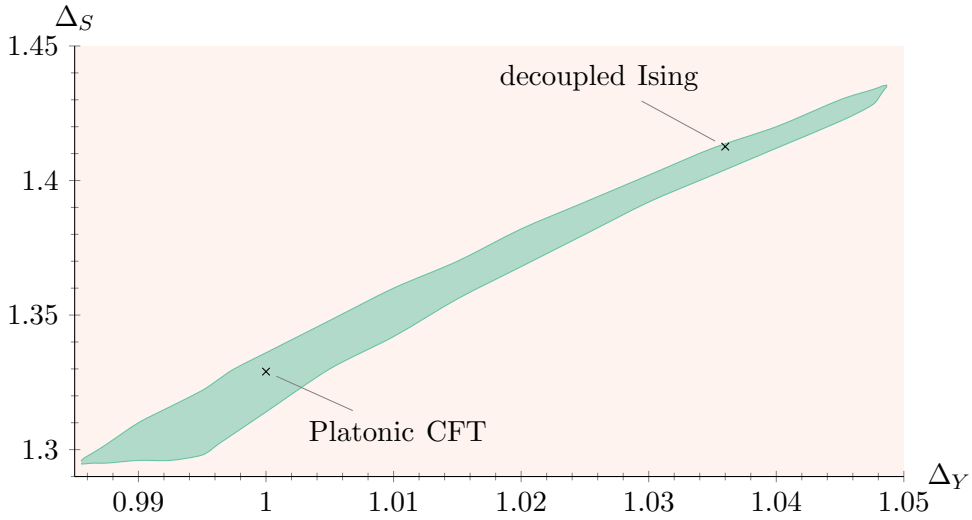


FIGURE 5.9: Projection onto the $(\Delta_S, \Delta_Y)$ plane of the isolated allowed region in $(\Delta_\phi, \Delta_S, \Delta_y)$ space (in green). In red are the disallowed values for the scaling dimension $\Delta_S$ as a function of $\Delta_Y$. In this plot we impose $\Delta_{X'} \geqslant 1.4126$, $\Delta_{S'} \geqslant 3.0$, $\Delta_{T_{\mu\nu}} = 3.7$, $\Delta_{T'_{\mu\nu}} \geqslant 4.0$ and $\Delta_{Y'} \geqslant 3.0$. We denote with crosses the positions of the $3D$ Ising CFT and the Platonic theory conjectured in the previous section. The decoupled Ising model appears in our plots since three decoupled Ising models have cubic global symmetry. To see this plug $g_2 = 0$ in 3.1. The position of the Platonic theory is approximate and corresponds to the island of the previous section. This figure was produced with PyCFTBoot [9] using the parameters $k_{max} = 36$, $l_{max} = 26$, $m_{max} = 5$ and $n_{max} = 7$. Figure reproduced from [63].

is that the problem is now in a form that can be systematically probed with stronger numerics in future work.

Fig 5.9 depicts the projection of the $3D$ scan $(\Delta_\phi, \Delta_S, \Delta_Y)$ onto the $(\Delta_S, \Delta_Y)$ plane. Whereas Fig 5.10 and Fig 5.11 depict cross sections of the allowed region at $\Delta_Y = 0.98575$ and $\Delta_Y = 1.025$ respectively. Lastly, we overlap the plot for fixed $\Delta_Y = 1.0$[7] with the island from Fig 5.5 with $\Delta_{S'} > 3.7$ from the previous section.

[7] Which is the value the extremal functional approximately gives for the theory saturating Fig 5.1.

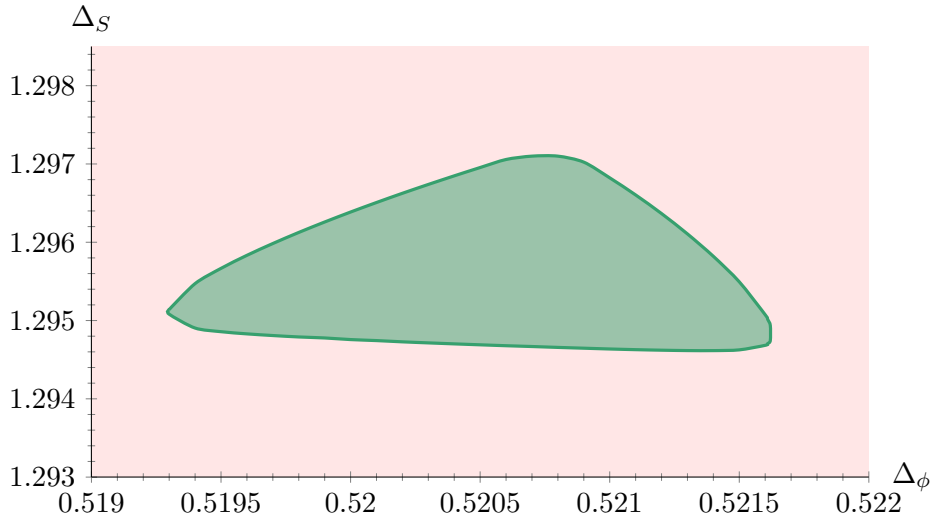


FIGURE 5.10: Projection onto the $(\Delta_S, \Delta_\phi)$ plane of the isolated allowed region in $(\Delta_\phi, \Delta_S, \Delta_y)$ space for $\Delta_Y = 0.98575$ (in green). In red are the disallowed values for the scaling dimension $\Delta_S$ as a function of $\Delta_\phi$. In this plot we impose $\Delta_{X'} \geqslant 1.4126$, $\Delta_{S'} \geqslant 3.0$, $\Delta_{T_{\mu\nu}} = 3.7$, $\Delta_{T'_{\mu\nu}} \geqslant 4.0$ and $\Delta_{Y'} \geqslant 3.0$. This figure was produced with PyCFTBoot [9] using the parameters $k_{max} = 36$, $l_{max} = 26$, $m_{max} = 5$ and $n_{max} = 7$. Figure reproduced from [63].

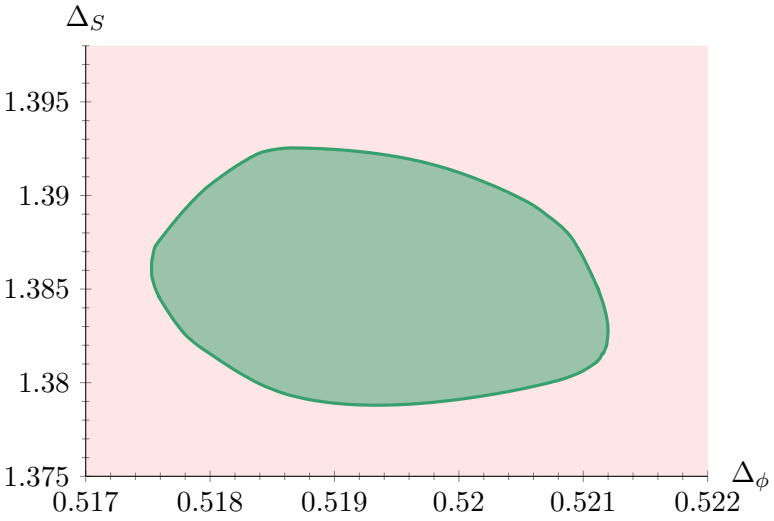


FIGURE 5.11: Projection onto the $(\Delta_S, \Delta_\phi)$ plane of the isolated allowed region in $(\Delta_\phi, \Delta_S, \Delta_y)$ space for $\Delta_Y = 1.025$ (in green). In red are the disallowed values for the scaling dimension $\Delta_S$ as a function of $\Delta_\phi$. In this plot we impose $\Delta_{X'} \geqslant 1.4126$, $\Delta_{S'} \geqslant 3.0$, $\Delta_{T_{\mu\nu}} = 3.7$, $\Delta_{T'_{\mu\nu}} \geqslant 4.0$ and $\Delta_{Y'} \geqslant 3.0$. This figure was produced with PyCFTBoot [9] using the parameters $k_{max} = 36$, $l_{max} = 26$, $m_{max} = 5$ and $n_{max} = 7$. Figure reproduced from [63].

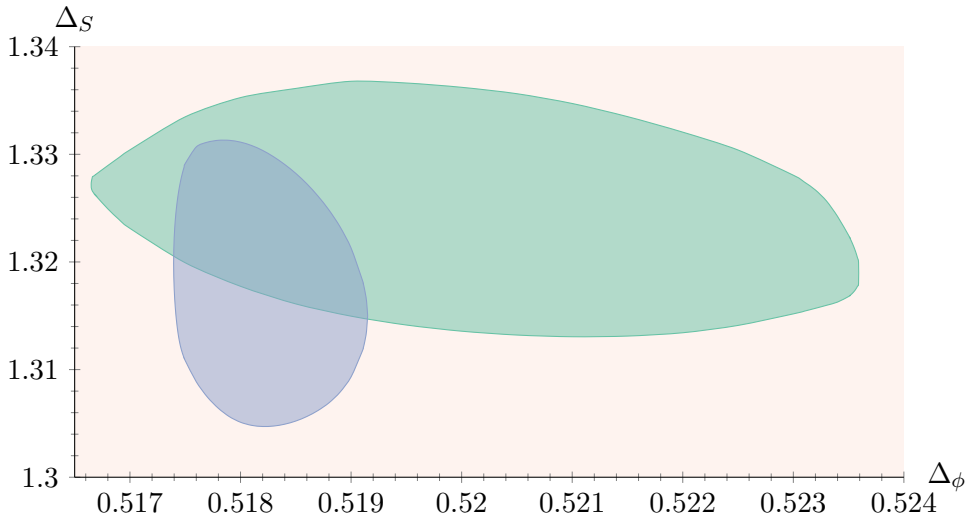


FIGURE 5.12: Projection onto the $(\Delta_S, \Delta_\phi)$ plane of the isolated allowed region in $(\Delta_\phi, \Delta_S, \Delta_y)$ space for $\Delta_Y = 1.0$ (in green). In blue we plot the the island with $\Delta_{S'} \geqslant 3.7$ from Fig 5.5 in the previous section. In red are the disallowed values for the scaling dimension $\Delta_S$ as a function of $\Delta_\phi$. In this plot we impose $\Delta_{X'} \geqslant 1.4126$, $\Delta_{S'} \geqslant 3.0$, $\Delta_{T_{\mu\nu}} = 3.7$, $\Delta_{T'_{\mu\nu}} \geqslant 4.0$ and $\Delta_{Y'} \geqslant 3.0$. This figure was produced with PyCFTBoot [9] using the parameters $k_{max} = 36$, $l_{max} = 26$, $m_{max} = 5$ and $n_{max} = 7$. Figure reproduced from [63].

# Chapter 6

# Scalar Field Theories with $O(m) \times O(n)/Z_2$ global symmetry

In this chapter we will consider scalar field theories with $O(m) \times O(n)/Z_2$ global symmetry. We have modded out a $Z_2$[1] since we will be interested in a field $\phi_{ar}$ where the indices $a$ and $r$ transform in $O(m)$ and $O(n)$ respectively. Thus, an action of the $Z_2$ due to $O(m)$ on $\phi_{ar}$ is indistinguishable from an action of the $Z_2$ due to $O(n)$. Note that if we had a theory with two separate scalar fields, one transforming in $O(m)$ and one transforming in $O(n)$ the situation would be different. In that case the symmetry would indeed be $O(m) \times O(n)$. For the rest of the thesis we will forget about this issue and refer to $O(m) \times O(n)/Z_2$ as $O(m) \times O(n)$ interchangeably.

There is plentiful motivation for studying theories with $O(m) \times O(n)$ global symmetry, both purely theoretical, as well as phenomenological. The purely theoretical motivation has to do with the nature of fixed points that arise, after resummations, in beta functions. These remain a controversial topic to the present day. We will elaborate further on this issue later on in the present chapter. The phenomenological motivation concerns physical systems undergoing phase transitions in with $O(m) \times O(n)$ global symmetry. This symmetry can be emergent. See for example Appendix E where we give two explicit examples of this, one for helimagnets and one for stacked triangular antiferromagnets. For both these examples the microscopic (global) symmetry of the system is $O(n)$. In the case of helimagnets the symmetry emerges due to the competition between nearest neighbour and next-nearest neighbour interactions in one of the directions (e.g. in the "x" direction). Whereas, in stacked triangular antiferromagnets the symmetry emerges due to the geometry of the lattice in combination with the antiferromagnetic nature of the interaction.

In the next two sections we will briefly review the fixed points one expects to see when using various techniques.

## 6.1 Fixed Points in $d = 4 - \varepsilon$ dimensions.

One can use two equivalent Hamiltonians to study $O(m) \times O(n)$ theories in $4 - \varepsilon$ dimensions

$$\mathcal{H} = \frac{1}{2}\partial_\mu \phi_{ar} \partial^\mu \phi^{ar} + \frac{\lambda}{8}(\phi_{ar}\phi_{ar})^2 + \frac{g}{24}\phi_{ar}\phi_{br}\phi_{as}\phi_{bs} \tag{6.1}$$

where summation is implicit above, and

[1] Which acts as $\phi_{ar} \to -\phi_{ar}$.

$$\mathcal{H} = \frac{1}{2}\sum_a \partial_\mu \vec{\phi}_a \cdot \partial^\mu \vec{\phi}^a + \frac{u}{24}\left(\sum_a \vec{\phi}_a{}^2\right)^2 + \frac{v}{24}\sum_{a,b}\left(\left(\vec{\phi}_a \cdot \vec{\phi}_b\right)^2 - \vec{\phi}_a{}^2\vec{\phi}_b{}^2\right) \tag{6.2}$$

these equations are related by coupling constant redefinition. We take "$a, b$" to be $O(m)$ indices, whereas "$r, s$" are $O(n)$ indices. Hence, the dot product in 6.2 refers to a product under $O(n)$. Equation 6.2 will be rather useful since it is directly related to the naming convention of fixed points in $O(m) \times O(n)$ theories. When the coupling $v$ is positive the fixed point is called either "Chiral" or "Antichiral". Whereas, when the coupling $v$ is negative it is called "Sinusoidal" or "Antisinusoidal" (the names "Collinear" and "Anti-Collinear" also appear in the literature). The names stem from the ordering of the physical spins in the $n$ dimensional space which the "$r, s$" indices live in[2]. The ordering of the physical spins can be worked out in mean field theory[3]. If $v > 0$, and e.g. $m = 2$, we find $\vec{\phi}_1 \cdot \vec{\phi}_2 = 0$, whereas if $v < 0$ then $\vec{\phi}_1$ is collinear/anti-collinear to $\vec{\phi}_2$. See paragraph 2.3 in [56] for further details.

Depending on the values of $m$ and $n$ we take, the type of fixed points we get are in general different. If we take $m$ fixed and vary $n$, we have four regimes of fixed points:

$$\begin{aligned} n > n_1(m) &: Regime_1 \\ n_1(m) > n > n_2(m) &: Regime_2 \\ n_2(m) > n > n_3(m) &: Regime_3 \\ n_3(m) > n &: Regime_4 \end{aligned} \tag{6.3}$$

where from [58] we have (for $m = 2$)

$$\begin{aligned} n_1(2) &= 5.96(19) \\ n_2(2) &= 1.970(3) \\ n_3(2) &= 1.462(13) \end{aligned} \tag{6.4}$$

The fixed points in each regime are as follows:

$Regime_1 : Gaussian, O(mn), Chiral, Antichiral$
Stable : $Chiral$

$Regime_2 : Gaussian, O(mn)$
Stable : $Non$

$Regime_3 : Gaussian, O(mn), Sinusoidal, Anti-Sinusoidal$
Stable: $Sinusoidal$

$Regime_4 : Gaussian, O(mn), Chiral, Sinusoidal$
Stable : $O(mn)$

A list of references for relevant $\varepsilon$ expansion studies is [80] [86] [54] [53] [56] [84]

[2] Whereas the indices $a$ and $b$ are emergent, in the sense that they do not appear in the original microscopic Hamiltonian.

[3] I.e. we just minimize the potential in the ordered phase.

[79] [95] [47] [58]. For a study in higher dimensions see [99]. See also [12] for the generalization to the tri-fundamental models.

## 6.2 Fixed Points in the Large $n$ limit

The Hamiltonians of the previous section can also be studied in the Large $n$ limit. In this case we expect the fixed points to correspond to $Regime_1$ of the previous section. One introduces two Hubbard-Stratonovich auxiliary fields $S$ and $W_{ab}$, where the first is a singlet of $O(m)$ and the second transforms in the traceless symmetric representation, and both are singlets of $O(n)$. Thus, 6.2 becomes

$$\mathcal{H} = \frac{1}{2}\sum_a \partial_\mu \vec{\phi}_a \cdot \partial^\mu \vec{\phi}^a + \frac{1}{2}\sum_a S\vec{\phi}_a \cdot \vec{\phi}_a + \frac{1}{2}\sum_{a,b} W_{ab}\vec{\phi}_a \cdot \vec{\phi}_b - \frac{3S^2}{2w} - \frac{3}{2v}\sum_{a,b} W_{ab}W_{ab} \quad (6.5)$$

where $w = u + (1 - 1/m)v$. Plugging in the equations of motion for $S$ and $W_{ab}$ one recovers 6.2. In this approach one finds three non-Gaussian fixed points: chiral, anti-chiral and O(mn). The chiral fixed point is the one that corresponds to both $S$ and $W_{ab}$ being non zero. If $W_{ab}$ is zero and $S$ is not, we are at the $O(mn)$ fixed point. Whereas if $S$ is zero and $W_{ab}$ is not we are in the anti-chiral fixed point, see [44] and [43]. The stable fixed point is found to be the chiral one. This is in agreement with the structure of $Regime_1$ in the $\varepsilon$ expansion fixed points.

A list of references for relevant Large-$n$ expansion studies is [54] [81] [43] [44] [47].

## 6.3 Fixed Points in Resummations

The most common way for finding fixed points in $d = 3$ is to consider the theory in $d = 4 - \varepsilon$ dimensions, and then solve for the couplings as a power series in $\varepsilon$ at the fixed point. Critical exponents are then expressed as a power series in $\varepsilon$, which may be resummed in order to obtain an approximation of the underlying non-perturbative function that gave us this power series. Lastly, after resummations one may plug in $\varepsilon = 1$ and find rather reliable[4] results for the critical exponents, assuming the initial perturbative expansion has been carried out to high enough order.

In a series of papers it was shown that in the $O(m) \times O(n)$ models if one performs a perturbative expansion directly in $3D$, then resums the series before looking for fixed points, starting at some loop order and above one finds new fixed points not visible in the ordinary $\varepsilon$ expansion [82] [25] [17]. Note that Monte Carlo [75] does seem to see these fixed points as well. These fixed points have gathered a considerable amount of criticism in the literature and have been argued to be spurious by various authors. For example they have drawn criticism in [102] [103] [27] [28] [30] [26] [29]. Some of the criticisms in [29] include: a) These fixed points were found to not have an upper critical dimension of $d = 4$, and they converged badly with loop order b) The fixed points could not be found in the Functional Renormalization Group (to the approximation order considered) c) The authors, using the same techniques, found a new cubic fixed point they claimed is an artefact given that no new cubic fixed point beyond the standard one had been previously reported (see e.g. their discussion between the end of page 9 and the start of page 10). The last point is rather interesting

[4] For some theories.

since as we demonstrated in previous chapters there does seem to be evidence for a cubic fixed point in $3D$ beyond the standard one of the $\epsilon$-expansion[5]. Unfortunately, experiments have not been able to shed light on these issues. For discussions about experiments see e.g. [55] and [84]. Note that the theoretical interpretation is made even more difficult since one may claim that something is not a continuous phase transition but a very weakly first order transition and vice versa. Also, a fixed point of interest may perfectly well exist but not be in the basin of attraction of the specific RG flow. Another complication is that these new fixed points are predicted to have spiral RG flows, see e.g. [75], thus approaching them may not be an easy task experimentally. These spiral RG flows are due to the complex valued scaling dimensions[6] of certain scalar singlets . We stress that the couplings that appear in the Hamiltonian are real at the fixed point, it should thus be experimentally accessible if one excludes the aforementioned issues. Curiously, there is a supersymmetric model with $O(m) \times O(n)$ symmetry that seems to have a fixed point with real couplings and complex stability matrix eigenvalues, see e.g. [52].

[5] We cannot comment on what, if any, relation these two fixed points may have.

[6] Which are related to the eigenvalues of the stability matrix, i.e. the derivative matrix of the $\phi^4$ coupling beta functions.

# Chapter 7

# Tensor Structures in $O(m) \times O(n)/Z_2$ Theories

The global symmetry tensor structures of 4-pt functions of scalars $\phi_{ar}$ that transform as vectors of both $O(m)$ ("$a$" index) and $O(n)$ ("$r$" index), are simply tensor products of tensor structures of $O(m)$ with tensor structures of $O(n)$, which are already known. The correlator of interest will be

$$\langle \phi_{ar} \phi_{bs} \phi_{ct} \phi_{du} \rangle \tag{7.1}$$

Next we define the three orthogonal group projectors we will need, these are

$$\begin{aligned} P^S_{N;ijkl} &= \frac{1}{N}\delta_{ij}\delta_{kl} \\ P^T_{N;ijkl} &= \frac{1}{2}(\delta_{ik}\delta_{jl} + \delta_{il}\delta_{jk} - \frac{2}{N}\delta_{ij}\delta_{kl}) \\ P^A_{N;ijkl} &= \frac{1}{2}(\delta_{ik}\delta_{jl} - \delta_{il}\delta_{jk}) \end{aligned} \tag{7.2}$$

where $S$, $T$ and $A$ refer to the singlet, traceless symmetric and antisymmetric representation respectively, and $N$ refers to the number of values the indices take. Then the $O(m) \times O(n)$ projectors are defined as

$$\begin{aligned} P^S_{arbsctdu} &= P^S_{m;abcd} P^S_{n;rstu} \\ P^W_{arbsctdu} &= P^T_{m;abcd} P^S_{n;rstu} \\ P^X_{arbsctdu} &= P^S_{m;abcd} P^T_{n;rstu} \\ P^Y_{arbsctdu} &= P^T_{m;abcd} P^T_{n;rstu} \\ P^Z_{arbsctdu} &= P^A_{m;abcd} P^A_{n;rstu} \\ P^A_{arbsctdu} &= P^A_{m;abcd} P^S_{n;rstu} \\ P^B_{arbsctdu} &= P^S_{m;abcd} P^A_{n;rstu} \\ P^C_{arbsctdu} &= P^A_{m;abcd} P^T_{n;rstu} \\ P^D_{arbsctdu} &= P^T_{m;abcd} P^A_{n;rstu} \end{aligned} \tag{7.3}$$

where we have made the following definitions for the names of the $O(m) \times O(n)$ representations ($S$, $W$, $X$, $Y$, $Z$, $A$, $B$, $C$, $D$) = ($SS$, $TS$, $ST$, $TT$, $AA$, $AS$, $SA$, $AT$, $TA$).

Note that the representations $A$ and $B$ contain the conserved vectors of $O(m)$ and $O(n)$ respectively.

# Chapter 8

# Bootstrap Constraints

## 8.1 Crossing Equations

The crossing equation

$$\langle \phi_{ar}\phi_{bs}\phi_{ct}\phi_{du}\rangle = \langle \phi_{ct}\phi_{bs}\phi_{ar}\phi_{du}\rangle \tag{8.1}$$

leads to the following sum rules [47]

$$\sum_{S^+} c_O^2 \begin{pmatrix} F^-_{\Delta,\ell} \\ 0 \\ 0 \\ 0 \\ 0 \\ F^+_{\Delta,\ell} \\ 0 \\ 0 \\ 0 \end{pmatrix} + \sum_{W^+} c_O^2 \begin{pmatrix} -\frac{2}{m}F^-_{\Delta,\ell} \\ 0 \\ F^-_{\Delta,\ell} \\ F^-_{\Delta,\ell} \\ 0 \\ -\frac{2}{m}F^+_{\Delta,\ell} \\ 0 \\ -F^+_{\Delta,\ell} \\ F^+_{\Delta,\ell} \end{pmatrix} + \sum_{X^+} c_O^2 \begin{pmatrix} -\frac{2}{n}F^-_{\Delta,\ell} \\ F^-_{\Delta,\ell} \\ F^-_{\Delta,\ell} \\ 0 \\ 0 \\ -\frac{2}{n}F^+_{\Delta,\ell} \\ F^+_{\Delta,\ell} \\ F^+_{\Delta,\ell} \\ 0 \end{pmatrix} + \sum_{Y^+} c_O^2 \begin{pmatrix} (1+\frac{4}{mn})F^-_{\Delta,\ell} \\ (1-\frac{2}{m})F^-_{\Delta,\ell} \\ -2(\frac{1}{m}+\frac{1}{n})F^-_{\Delta,\ell} \\ (1-\frac{2}{n})F^-_{\Delta,\ell} \\ 2F^-_{\Delta,\ell} \\ -(1-\frac{4}{mn})F^+_{\Delta,\ell} \\ -(1+\frac{2}{m})F^+_{\Delta,\ell} \\ -2(\frac{1}{m}-\frac{1}{n})F^+_{\Delta,\ell} \\ -(1+\frac{2}{n})F^+_{\Delta,\ell} \end{pmatrix}$$
$$+ \sum_{Z^+} c_O^2 \begin{pmatrix} F^-_{\Delta,\ell} \\ -F^-_{\Delta,\ell} \\ 0 \\ -F^-_{\Delta,\ell} \\ 2F^-_{\Delta,\ell} \\ -F^+_{\Delta,\ell} \\ F^+_{\Delta,\ell} \\ 0 \\ F^+_{\Delta,\ell} \end{pmatrix} + \sum_{A^-} c_O^2 \begin{pmatrix} 0 \\ 0 \\ -F^-_{\Delta,\ell} \\ F^-_{\Delta,\ell} \\ 0 \\ 0 \\ 0 \\ F^+_{\Delta,\ell} \\ F^+_{\Delta,\ell} \end{pmatrix} + \sum_{B^-} c_O^2 \begin{pmatrix} 0 \\ F^-_{\Delta,\ell} \\ -F^-_{\Delta,\ell} \\ 0 \\ 0 \\ 0 \\ F^+_{\Delta,\ell} \\ -F^+_{\Delta,\ell} \\ 0 \end{pmatrix}$$
$$+ \sum_{C^-} c_O^2 \begin{pmatrix} -F^-_{\Delta,\ell} \\ -F^-_{\Delta,\ell} \\ \frac{2}{n}F^-_{\Delta,\ell} \\ (1-\frac{2}{n})F^-_{\Delta,\ell} \\ 2F^-_{\Delta,\ell} \\ F^+_{\Delta,\ell} \\ F^+_{\Delta,\ell} \\ -\frac{2}{n}F^+_{\Delta,\ell} \\ -(1+\frac{2}{n})F^+_{\Delta,\ell} \end{pmatrix} + \sum_{D^-} c_O^2 \begin{pmatrix} -F^-_{\Delta,\ell} \\ (1-\frac{2}{m})F^-_{\Delta,\ell} \\ \frac{2}{m}F^-_{\Delta,\ell} \\ -F^-_{\Delta,\ell} \\ 2F^-_{\Delta,\ell} \\ F^+_{\Delta,\ell} \\ -(1+\frac{2}{m})F^+_{\Delta,\ell} \\ \frac{2}{m}F^+_{\Delta,\ell} \\ F^+_{\Delta,\ell} \end{pmatrix} = \begin{pmatrix} 0 \\ 0 \\ 0 \\ 0 \\ 0 \\ 0 \\ 0 \\ 0 \\ 0 \end{pmatrix}. \tag{8.2}$$

The notation $c_O^2$ is shorthand for the OPE coefficient squared of the exchanged operators in the corresponding irrep that is being summed over. Superscripts on irreps denote the spins that appear in each sum (even, odd). For the sum rules resulting from the $\phi_{ar}$ - $S$ system of mixed correlators see Appendix D.

## 8.2 Results

In what follows we will study the behavior of $O(2) \times O(n)$ CFTs from the Large $n$ limit all the way down to the upper edge of Regime I of 6.3 and 6.4. Consequently, we will study the case $O(2) \times O(3)$ that is considered phenomenologically relevant for condensed matter systems. We will not discuss the $O(2) \times O(2)$ case in this Chapter, but in Chapter 9 instead since it is equivalent to $O(2)^2 \rtimes S_2$ due to symmetry enhancement[1], see [56]. CFTs with $O(m) \times O(n)$ global symmetry were first studied in the numerical bootstrap by [76] and [77], consequently [36] appeared the same day as [47]. In [76] and [77] the authors considered various values of $m$ and $n$ in a single correlator bootstrap system. In [76] they studied the large $n$ limit and in [77] they conjectured that various changes of slope for $m$ and $n$ small where due to the fixed points found in resummations. Whereas, the authors of [36] considered the $O(3) \times O(15)$ case using a mixed correlator system involving the operators $\phi_{ar}$ and $S$, and showed that known fixed points lie on the edges of the allowed region peninsula.

In the interest of clearness of presentation, given that we will present many plots, we will include the assumptions and numerical parameters used to produce each plot in its corresponding caption only.

### 8.2.1 Comparing With Perturbation Theory and Regime I

The starting point will be to present the single correlator plots for the $W$ and $X$ sectors[2] keeping $m = 2$ fixed and varying $n$. These can be seen in Fig 8.1 and Fig 8.2. In these plots we compare the Large $n$ data of [43] [44] [47] and [81] with the numerical bootstrap. In both Fig 8.1 and Fig 8.2 we use circles to denote the position of the antichiral fixed point for the corresponding values of $m$ and $n$, whereas we use squares to denote the chiral fixed point. The line between the square and the circle is used to demonstrate that both correspond to fixed points with the same values of $m$ and $n$. It thus apparent that the exclusion plots for the $W$ sector are saturated by the Large $n$ antichiral fixed points whereas the exclusion plots for the $X$ sector are saturated by the Large $n$ chiral fixed points. Unsurprisingly, as we decrease the value of $n$ the agreement becomes worse. Nevertheless, it is very interesting that for $n$ as low as $n = 10$ we get excellent agreement between the position of the kinks and the predicted fixed points. This is important since it reinforces/supports the bootstrap intuition that CFTs are quite often the reason for the appearance of kinks/features in bootstrap exclusion plots.

In Fig 8.3 we present the corresponding exclusion plots for the $X$ and $W$ sectors specifically for $m = 2$ and $n = 6$. This case is of special interest since it is located on the upper edge of Regime I of the $\varepsilon$ expansion fixed points, as seen in 6.4. In this case there exist six loop resummed results in the literature [58] that we can compare to.

[1] At least perturbatively.
[2] Remember $W = TS$ and $X = ST$.

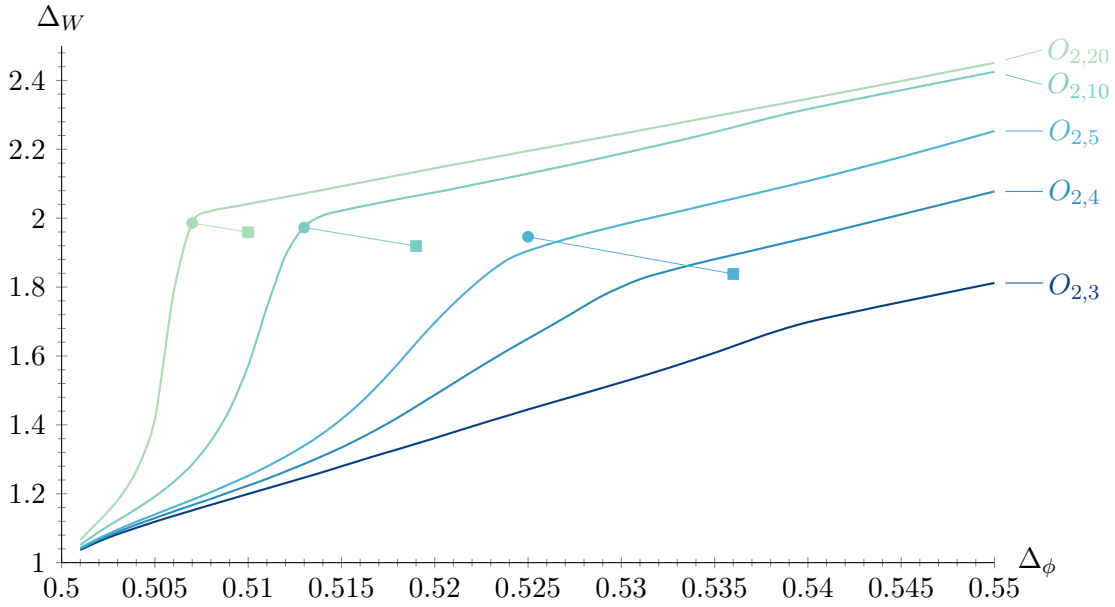


FIGURE 8.1: Single correlator exclusion plots for the scaling dimension of the first $W$ operator, for $m = 2$ and various values of $n$. The circles on the plot denote the Large $n$ predictions for the dimension of this operator at the anti-chiral fixed point. The box, connected to the circle by a line, represents the Large $n$ predictions for the dimensions of this operator at the chiral fixed point. It is thus clear that the kinks are saturated by the anti-chiral fixed point. The figure was produced using the following parameters in PyCFTBoot [9]: $m_{max} = 8$, $n_{max} = 11$, $l_{max} = 36$ and $k_{max} = 42$. Figure reproduced from [47].

Remember that the Large $n$ fixed points should correspond to the $\varepsilon$ expansion fixed points in Regime I when $n$ is took sufficiently large.

The next natural step it to attempt to find isolated self consistent regions in parameter space (i.e. islands) that correspond to the CFTs that saturate the kinks in Figs 8.1, 8.2 and 8.3. To do this we consider, in addition to those of 8.2, the sum rules of Appendix D. In other words, we consider the $\phi_{ar}$ - $S$ mixed correlator system of sum rules. In Fig 8.4 and Fig 8.5 we present the islands corresponding to chiral and anti-chiral fixed points with $m = 2$ and $n = 10$ and $n = 20$ respectively. For $n = 20$ we observe excellent agreement with Large $n$ predictions. For $n = 10$ there is a very small deviation, which is not unexpected since $1/n = 0.1$ is not very small. Interestingly, in the $m = 2$ and $n = 6$ case in Fig 8.6, where we compare the chiral island[3] to the data of [58] we find that there is some tension. This is not too worrying since if one considers the $3\sigma$ deviation of the $\epsilon$ expansion error bars the results do overlap.

### 8.2.2 $O(2) \times O(3)$

It is useful to emphasize at this point that we name islands based on the CFTs we expect/hope to match them to. We cannot actually prove though that the islands

[3]We identify the island in the $X$ sector as the chiral island for $m = 2$ and $n = 6$ given the excellent agreement down to $n = 10$ of the Large $n$ data and the conformal bootstrap. We cannot exclude though the possibility that for $n < 10$ some new, different, fixed point saturates the kink. However, we consider this scenario unlikely.

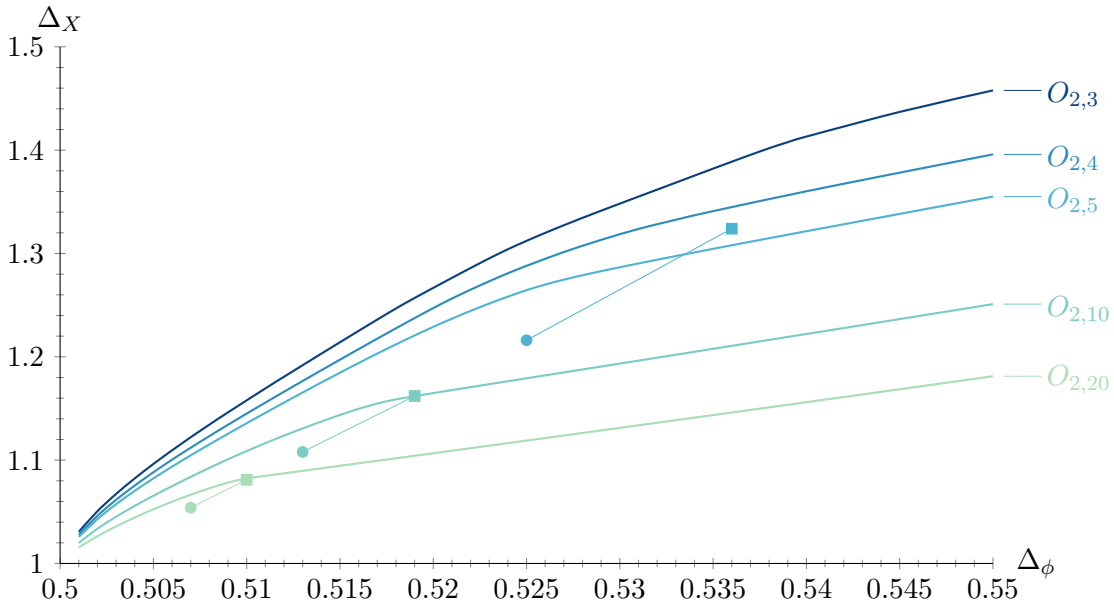


FIGURE 8.2: Single correlator exclusion plots for the scaling dimension of the first $X$ operator, for $m = 2$ and various values of $n$. The circles on the plot denote the Large $n$ predictions for the dimension of this operator at the anti-chiral fixed point. The box, connected to the circle by a line, represents the Large $n$ predictions for the dimensions of this operator at the chiral fixed point. It is thus clear that the kinks are saturated by the chiral fixed point. The figure was produced using the following parameters in PyCFTBoot [9]: $m_{max} = 8$, $n_{max} = 11$, $l_{max} = 36$ and $k_{max} = 42$. Figure reproduced from [47].

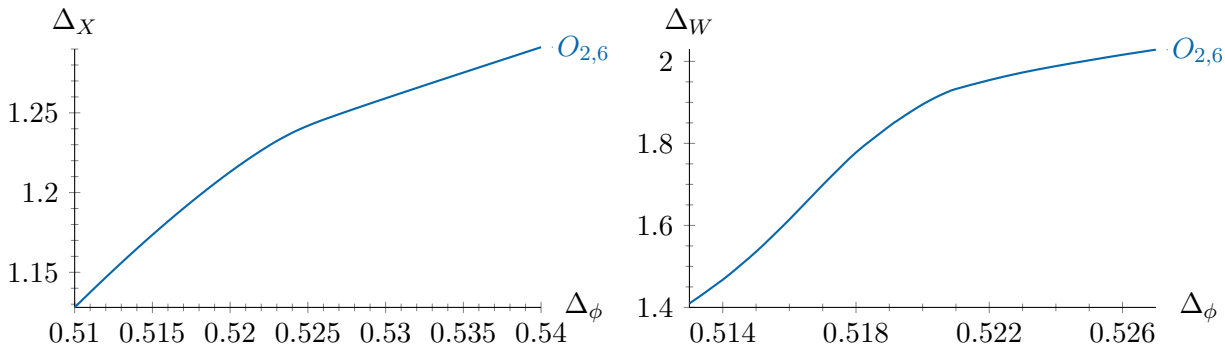


FIGURE 8.3: Single correlator exclusion plots for the scaling dimension of the first $X$ and $W$ operators respectively, for $m = 2$ and $n = 6$. This case is of particular interest since it sits at the edge of Regime$_1$ in 6.4 from the results of [58]. The figure was produced using the following parameters in PyCFTBoot [9]: $m_{max} = 8$, $n_{max} = 11$, $l_{max} = 36$ and $k_{max} = 42$. Figure reproduced from [47].

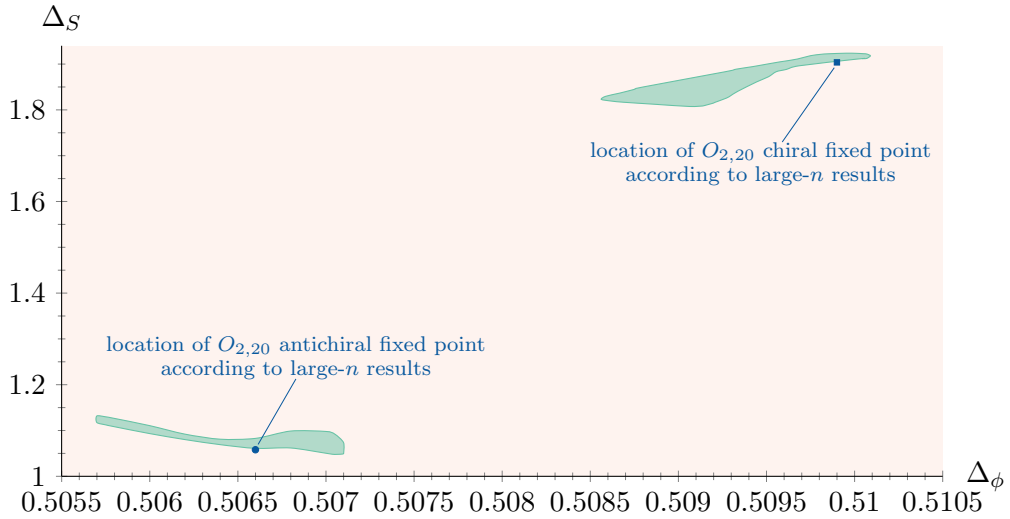


FIGURE 8.4: Islands corresponding to the Chiral and Anti-Chiral fixed points with $m = 2$ and $n = 20$ obtained using the mixed $\phi_{ar}$ - $S$ system of correlators. These islands assume that the first $X$ (for the chiral island) and $W$ (for the anti-chiral island) operators have a scaling dimension that saturates the corresponding single correlator plots Fig 8.2 and Fig 8.1 respectively. We also assume in both that the first $B$ operator has a scaling dimension of $\Delta_B = 2.0$ since it is a conserved vector (remember $B = S \times A$). For the second $B$ operator in both we impose $\Delta_{B'} \geqslant 3.0$. For the second defining operator $\phi'$ we impose $\Delta_{\phi'} \geqslant \Delta_\phi + 0.01$ in both. Lastly, in the Chiral island we impose $\Delta_{S'} \geqslant 3.0$ whereas for the Anti-Chiral island we impose $\Delta'_S \geqslant 1.5$. The figure was produced using the following parameters in PyCFTBoot [9]: $m_{max} = 7$, $n_{max} = 9$, $l_{max} = 30$ and $k_{max} = 40$. Figure reproduced from [47].

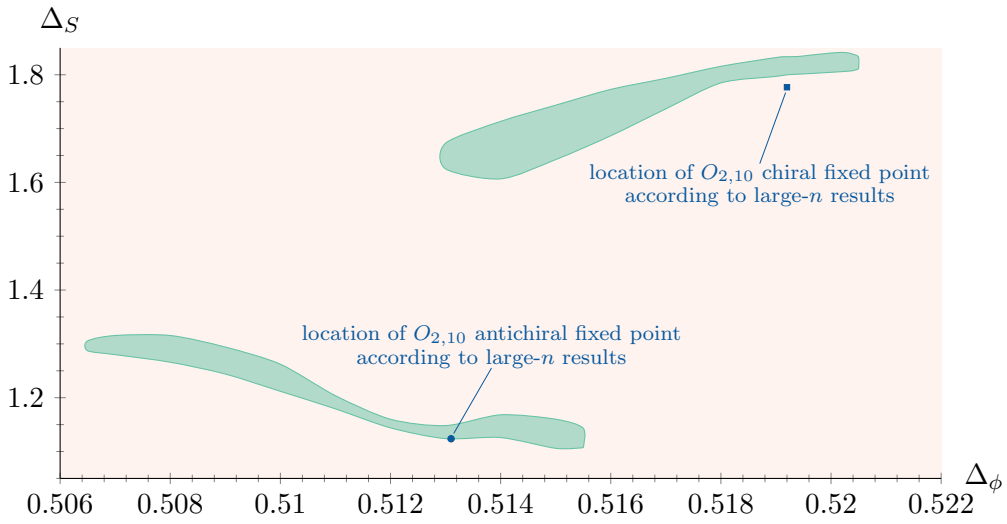


FIGURE 8.5: Islands corresponding to the Chiral and Anti-Chiral fixed points with $m = 2$ and $n = 10$ obtained using the mixed $\phi_{ar}$ - $S$ system of correlators. These islands assume that the first $X$ (for the chiral island) and $W$ (for the anti-chiral island) operators have a scaling dimension that saturates the corresponding single correlator plots Fig 8.2 and Fig 8.1 respectively. We also assume in both that the first $B$ operator has a scaling dimension of $\Delta_B = 2.0$ since it is a conserved vector (remember $B = S \times A$). For the second $B$ operator in both we impose $\Delta_{B'} \geqslant 3.0$. Lastly, in the Chiral fixed point we impose $\Delta_{S'} \geqslant 3.0$ and $\Delta_{\phi'} \geqslant \Delta_\phi + 0.01$ whereas for the Anti-Chiral fixed point we impose $\Delta_{S'} \geqslant 1.6$ and $\Delta_{\phi'} \geqslant 1.6$. We note that there seems to be some minor deviation between the island and the Large $n$ prediction in the Chiral case, however this is not very worrying since $n = 10$ is quite far from $n \to \infty$. The figure was produced using the following parameters in PyCFTBoot [9]: $m_{max} = 7$, $n_{max} = 9$, $l_{max} = 30$ and $k_{max} = 40$. Figure reproduced from [47].

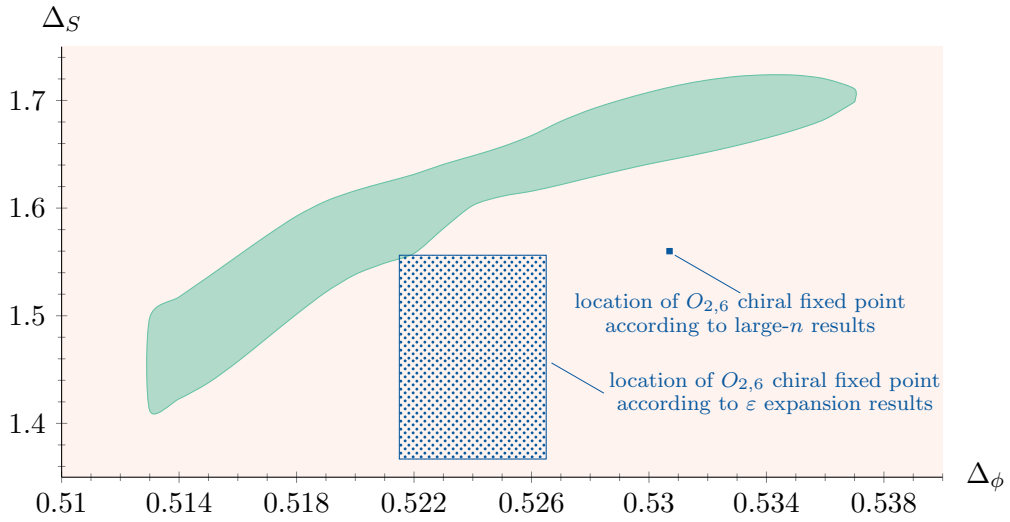


FIGURE 8.6: Island corresponding to the Chiral fixed point with $m = 2$ and $n = 6$ obtained using the mixed $\phi_{ar}$ - $S$ system of correlators. This island assumes that the first $X$ operator has a scaling dimension that saturates the corresponding single correlator plot Fig 8.3. We also assume that the first $B$ operator has a scaling dimension of $\Delta_B = 2.0$ since it is a conserved vector (remember $B = S \times A$). For the second $B$ operator we impose $\Delta_{B'} \geqslant 3.0$. Lastly, we impose $\Delta_{S'} \geqslant 3.0$ and $\Delta_{\phi'} \geqslant \Delta_\phi + 0.01$. We note that there seems to be some tension between the island and the six loop resummed $\varepsilon$-expansion results of [58]. The figure was produced using the following parameters in PyCFTBoot [9]: $m_{max} = 7$, $n_{max} = 9$, $l_{max} = 30$ and $k_{max} = 40$. Figure reproduced from [47].

are necessarily due to the CFTs we named them after. Of course, in cases like the $Regime_1$ fixed points for $n = 10$ and $n = 20$ we are confident that the islands are due to the CFTs we named them after. This is because in these cases we have excellent agreement with concrete perturbative predictions. In the case of the fixed points found in resummations, one can see e.g. in Table 8.1, that theoretical predictions vary wildly. Thus the naming of our islands in this section should be taken with a grain of salt.

Now we turn our attention to the $O(2) \times O(3)$ case. We emphasize once again that these are qualitatively different from the islands/CFTs/fixed points studied in the previous section in that they are found after resummations are performed. In other words they cannot be calculated by setting a beta function to zero order by order in some control parameter such as e.g. $\varepsilon$. See 6.3 for further details. The possibility that changes in slope in the $O(2) \times O(3)$ exclusion bounds might correspond to these new, controversial fixed points was originally proposed in [77]. We present the single correlator $W$ sector exclusion plot for $m = 2$ and $n = 3$ in Fig 8.7 and the one for the $Z$ sector in Fig 8.10. We see that there is a change of slope, but given that it is a bit hard to see, we show in Fig 8.8 two fits of the points on the bound that indeed show a well defined change of slope around roughly $\Delta_\phi = 0.54$. Consequently, in Fig 8.9 and Fig 8.11 one can see the chiral and collinear islands which correspond the the changes of slope in Fig 8.7 and Fig 8.10 respectively. Note that both seem to be RG stable, since both continue to exist if we impose that the second scalar singlet is irrelevant in the RG sense of the word ($\Delta_{S'} > 3$). We remind the reader that the names chiral and collinear are simply indicative of whether the coupling $v$ in 6.2 is positive or not at the fixed point. We once again emphasize this, since the chiral fixed point of this section is qualitatively different from the chiral fixed point of the previous section. We understand that calling them both chiral can be confusing, but continue to do so to make contact with the literature. In tables 8.1 and 8.2 we give the critical exponents corresponding to the islands in Fig 8.9 and Fig 8.11 respectively, and compare to corresponding values in the literature. We note that the error bars that we give for the bootstrap results are non-rigorous since we assume that our theories saturate their corresponding exclusion plots, an assumption whose error is hard to estimate systematically. Also, note that we have not mentioned experimental results, since experimental data seems to vary quite a lot, see e.g. the discussions and data in [84], [56]. There could be various reasons for this, such as a spiral RG flow due to the conjectured complex scaling dimensions[4] at the fixed point, or depending on the choice of initial parameters in the experiment it may not be in the basin of attraction of the fixed point.

[4]Note that even though we are using the unitary bootstrap, it has been know to pick up non-unitary theories in the past. See the discussion in Chapter 10.

TABLE 8.1: $O(2) \times O(3)$ "chiral" critical exponents. Reproduced from [47].

| **Method** | $\alpha$ | $\beta$ | $\nu$ | $\gamma$ | $\delta$ | $\eta$ | $\phi_W$ |
|---|---|---|---|---|---|---|---|
| Figs. 8.7, 8.9 | 0.082(22) | 0.344(5) | 0.639(7) | 1.23(3) | 4.573(14) | 0.077(3) | 0.818(16) |
| $\overline{\text{MS}}$ scheme [17, 16] | 0.11(15) | 0.34(4) | 0.63(5) | 1.20(24) | 4.5(2) | 0.09(4) | 0.76(12) |
| MZM scheme [82, 16] | 0.35(9) | 0.30(4) | 0.55(3) | 1.04(18) | 4.5(5) | 0.1(1) | 0.58(6) |
| Monte Carlo [75] | 0.44(3) | 0.26(3) | 0.52(1) | 1.04(9) | 5.0(5) | 0.00(8) | – |

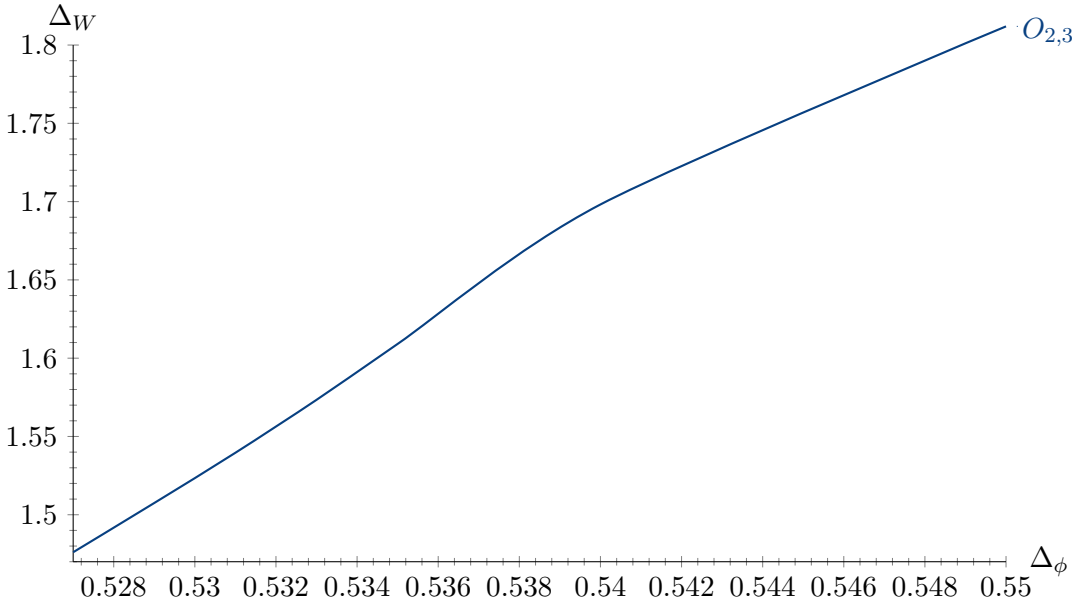


FIGURE 8.7: Single correlator exclusion plot for the scaling dimension of the first $W$ operator for $m = 2$ and $n = 3$. The figure was produced using the following parameters in PyCFTBoot [9]: $m_{max} = 8$, $n_{max} = 11$, $l_{max} = 36$ and $k_{max} = 42$. Figure reproduced from [47].

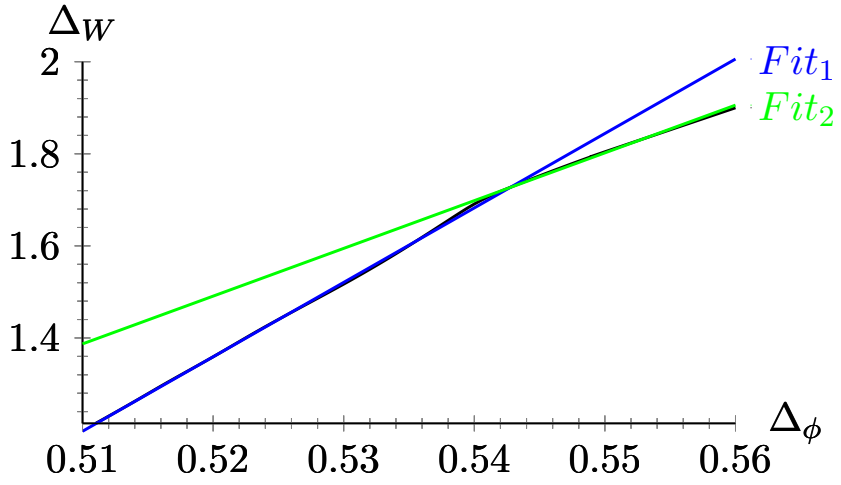


FIGURE 8.8: Single correlator exclusion plot for the scaling dimension of the first $W$ operator for $m = 2$ and $n = 3$. The same as in Fig 8.7 but with least square fits adapted to the left and right of the plot in order to indicate that even though it is not very pronounced, there does seems to be a well defined change of slope. The figure was produced using the following parameters in PyCFTBoot [9]: $m_{max} = 8$, $n_{max} = 11$, $l_{max} = 36$ and $k_{max} = 42$.

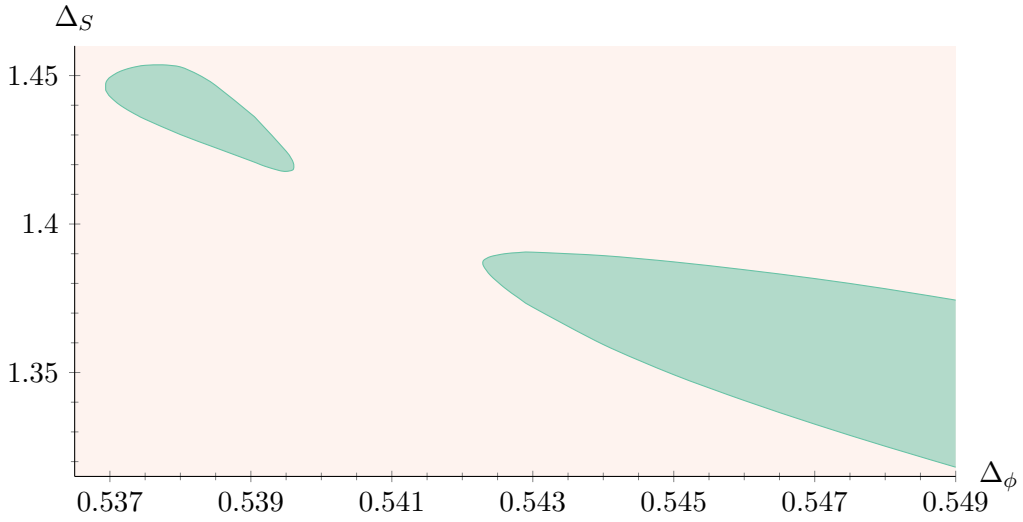


FIGURE 8.9: Island corresponding to the Chiral fixed point with $m = 2$ and $n = 3$ obtained using the mixed $\phi_{ar}$ - $S$ system of correlators. This island assumes that the first $W$ operator has a scaling dimension that saturates the corresponding single correlator plot Fig 8.7. We also assume that the first $B$ operator has a scaling dimension of $\Delta_B = 2.0$ since it is a conserved vector (remember $B = S \times A$). For the second $B$ operator we impose $\Delta_{B'} \geqslant 2.4$. Lastly, we impose $\Delta_{S'} \geqslant 2.0$ and $\Delta_{\phi'} \geqslant 1.5$. We note that we have checked that the island remains even if we impose $\Delta_{S'} \geqslant 3.0$ which corresponds to it being a stable fixed point in the language of RG. We once again stress that this island is unrelated to the Chiral islands of the $\varepsilon$ expansion but they have the same name in the literature since the coupling $v$ in 6.2 is positive for both types of fixed points. The figure was produced using the following parameters in PyCFTBoot [9]: $m_{max} = 7$, $n_{max} = 9$, $l_{max} = 30$ and $k_{max} = 40$. Figure reproduced from [47].

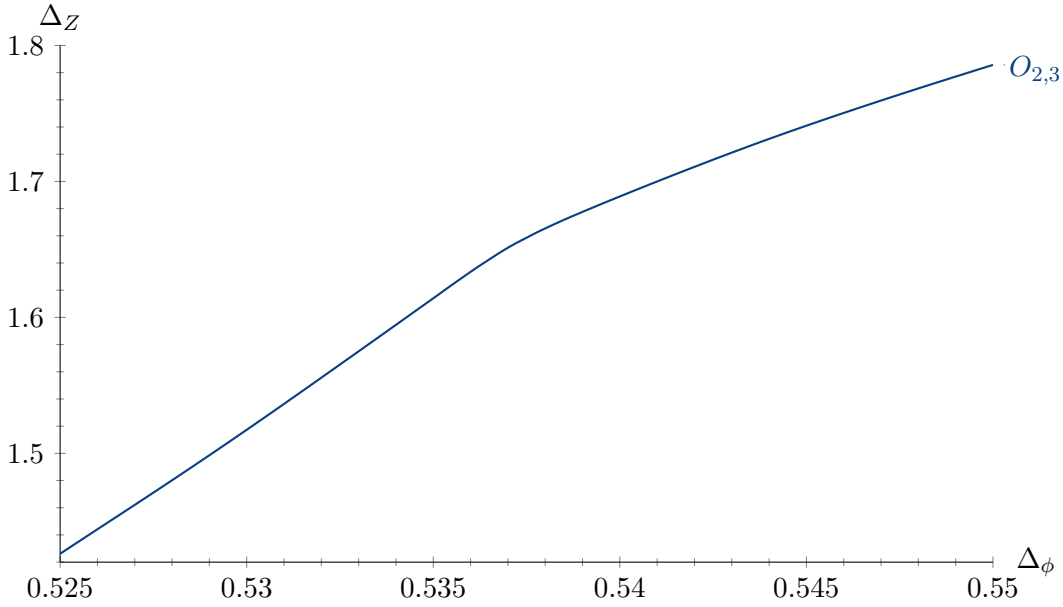


FIGURE 8.10: Single correlator exclusion plot for the scaling dimension of the first $Z$ operator for $m = 2$ and $n = 3$. The figure was produced using the following parameters in PyCFTBoot [9]: $m_{max} = 8$, $n_{max} = 11$, $l_{max} = 36$ and $k_{max} = 42$. Figure reproduced from [47].

TABLE 8.2: $O(2) \times O(3)$ "antichiral/collinear" critical exponents. Reproduced from [47].

| **Method** | $\alpha$ | $\beta$ | $\nu$ | $\gamma$ | $\delta$ | $\eta$ | $\phi_Z$ |
|---|---|---|---|---|---|---|---|
| Figs. 8.10, 8.11 | 0.05(7) | 0.341(19) | 0.650(23) | 1.27(11) | 4.72(13) | 0.049(23) | 0.89(4) |
| $\overline{\text{MS}}$ scheme [17, 16] | 0.11(24) | 0.34(5) | 0.63(8) | 1.2(3) | 4.52(12) | 0.086(24) | 0.75(16) |
| MZM scheme [82, 16] | 0.22(12) | 0.319(23) | 0.59(4) | 1.14(16) | 4.56(4) | 0.079(7) | 0.74(11) |

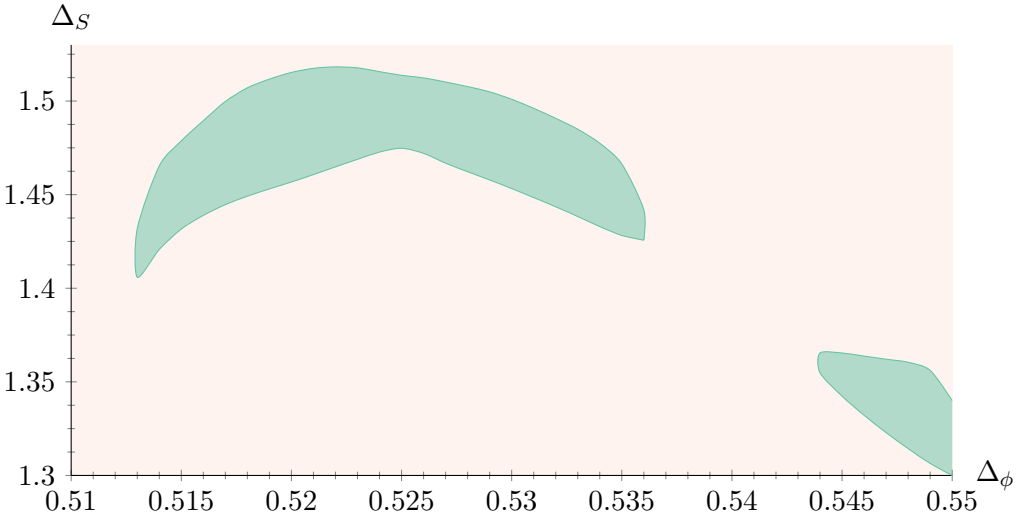


FIGURE 8.11: Island corresponding to the Collinear fixed point with $m = 2$ and $n = 3$ obtained using the mixed $\phi_{ar}$ - $S$ system of correlators. This island assumes that the first $Z$ operator has a scaling dimension that saturates the corresponding single correlator plot Fig 8.10. We also assume that the first $B$ operator has a scaling dimension of $\Delta_B = 2.0$ since it is a conserved vector (remember $B = S \times A$). For the second $B$ operator we impose $\Delta_{B'} \geqslant 2.5$. Lastly, we impose $\Delta_{S'} \geqslant 3.0$ and $\Delta_{\phi'} \geqslant \Delta_\phi + 0.01$. The figure was produced using the following parameters in PyCFTBoot [9]: $m_{max} = 7$, $n_{max} = 9$, $l_{max} = 30$ and $k_{max} = 40$. Figure reproduced from [47].

# Chapter 9

# Tensor structures in $G^N \rtimes S_N$ theories

## 9.1 The OPE decomposition

In this chapter we will study global symmetry tensor structures that appear in theories with $G' = G^N \rtimes S_N$ symmetry for $G$ arbitrary. To rephrase, this is simply the group theory of $N$ copies of $G$ which can be permuted with each other. This generalizes several previously studied cases, such as the Hypercubic theories ($G' = Z_2^N \rtimes S_N$), and the MN theories ($G' = O(m)^N \rtimes S_N$) and Tetragonal theories ($G' = (Z_2^M \rtimes S_M)^N \rtimes S_N$) which where first bootstrapped in [101]. We note that the class of groups $G'$ contains a lot of groups not included in Autoboot [42].

We start by defining a field $\phi_i^a$ that transforms in the defining representation of $G' = G^N \rtimes S_N$. The upper indices in all the subsequent discussion will label the copy of $G$ that $\phi$ transforms in, i.e. it is an $S_N$ index. Whereas the lower index $i$ is an index transforming in $G$. Hence, the upper indices are acted upon by $S_N$ and the lower indices by $G$. Note that previous works, such as e.g. [101], have used a one index notation, i.e. $\phi_i$ where $i$ runs over $M * N$ values. The notation we will use in this work has the advantage that all invariant tensors will be expressible in multi-index Kronecker delta functions. However, see Appendix G for a workaround in expressing the one index notation in terms of Kronecker deltas, the caveat is that one has to write out explicitly the index values, e.g. $\delta_{i1}$.

Let us start by considering the product of $\phi_i^a$ with itself, $\phi_i^a \times \phi_j^b$. The first observation is that elements with $a \neq b$ can never mix with elements with $a = b$ under the action of $S_N$. As a concrete example consider the following objects with $N = 3$, take

$$A = (\phi_i^1 \phi_j^2,\ \phi_i^2 \phi_j^3,\ \phi_i^3 \phi_j^1) \tag{9.1}$$

and

$$B = (\phi_i^1 \phi_j^1,\ \phi_i^2 \phi_j^2,\ \phi_i^3 \phi_j^3) \tag{9.2}$$

one can easily be convinced that the elements of $A$ and $B$ will never mix under permutation of the upper indices. This is a general fact, i.e. the elements with $a \neq b$ never mix with elements with $a = b$. Hence, the OPE may be split as

$$\phi_i^a \times \phi_j^b = \left(\phi_i^a \times \phi_j^b\right)_{a \neq b} + \left(\phi_i^a \times \phi_j^b\right)_{a = b} \tag{9.3}$$

The first term on the RHS multiplies fields from different copies of $G$, hence the indices $i$ and $j$ cannot be decomposed onto irreducible representations of $G$. Thus

in order to get irreducible representations of $G'$ we simply symmetrize and anti-symmetrize the fields

$$\left(\phi_i^a \times \phi_j^b\right)_{a\neq b} = \frac{1}{2}\left(\phi_i^a\phi_j^b + \phi_j^b\phi_i^a\right)_{a\neq b} + \frac{1}{2}\left(\phi_i^a\phi_j^b - \phi_j^b\phi_i^a\right)_{a\neq b} \tag{9.4}$$

the representations on the right hand side of 9.4 cannot be reduced further, hence they are irreducible. To make contact with [101] we call them $Z_{ij}^{ab}$ and $B_{ij}^{ab}$ respectively. Note also that they exist for any choice of group $G$.

We now turn our attention to the second term in 9.3, since $a = b$, i.e. both fields are in the same copy of $G$, we can decompose the product of the two fields onto irreducible representations of $G$.

$$\left(\phi_i^a \times \phi_j^b\right)_{a=b} = \delta_{ij}\left(\phi_k^a\phi_k^b\right)_{a=b} + \left(R_{1\,ij}^{ab}\right)_{a=b} + ... + \left(R_{\mathcal{N}\,ij}^{ab}\right)_{a=b} \tag{9.5}$$

note that we have separated the contribution of the singlet under $G$ in the first term. The other terms correspond to the remaining irreducible representations under $G$, which we named $R_1$, $R_2$, ... $R_{\mathcal{N}}$. We emphasize that $\mathcal{N}$ is equal to the number of (non-singlet) irreducible representations that appear in the OPE of the $G$ defining representation with itself.

The first term in 9.5 is reducible, this is because we can subtract the trace of copies

$$\left(\phi_k^a\phi_k^b\right)_{a=b} = \left(\phi_k^a\phi_k^b - \frac{\delta^{ab}}{N}\phi_k^c\phi_k^c\right)_{a=b} + \left(\frac{\delta^{ab}}{N}\phi_k^c\phi_k^c\right)_{a=b} \tag{9.6}$$

we may name the first irrep on the right hand side of 9.6 $X^{ab}$. The second term is simply the singlet of $G'$ which we call $S$. Regarding $X^{ab}$ we note that this operator is the same for all groups $G'$ independently of the choice of $G$, since it is a singlet with respect to $G$. Remember also from our analysis in Section 4.2 that it is equivalent to the defining representation of $S_N$, hence its group theory and its tensor structures are known. Thus if we name $\left(R_{\mathcal{N}\,ij}^{ab}\right)_{a=b}$ as $I_{\mathcal{N}\,ij}^{ab}$. We obtain the full decomposition of the OPE 9.3

$$\phi_i^a \times \phi_j^b \sim \delta^{ab}\delta_{ij}S + \delta_{ij}X^{ab} + I_{1\,ij}^{ab} + ... + I_{\mathcal{N}\,ij}^{ab} + Z_{ij}^{ab} + B_{ij}^{ab} \tag{9.7}$$

## 9.2 Projectors

Having fully decomposed the OPE $\phi_i^a \times \phi_j^b$ onto irreducible representations of $G'$ for a generic generic number of copies, and generic group $G$, we are ready to write down the projectors corresponding to the decomposition of the four point function $\langle\phi_i^a\phi_j^b\phi_k^c\phi_l^d\rangle$ onto each irreducible representation. We have

$$
\begin{aligned}
P^{S}{}_{ijkl}^{abcd} &= \frac{1}{MN}\delta^{ab}\delta^{cd}\delta_{ij}\delta_{kl} \\
P^{X}{}_{ijkl}^{abcd} &= \frac{1}{M}\delta_{ij}\delta_{kl}\left(\delta^{abcd} - \frac{1}{N}\delta^{ab}\delta^{cd}\right) \\
P^{I_1}{}_{ijkl}^{abcd} &= \delta^{abcd}\, P^{R_1}{}_{ijkl} \\
&\dots \\
P^{I_{\mathcal{N}}}{}_{ijkl}^{abcd} &= \delta^{abcd}\, P^{R_{\mathcal{N}}}{}_{ijkl} \\
P^{Z}{}_{ijkl}^{abcd} &= \frac{1}{2}\left(\left(\delta^{ac}\delta^{bd} - \delta^{abcd}\right)\delta_{ik}\delta_{jl} + \left(\delta^{ad}\delta^{bc} - \delta^{abcd}\right)\delta_{il}\delta_{jk}\right) \\
P^{B}{}_{ijkl}^{abcd} &= \frac{1}{2}\left(\left(\delta^{ac}\delta^{bd} - \delta^{abcd}\right)\delta_{ik}\delta_{jl} - \left(\delta^{ad}\delta^{bc} - \delta^{abcd}\right)\delta_{il}\delta_{jk}\right)
\end{aligned}
\tag{9.8}
$$

one can check that the above projectors once contracted onto a pair of fields $\phi_k^c\phi_l^d$ reproduce the operators in 9.7. For example

$$
\frac{1}{2}\left(\phi_i^a\phi_j^b - \phi_j^b\phi_i^a\right)_{a\neq b} = P^{B}{}_{ijkl}^{abcd}\,\phi_k^c\phi_l^d \tag{9.9}
$$

Also, the tensors $P^{R_{\mathcal{N}}}{}_{ijkl}$ refer to the projectors in $G$, this should become clear from our examples in what follows. Lastly, note that the representations $(S,\ X,\ I_1,\ ...,\ I_{\mathcal{N}},\ Z,\ B)$ have dimensions $(1,\ N-1,\ NdimR_1,\ ...,\ NdimR_{\mathcal{N}},\ M^2\frac{N(N-1)}{2},\ M^2\frac{N(N-1)}{2})$ respectively.

## 9.3 Examples

### 9.3.1 Hypercubic

The first and simplest example to look at is $G = Z_2$. In this case we may simply drop the indices $(i,\ j,\ k,\ l)$. Also, since the product of two defining operators of $Z_2$ only gives rise to the singlet representation, we will not have any $R_{\mathcal{N}}$ representations in this case. The projectors in 9.8 then become

$$
\begin{aligned}
P^{S}{}_{ijkl}^{abcd} &= \frac{1}{N}\delta^{ab}\delta^{cd} \\
P^{X}{}_{ijkl}^{abcd} &= \left(\delta^{abcd} - \frac{1}{N}\delta^{ab}\delta^{cd}\right) \\
P^{Z}{}_{ijkl}^{abcd} &= \frac{1}{2}\left(\left(\delta^{ac}\delta^{bd} - \delta^{abcd}\right) + \left(\delta^{ad}\delta^{bc} - \delta^{abcd}\right)\right) \\
P^{B}{}_{ijkl}^{abcd} &= \frac{1}{2}\left(\left(\delta^{ac}\delta^{bd} - \delta^{abcd}\right) - \left(\delta^{ad}\delta^{bc} - \delta^{abcd}\right)\right)
\end{aligned}
\tag{9.10}
$$

but these are just 4.6 having renamed $A$ to $B$ and $Y$ to $Z$. Their dimensions are $(S,\ X,\ Z,\ B) = (1,\ N-1,\ \frac{N(N-1)}{2},\ \frac{N(N-1)}{2})$ which can be found by plugging in $M = 1$.

### 9.3.2 MN

To recover the MN models bootstrapped in [101] we plug in $G = O(M)$. In this case we have $R_1 = T$ the traceless symmetric representation of $O(M)$ and $R_2 = A$

the antisymmetric representation. Thus $P^{R_1}_{ijkl} = \frac{1}{2}(\delta_{ik}\delta_{jl} + \delta_{il}\delta_{jk} - \frac{2}{M}\delta_{ij}\delta_{kl})$ and $P^{R_2}_{ijkl} = \frac{1}{2}(\delta_{ik}\delta_{jl} - \delta_{il}\delta_{jk})$. The projectors then become

$$\begin{aligned}
P^{S\ abcd}_{\ ijkl} &= \frac{1}{MN}\delta^{ab}\delta^{cd}\delta_{ij}\delta_{kl} \\
P^{X\ abcd}_{\ ijkl} &= \frac{1}{M}\delta_{ij}\delta_{kl}\left(\delta^{abcd} - \frac{1}{N}\delta^{ab}\delta^{cd}\right) \\
P^{I_1\ abcd}_{\ ijkl} &= \delta^{abcd}\ P^{R_1}{}_{ijkl} \\
P^{I_2\ abcd}_{\ ijkl} &= \delta^{abcd}\ P^{R_2}{}_{ijkl} \\
P^{Z\ abcd}_{\ ijkl} &= \frac{1}{2}\left(\left(\delta^{ac}\delta^{bd} - \delta^{abcd}\right)\delta_{ik}\delta_{jl} + \left(\delta^{ad}\delta^{bc} - \delta^{abcd}\right)\delta_{il}\delta_{jk}\right) \\
P^{B\ abcd}_{\ ijkl} &= \frac{1}{2}\left(\left(\delta^{ac}\delta^{bd} - \delta^{abcd}\right)\delta_{ik}\delta_{jl} - \left(\delta^{ad}\delta^{bc} - \delta^{abcd}\right)\delta_{il}\delta_{jk}\right)
\end{aligned} \tag{9.11}$$

the dimensions of the representations are $(S,\ X,\ I_1,\ I_2,\ Z,\ B)$ $= (1,\ N-1,\ N\frac{(M-1)(M+2)}{2},\ N\frac{M(M-1)}{2},\ M^2\frac{N(N-1)}{2},\ M^2\frac{N(N-1)}{2})$ which agree with those of [101]. Where $I_1$ here corresponds to $Y$ and $I_2$ to $A$ in that publication.

### 9.3.3 Tetragonal

For the tetragonal case we take $G = Z_2^M \rtimes S_M$. Repeating the same exercise as the two cases above we get

$$\begin{aligned}
P^{S\ abcd}_{\ ijkl} &= \frac{1}{MN}\delta^{ab}\delta^{cd}\delta_{ij}\delta_{kl} \\
P^{X\ abcd}_{\ ijkl} &= \frac{1}{M}\delta_{ij}\delta_{kl}\left(\delta^{abcd} - \frac{1}{N}\delta^{ab}\delta^{cd}\right) \\
P^{I_1\ abcd}_{\ ijkl} &= \delta^{abcd}\ (\delta_{ijkl} - \frac{1}{M}\delta_{ij}\delta_{kl}) \\
P^{I_2\ abcd}_{\ ijkl} &= \delta^{abcd}\ \frac{1}{2}(\delta_{ik}\delta_{jl} + \delta_{il}\delta_{jk} - 2\delta_{ijkl}) \\
P^{I_3\ abcd}_{\ ijkl} &= \delta^{abcd}\ \frac{1}{2}(\delta_{ik}\delta_{jl} - \delta_{il}\delta_{jk}) \\
P^{Z\ abcd}_{\ ijkl} &= \frac{1}{2}\left(\left(\delta^{ac}\delta^{bd} - \delta^{abcd}\right)\delta_{ik}\delta_{jl} + \left(\delta^{ad}\delta^{bc} - \delta^{abcd}\right)\delta_{il}\delta_{jk}\right) \\
P^{B\ abcd}_{\ ijkl} &= \frac{1}{2}\left(\left(\delta^{ac}\delta^{bd} - \delta^{abcd}\right)\delta_{ik}\delta_{jl} - \left(\delta^{ad}\delta^{bc} - \delta^{abcd}\right)\delta_{il}\delta_{jk}\right)
\end{aligned} \tag{9.12}$$

whereas the dimensions of the representations are $(S,\ X,\ I_1,\ I_2,\ I_3,\ Z,\ B)$ $= (1,\ N-1,\ N(M-1),\ N\frac{M(M-1)}{2},\ N\frac{M(M-1)}{2},\ M^2\frac{N(N-1)}{2},\ M^2\frac{N(N-1)}{2})$ plugging in $M = 2$ we recover the results of [101].

## 9.4 Applications

### 9.4.1 $\phi$ - $X$ System Islands

We will use the above results to study the mixed $\phi_i^a$ - $X^{bc}$ system of correlators in the case where $G = O(M)$ [64]. The sum rules derived from the $\langle XXXX\rangle = \langle XXXX\rangle$ crossing equation have already been worked out in 4.2. Also the due to the analysis

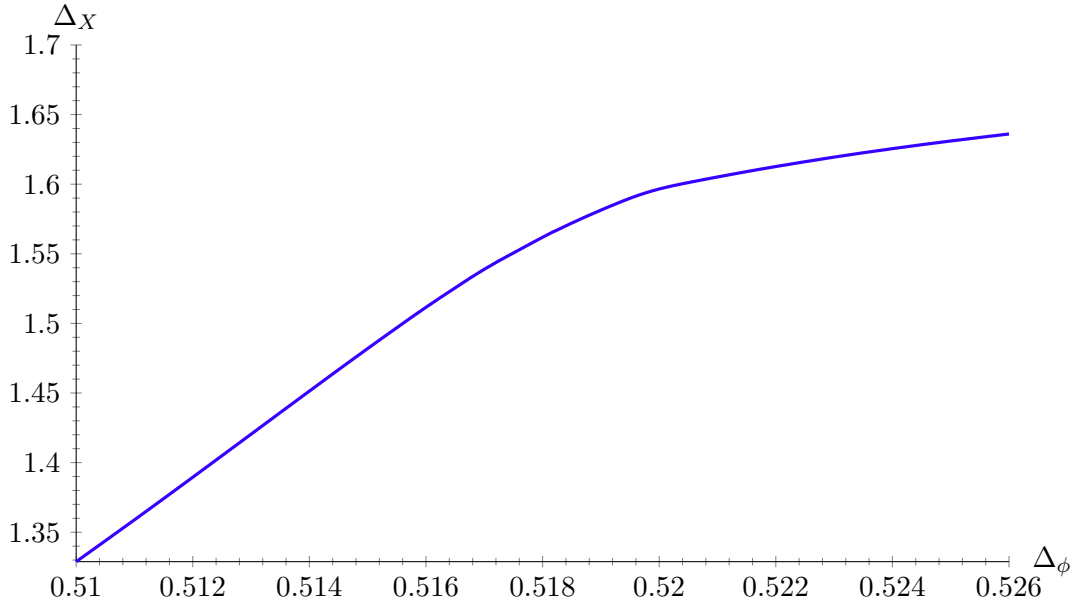


FIGURE 9.1: Single correlator exclusion plot for the scaling dimension of the first $X$ operator for $M = 2$ and $N = 3$. Points above the line are disallowed. The figure was produced using the following parameters in qboot [41]: $\Lambda = 45$, $l = (0 - 50, 55, 56, 59, 60, 64, 65, 69, 70, 74, 75, 79, 80, 84, 85, 89, 90)$ and $\nu_{max} = 20$.

of Appendix B the sum rules due to the crossing equations $\langle\phi X\phi X\rangle = \langle\phi X\phi X\rangle$ and $\langle\phi\phi XX\rangle = \langle X\phi\phi X\rangle$ are already known and we have worked them out in Appendix C. Hence, all that remains to write down the full $\phi$-$X$ system of sum rules, are the sum rules from $\langle\phi\phi\phi\phi\rangle = \langle\phi\phi\phi\phi\rangle$. For $G = O(M)$ these are[1]

$$\sum_{S^+} c_O^2 \begin{pmatrix} 0 \\ F^-_{\Delta,\ell} \\ 0 \\ 0 \\ F^+_{\Delta,\ell} \\ 0 \end{pmatrix} + \sum_{X^+} c_O^2 \begin{pmatrix} 0 \\ -F^-_{\Delta,\ell} \\ nF^-_{\Delta,\ell} \\ 0 \\ -F^+_{\Delta,\ell} \\ nF^+_{\Delta,\ell} \end{pmatrix} + \sum_{Y^+} c_O^2 \begin{pmatrix} 0 \\ 0 \\ \frac{m-2}{2} F^-_{\Delta,\ell} \\ mF^-_{\Delta,\ell} \\ 0 \\ \frac{m-2}{2} F^+_{\Delta,\ell} \end{pmatrix} + \sum_{Z^+} c_O^2 \begin{pmatrix} F^-_{\Delta,\ell} \\ \frac{1}{2} F^-_{\Delta,\ell} \\ -\frac{1}{2} F^-_{\Delta,\ell} \\ -F^-_{\Delta,\ell} \\ -\frac{1}{2} F^+_{\Delta,\ell} \\ +\frac{1}{2} F^+_{\Delta,\ell} \end{pmatrix}$$
$$+ \sum_{A^-} c_O^2 \begin{pmatrix} 0 \\ 0 \\ -\frac{1}{2} F^-_{\Delta,\ell} \\ F^-_{\Delta,\ell} \\ 0 \\ \frac{1}{2} F^+_{\Delta,\ell} \end{pmatrix} + \sum_{B^-} c_O^2 \begin{pmatrix} F^-_{\Delta,\ell} \\ -\frac{1}{2} F^-_{\Delta,\ell} \\ \frac{1}{2} F^-_{\Delta,\ell} \\ -F^-_{\Delta,\ell} \\ \frac{1}{2} F^+_{\Delta,\ell} \\ -\frac{1}{2} F^+_{\Delta,\ell} \end{pmatrix} = \begin{pmatrix} 0 \\ 0 \\ 0 \\ 0 \\ 0 \\ 0 \end{pmatrix}. \tag{9.13}$$

These are completely equivalent to those of [101]. As was noticed in [101] there exist kinks in the $X$ sector, see e.g. Fig 9.1 and Fig 9.4.

Using the multi-correlator system described just above, we may isolate an island

[1] Where we have rescaled some OPE coefficients to simplify some factors of $M$ and $N$. We also wrote $m$ instead of $M$ and $n$ instead of $N$.

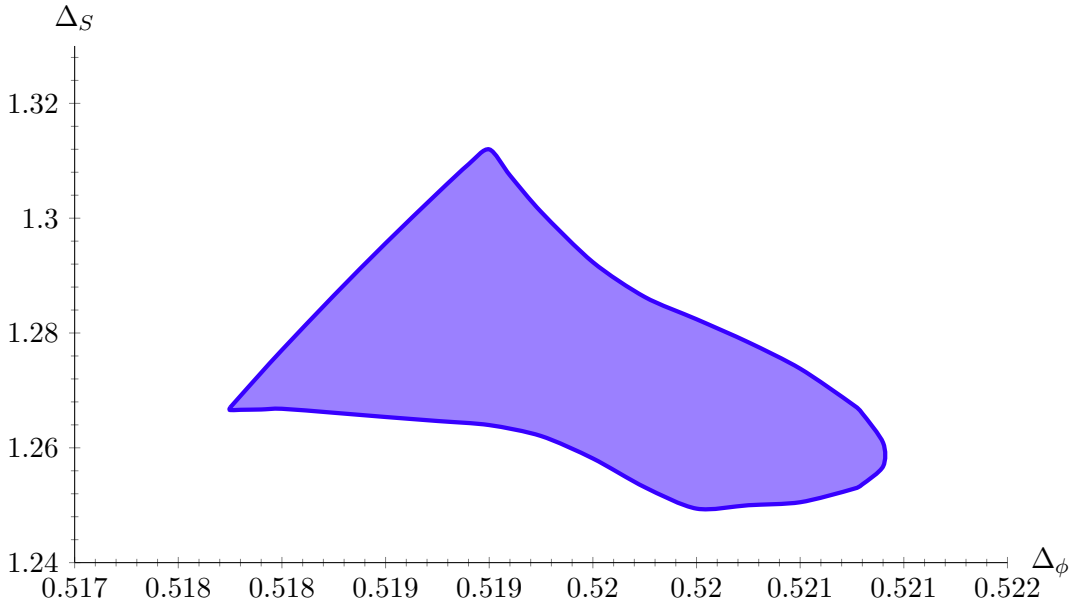


FIGURE 9.2: MN = 2, 3 island corresponding to the fixed point saturating Fig 9.1 obtained using the mixed $\phi_i^a$ - $X^{bc}$ system of correlators. The island assumes that the second $S$, $X$ and $A$ operators have scaling dimensions that satisfy $\Delta \geqslant 3.0$. The first $X$ operator is assumed to have a scaling dimension that saturates Fig 9.1, also the first $A$ operator satisfies $\Delta_A = 2.0$ since it is the conserved vector of $O(M)$. Lastly, we impose $\Delta_{\phi'} \geqslant 1.0$ for the second operator in the defining representation. The figure was produced using the following parameters in qboot [41]: $\Lambda = 27$, $l = (0 - 50, 55, 56, 59, 60, 64, 65, 69, 70, 74, 75, 79, 80, 84, 85, 89, 90)$ and $\nu_{max} = 25$.

corresponding to the $M = 2$ and $N = 3$ $X$ sector kink. This is done in Fig 9.2, the corresponding assumptions are described in the caption. Also, in Fig 9.3 we display the same island but with bigger gaps imposed on various sectors in order to demonstrate that it obtains a more "regular" shape when gaps are pushed higher. Since in Fig 9.3 we are only interested in the shape of the island we only use $\Lambda = 20$. In Fig 9.4 and 9.5 we show the kink in the $X$ sector and its corresponding island for the $M = 2$ and $N = 2$ case. Note that the crossing sum rules are somewhat simpler now. The crossing sum rules in this case are the ones in 9.13, plus the ones in Appendix D in which one must replace the external $S$ operator with an $X$ operator. This simplification occurs because the representation $X$ becomes one dimensional for $N = 2$.

Note that both our islands ($N = 2$ and $N = 3$) do not seem to agree with resummed $\varepsilon$ expansion predictions [70]. This is something that was already noticed in [101] from the single correlator study. For $N = 2$ the $\varepsilon$ expansion gives $\Delta_S = 1.60(2)$ and $\Delta_\phi = 0.517(1)$, whereas for $N = 3$ it gives $\Delta_S = 1.57(2)$ and $\Delta_\phi = 0.5172(8)$.

### 9.4.2 $\langle ZZZZ \rangle$ Single Correlator Bootstrap

As a final application we will bootstrap the crossing equation $\langle Z_{ij}^{ab} Z_{kl}^{cd} Z_{mn}^{ef} Z_{op}^{gh} \rangle = \langle Z_{mn}^{ef} Z_{kl}^{cd} Z_{ij}^{ab} Z_{op}^{gh} \rangle$, where $Z_{ij}^{ab}$ is the operator appearing in 9.7. One motivation for studying this crossing equation are the second kinks that have appeared in the $X$

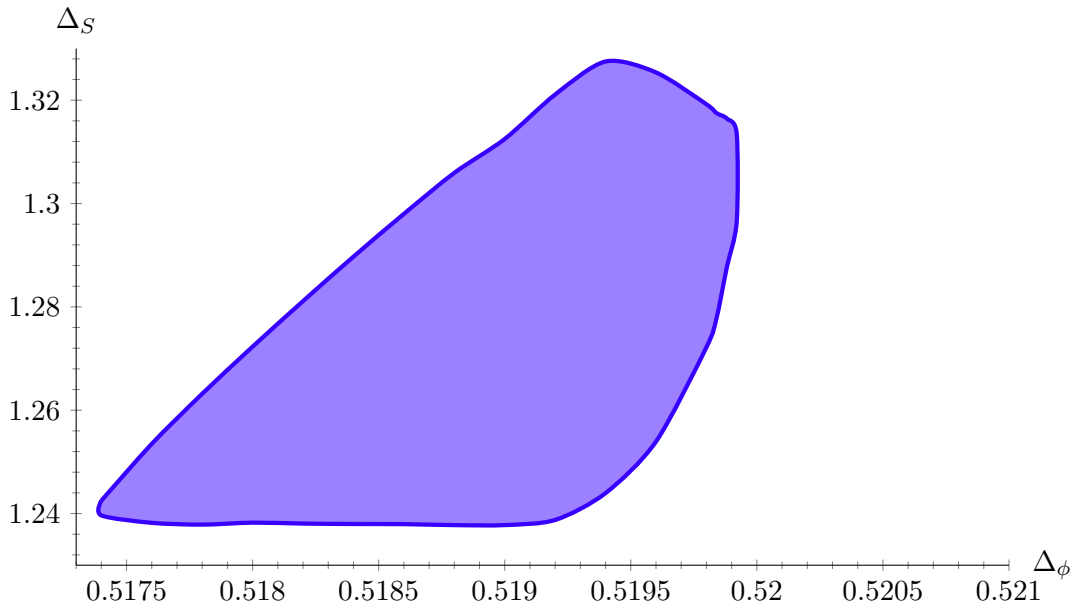


FIGURE 9.3: MN = 2, 3 island corresponding to the fixed point saturating Fig 9.1 obtained using the mixed $\phi_i^a$ - $X^{bc}$ system of correlators. The island assumes that the second $S$, $X$ and $A$ operators have scaling dimensions that satisfy $\Delta_{S'} \geqslant 3.5$, $\Delta_{X'} \geqslant 3.0$ and $\Delta_{A'} \geqslant 3.9$ respectively. The first $X$ operator is assumed to have a scaling dimension that saturates Fig 9.1, also the first $A$ operator satisfies $\Delta_A = 2.0$ since it is the conserved vector of $O(M)$. Lastly, we impose $\Delta_{\phi'} \geqslant 1.5$ for the second operator in the defining representation. The figure was produced using the following parameters in qboot [41]: $\Lambda = 20$, $l = (0 - 50, 55, 56, 59, 60, 64, 65, 69, 70, 74, 75, 79, 80, 84, 85, 89, 90)$ and $\nu_{max} = 25$.

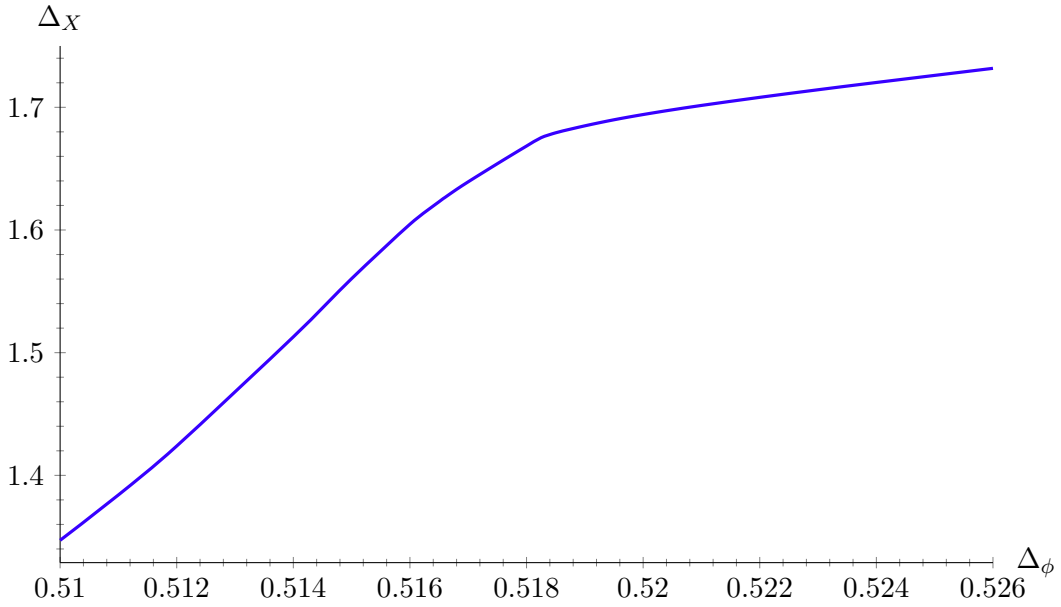


FIGURE 9.4: $\phi$ - $X$ mixed correlator system exclusion plot for the scaling dimension of the first $X$ operator for $M = 2$ and $N = 2$. Points above the line are disallowed. The figure was produced using the following parameters in qboot [41]: $\Lambda = 45$, $l = (0 - 50, 55, 56, 59, 60, 64, 65, 69, 70, 74, 75, 79, 80, 84, 85, 89, 90)$ and $\nu_{max} = 20$. Note that in contrast with Fig 9.1, here we use the full $\phi$ - $X$ system of correlators since it contains less sum rules, and thus is numerically less costly, than the $N = 3$ one.

sector of $S_N \ltimes O(M)^N$ theories, such as in [101] and [48]. We note that the aforementioned studies used the $\langle\phi\phi\phi\phi\rangle = \langle\phi\phi\phi\phi\rangle$ single correlator system. Notably, in [48] the authors found that whatever theory is responsible for the second kink in the $X$ sector has a scaling dimension for the first $Z$ operator very close to the unitarity bound. This makes it a prime candidate for the $\langle Z^{ab}_{ij} Z^{cd}_{kl} Z^{ef}_{mn} Z^{gh}_{op}\rangle = \langle Z^{ef}_{mn} Z^{cd}_{kl} Z^{ab}_{ij} Z^{gh}_{op}\rangle$ (single correlator) bootstrap. In what follows we will work out the crossing equation sum rules only for the $G = O(M)$ and $N = 2$ case for simplicity of demonstration. Since the indices can now only take values 1 and 2, without loss of generality we can work out the tensor structures for $\langle Z^{12}_{ij} Z^{12}_{kl} Z^{12}_{mn} Z^{12}_{op}\rangle = \langle Z^{12}_{mn} Z^{12}_{kl} Z^{12}_{ij} Z^{12}_{op}\rangle$, i.e. we get rid of eight indices in the projectors. In order to decompose onto irreps, whenever lower indices are in the same copy of $O(M)$ we decompose them onto irreps of $O(M)$. Thus, we obtain the following projectors

$$\begin{aligned}
P^{S}{}_{ijklmnop} &= P^{S}_{ikmo} P^{S}_{jlnp} \\
P^{SY}{}_{ijklmnop} &= P^{S}_{ikmo} P^{Y}_{jlnp} + P^{Y}_{ikmo} P^{S}_{jlnp} \\
P^{SA}{}_{ijklmnop} &= P^{S}_{ikmo} P^{A}_{jlnp} + P^{A}_{ikmo} P^{S}_{jlnp} \\
P^{YA}{}_{ijklmnop} &= P^{Y}_{ikmo} P^{A}_{jlnp} + P^{A}_{ikmo} P^{Y}_{jlnp} \\
P^{YY}{}_{ijklmnop} &= P^{Y}_{ikmo} P^{Y}_{jlnp} \\
P^{AA}{}_{ijklmnop} &= P^{A}_{ikmo} P^{A}_{jlnp}
\end{aligned} \tag{9.14}$$

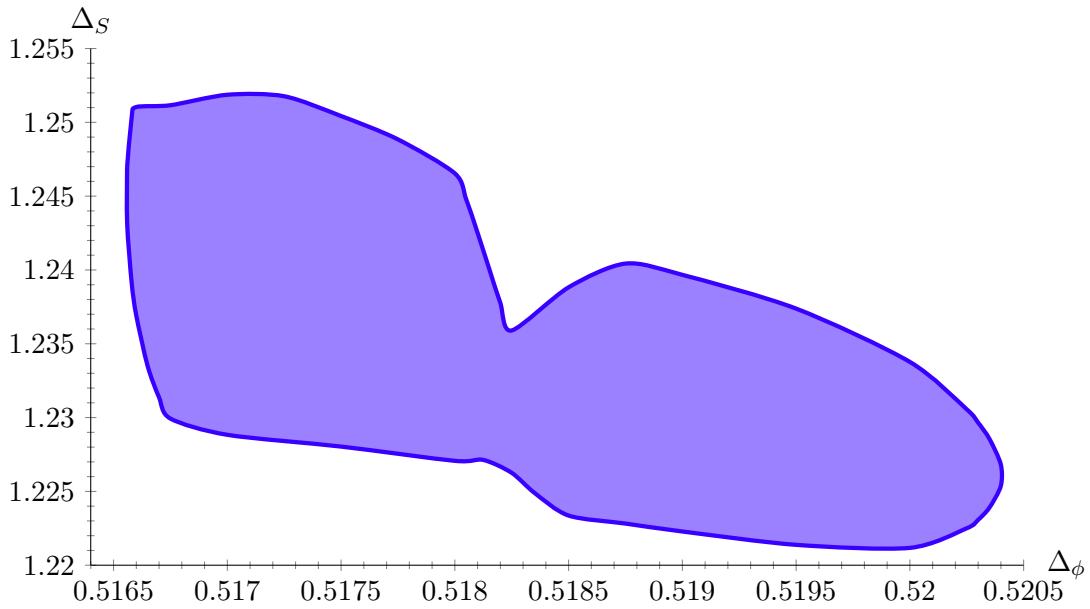


FIGURE 9.5: MN = 2, 2 island corresponding to the fixed point saturating Fig 9.4 obtained using the mixed $\phi_i^a$ - $X^{bc}$ system of correlators. The island assumes that the second $S$, $X$ and $A$ operators have scaling dimensions that satisfy $\Delta \geqslant 3.0$. The first $X$ operator is assumed to have a scaling dimension that saturates Fig 9.1, also the first $A$ operator satisfies $\Delta_A = 2.0$ since it is the conserved vector of $O(M)$. Lastly, we impose $\Delta_{\phi'} \geqslant 1.0$ for the second operator in the defining representation. The figure was produced using the following parameters in qboot [41]: $\Lambda = 35$, $l = (0 - 50, 55, 56, 59, 60, 64, 65, 69, 70, 74, 75, 79, 80, 84, 85, 89, 90)$ and $\nu_{max} = 25$.

where $P^S$, $P^A$ and $P^Y$ are the projectors corresponding to the singlet, the antisymmetric and the traceless symmetric representations of $O(M)$ respectively. From these we obtain the following sum rules[2]

$$\sum_{S^+} c_O^2 \begin{pmatrix} 0 \\ F^-_{\Delta,\ell} \\ 0 \\ 0 \\ 0 \\ F^+_{\Delta,\ell} \end{pmatrix} + \sum_{SY^+} c_O^2 \begin{pmatrix} 0 \\ -2F^-_{\Delta,\ell} \\ F^-_{\Delta,\ell} \\ 2F^-_{\Delta,\ell} \\ -2F^+_{\Delta,\ell} \\ \frac{m-4}{2} F^+_{\Delta,\ell} \end{pmatrix} + \sum_{YY^+} c_O^2 \begin{pmatrix} F^-_{\Delta,\ell} \\ F^-_{\Delta,\ell} \\ -F^-_{\Delta,\ell} \\ (m-2)F^-_{\Delta,\ell} \\ (m+2)F^+_{\Delta,\ell} \\ \frac{2-m-m^2}{2} F^+_{\Delta,\ell} \end{pmatrix} + \sum_{AA^+} c_O^2 \begin{pmatrix} F^-_{\Delta,\ell} \\ 0 \\ 0 \\ 0 \\ -mF^+_{\Delta,\ell} \\ 0 \end{pmatrix}$$
$$+ \sum_{SA^-} c_O^2 \begin{pmatrix} 0 \\ 0 \\ -F^-_{\Delta,\ell} \\ 0 \\ -2F^+_{\Delta,\ell} \\ \frac{m}{2} F^+_{\Delta,\ell} \end{pmatrix} + \sum_{YA^-} c_O^2 \begin{pmatrix} 2F^-_{\Delta,\ell} \\ -m^2 F^-_{\Delta,\ell} \\ F^-_{\Delta,\ell} \\ mF^-_{\Delta,\ell} \\ 2F^+_{\Delta,\ell} \\ \frac{m^2-m}{2} F^+_{\Delta,\ell} \end{pmatrix} = \begin{pmatrix} 0 \\ 0 \\ 0 \\ 0 \\ 0 \\ 0 \end{pmatrix}. \tag{9.15}$$

We can now apply 9.15 to e.g. the $M = 100$ and $N = 2$ case, which we present in Fig 9.6. Note that the kink in Fig 9.6 does not seem to correspond to a known Large $m$ fixed point. This is because the value $\Delta_Z = 0.53$ is much further away from $\Delta_Z = 0.5$ than what is typically expected for a Large $m$ fixed point with $m = 100$. See e.g. the analytic predictions in [48]. Notably, the position of the kink in 9.6 seems to be in agreement with the extremal functional prediction of [48] with respect to the position of the fixed point in the $\Delta_Z$ axis. In the $\Delta_Y$ axis the kink in our plot seems to be in agreement with the second $Y$ operator in the spectrum of [48]. In other words our plot does not "see" the first $Y$ operator seen in [48][3]. One possible explanation for this would be that the first $Y$ operator appears in the $\phi \times \phi$ OPE but not the $Z \times Z$ OPE. We cannot presently comment further on this.

[2] With various rescalings in order to simplify some factors. Also we again denote $M$ by $m$.

[3] It has been checked that the zero in the extremal functional presented in [48] which corresponds to the first $Y$ operator in the $\phi \times \phi$ OPE is not spurious. This was done by raising the gap in the $Y$ sector above the dimension of the first $Y$ operator, and checking that the corresponding kink in the $X$ sector disappears.

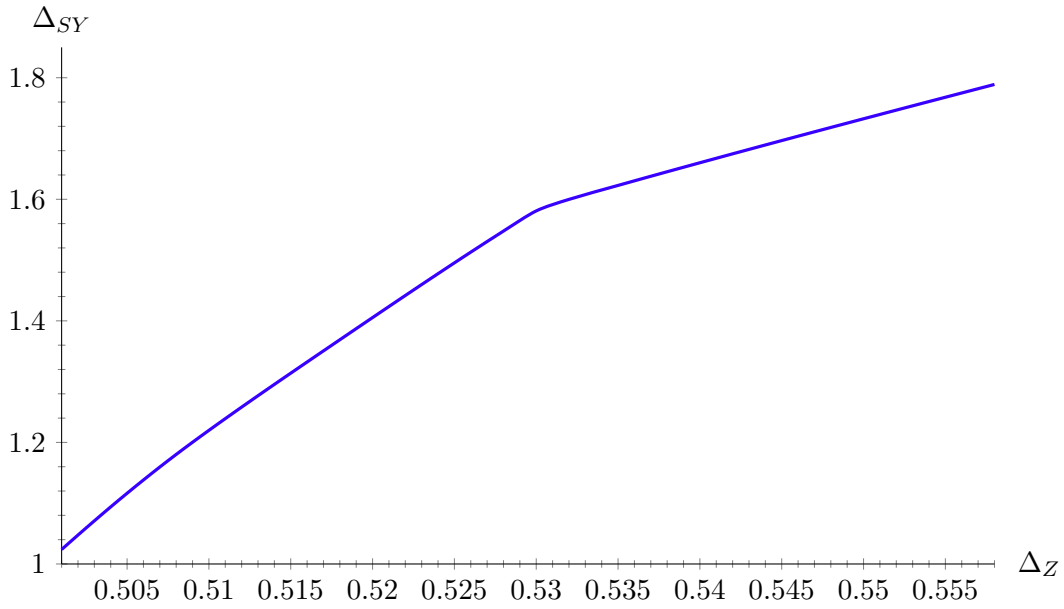


FIGURE 9.6: Single correlator exclusion plot for the scaling dimension of the first $SY$ (note that $SY = Y$) operator for $M = 100$ and $N = 2$ appearing in the $Z \times Z$ OPE. Points above the line are disallowed. The figure was produced using the following parameters in qboot [41]: $\Lambda = 20$, $l = (0 - 50, 55, 56, 59, 60, 64, 65, 69, 70, 74, 75, 79, 80, 84, 85, 89, 90)$ and $\nu_{max} = 25$.

# Chapter 10

# Discussion and Future Directions

In the main part of the thesis we studied three classes of CFTs numerically. These were CFTs with $S_n \ltimes (Z_2)^n$, $O(m) \times O(n)/Z_2$ and $S_n \ltimes O(m)^n$ global symmetry. In the case of cubic CFTs we found evidence of a new CFT that appears to be in very good agreement with certain experimental data for perovskites. Specifically, in one of the experiments our conjectured Platonic CFT is closer to the experimental data for critical exponents than any other known relevant CFT. Consequently, we aimed to obtain a closed isolated region in parameter space, without assuming that the theory lives on the $X$ sector exclusion bound. One of the main motivations in doing this is to show that one can still obtain a theory without imposing that it must extremize a direction in parameter space. An assumption which is somewhat arbitrary from the physics point of view. We were able to drop the assumption of $X$ sector saturation by scanning over the dimensions of three low lying operators of the theory. This has the upshot of bringing the theory to a form that is systematically improvable in the future. By e.g. using of the new technology developed in [92] we may scan over OPE coefficient ratios in addition to the scaling dimensions. We expect this to dramatically shrink the allowed region, and hence drastically improve our determinations of the critical exponents.

In our study of $O(m) \times O(n)/Z_2$ theories we found the technique that provided the most robust predictions to be the large $n$ expansion. We found excellent agreement in all sectors we looked at. More specifically, we found that the chiral and anti-chiral fixed points in the large $n$, and fixed $m = 2$, limit saturate the single correlator exclusion bound in two different sectors. Consequently, assuming the saturation of these bounds we found islands which determined the scaling dimensions of the scalar singlet $S$ and the bifundamental $\phi_{ar}$ operators. We again found good agreement between these operators and their large $n$ predictions. In order to make contact with six loop resummed $\varepsilon$ expansion predictions, we studied the $m = 2$ and $n = 6$ case. We found the predictions here to be less accurate than the large $n$ predictions, but still in the correct ballpark. Lastly, in order to investigate the possible fixed points found in resummations we looked at the $m = 2$ and $n = 3$ cases, in which we found two islands. Unfortunately, given the large spread in the theoretical predictions we could not make a meaningful comparison between the bootstrap and the perturbative data. Note that the fixed points found in resummations are expected to have operators with complex scaling dimensions. More specifically, these operators are certain subleading (in terms of scaling dimension) scalar singlets which happen to be the eigenvectors of the stability matrix[1]. The key point, though, is that the couplings in these theories are real, hence they should be experimentally accessible. Although the numerical bootstrap in its current implementation is only supposed

[1] We remind the reader that by stability matrix we mean the matrix of derivatives of the beta functions corresponding to the quartic couplings.

to find unitary theories, it has been known to also pick up islands for non-unitary theories, see e.g. [9], [68]. Notably, in [68] the island disappeared once the numerical precision was pushed. We cannot comment at the present stage whether the islands we find correspond to the non-unitary theories from the resummations or some other hitherto unknown CFTs. If our islands do correspond to the non-unitary theories we expect them to eventually disappear once we push the numerics further.

In the last main part of the thesis we presented work in progress for $S_n \ltimes O(m)^n$ theories and also worked out the projectors in the general case of $S_n \ltimes G^n$, where $G$ is arbitrary. We presented two islands, one for $n = 2$ and one for $n = 3$ both with $G = O(2)$, which are relevant to experiments[2]. Consequently, we studied the single correlator bootstrap of a 4-pt function consisting of $Z$ operators. Doing this we found a kink that seems to correspond to the second kinks in the $X$ sector reported in [101] and [48].

Many natural extensions can be considered regarding the work presented in this thesis. One first direction, especially since the development of [92] which simplified higher dimensional scans, is to improve upon the results of Chapter 5 where we performed a $3D$ scan in parameter space. See e.g. Fig 5.9. Since we have already proven that the three dimensional space which is spanned by the scaling dimensions $(\Delta_\phi, \Delta_S, \Delta_Y)$ can be reduced to an island around the Platonic theory[3], we may improve our results by including $Y_{ij}$ as an external operator and furthermore scanning over OPE coefficient ratios. This should lead to a considerably smaller island which would give very precise estimates for critical exponents. These precision critical exponents should then provide significant motivation for experimentalists to study the theory. Another similar direction is the study of the two flavour "cubic" theory, i.e. $C_2 = S_2 \ltimes Z_2^2$. This is expected to be somewhat similar to the Platonic theory (unpublished work). Using the techniques described above we would like to also provide precision exponents for this theory as well. Lastly, with regards to cubic theories we would also like to study the theories responsible for the kinks in 5.2. One possibility that needs to be tested, is the existence of a theory responsible for the kinks which is close to the unitarity bound. Such as what we found in Fig 9.6. This would be important since the bootstrap tends to lose constraining power away from the unitarity bound. Additionally, proximity to the unitarity bound might hint at perturbative accessibility.

With regards to $O(m) \times O(n)$ theories, although fixed points in the large $n$ limit seem to be understood quite well, the small $n$ fixed points remain contentious. We would like to study e.g. the $O(2) \times O(3)$ case in Fig 8.9 and try and determine with certainty if it is indeed the fixed point found in resummations or some other new unknown (or known) fixed point. If it is the fixed point found in resummations it is expected to have operators with complex scaling dimensions, hence we expect the unitary numerical bootstrap to exclude it once it is able to see the non-unitarity in practice. This could happen at some a priory unknown number of components included in the bootstrap functional. A similar strategy was employed in [68], where the island the authors were studying disappeared once the constraints were sufficiently increased. This strategy, should in the worst case scenario shrink the island considerably providing tighter estimates of critical exponents.

[2] See for example [71] [72] [7] and [73]. See also Appendix E.

[3] Plus other possible disconnected allowed regions we do not currently need to know about.

We also plan to study the cubic fixed point of the $\varepsilon$ expansion[4]. Although one can get preliminary islands including the $\varepsilon$ expansion cubic theory, these islands also include the $O(3)$ theory (unpublished work). Using the results of [92] we plan to shrink this island enough such that it is finally distinct from the $O(3)$ island.

There are numerous other projects, in addition to the ones described above, that we may also pursue. Such as the study of biconical (type) theories, these can be expressed with e.g. a Hamiltonian $\mathcal{H} = \mathcal{H}_1 + \mathcal{H}_2 + \mathcal{H}_{12}$ where $\mathcal{H}_1$ is a Hamiltonian with symmetry $G_1$, $\mathcal{H}_2$ a Hamiltonian with symmetry $G_2$ and $\mathcal{H}_{12}$ is a term that couples $G_1$ with $G_2$. Hopefully, though, we have at this point convinced the reader that the study of $3D$ CFTs, even in arguably the simplest case i.e. scalar field theories is a largely unresolved and exciting field of research. Their systematic study should have a direct impact on phenomenology and experiments, and in addition deepen our understanding of field theory both perturbative and non-perturbative.

[4]Which we remind is different from the Platonic one.

# Appendix A

# Generic Projectors of 4-pt Functions

## A.1 $\langle\phi_i\phi_j\phi_k\phi_l\rangle$ and $\langle\phi_i O_{jk}\phi_l O_{mn}\rangle$ Type Projectors

We remind the reader that we use the terms "tensor structure" and "projector" interchangeably, usually by slight abuse of terminology since we do not always normalize the tensor structures appropriately. It is useful to recall/re-derive some generic properties these projectors have that are independent of the respective global symmetry. Let us first for simplicity consider the 4-pt function of operators in the defining [1] representation of some arbitrary global symmetry group $G$.

$$\langle\phi_i\phi_j\phi_k\phi_l\rangle \sim \sum_R P^R_{ijkl}(....) \tag{A.1}$$

where $P^R_{ijkl}$ is what we call the projector. It is typically made up of invariant tensors of $G$. We label the irreps of $G$ with $R$. Lastly, the .... in A.1 contains everything independent of the global symmetry tensor structures. Next we assume a decomposition of the following schematic form for the OPE

$$\phi_i \times \phi_j \sim \sum_R O^R_{ij} \tag{A.2}$$

where we leave OPE coefficients implicit, thus

$$\sum_R \sum_{R'} \langle O^R_{ij} O^{R'}_{kl}\rangle \sim \sum_R P^R_{ijkl}(....) \tag{A.3}$$

using the fact that a two point function between non-identical operators vanishes we get

$$P^R_{ijkl} \sim \langle O^R_{ij} O^R_{kl}\rangle \tag{A.4}$$

contracting both sides with $P^R_{klmn}$ and using one of the defining properties of projectors, namely $P^R_{ijkl}P^R_{klmn} = P^R_{ijmn}$ , we obtain

$$O^R_{ij} = P^R_{ijkl} O^R_{kl} \tag{A.5}$$

which can be solved leading to

$$O^R_{ij} = P^R_{ijkl}\phi_k\phi_l \tag{A.6}$$

[1] See the "List of Abbreviations" in the beginning of the thesis.

At this point it is important to stress that A.6 is only correct at the level of group theory. This is because, in general, we can have arbitrary powers of $\phi$ appearing in the OPE of $\phi$ with itself. The fact that we include only two powers of $\phi$ in A.6 will not affect any of our results with respect to the projectors. With this in mind, we plug A.6 into A.2

$$\phi_i \times \phi_j \sim \sum_R P^R_{ijkl}\phi_k\phi_l \tag{A.7}$$

this leads to

$$\sum_R P^R_{ijkl} \sim \delta_{ik}\delta_{jl} \tag{A.8}$$

We can also generalize A.7 for operators in different representations, two particularly useful examples are:

$$\phi_i O^R_{jk} \sim \sum_{R'} P^{R'}_{ijklmn}\phi_l O^R_{mn} \tag{A.9}$$

and

$$O^R_{ij}O^R_{kl} \sim \sum_{R'} P^{R'}_{ijklmnop}O^R_{mn}O^R_{op} \tag{A.10}$$

where in A.9 and A.10 $R$ may, or may not, appear in the sum over $R'$, depending on the specific group $G$. For an explicit application of A.9 in calculating a tensor structure see Appendix B.

## A.2 $\langle\phi_i\phi_j O_{kl}O_{mn}\rangle$ Type Projectors

When our 4-pt function of interest looks like $\langle\phi_i\phi_j O_{kl}O_{mn}\rangle$, we can obtain some slightly different consistency equations for the projectors. Assume that the $\phi \times \phi$ and $O \times O$ OPEs have at least one representation in common which we will call $R$, we then have

$$\langle\phi_i\phi_j O_{kl}O_{mn}\rangle \sim P^R_{ijklmn} + ... \tag{A.11}$$

consequently, following the analysis of the previous section we may act on both sides with the four-index projector remembering that $O^R_{ij} = P^R_{ijkl}\phi_k\phi_l$ from A.6, hence

$$\langle O^R_{op}O_{kl}O_{mn}\rangle \sim P^R_{opij}P^R_{ijklmn} + ... \tag{A.12}$$

now the left hand side is only non zero if the $O \times O$ OPE exchanges the operator $O^R$. For the right hand side to match we must then have

$$P^R_{opij}P^R_{ijklmn} = P^R_{opklmn} \tag{A.13}$$

and

$$P^{R'}_{opij}P^R_{ijklmn} = 0 \tag{A.14}$$

where in A.14 $R'$ is assumed to be different from $R$. These equations, and those of the preceding section, are extremely useful for calculating projectors in practice, as well as checking that all calculations are consistent.

# Appendix B

# Six Index Projectors in Cubic Theories

We start with relation A.9, for six index projectors, restricted to the case of two irreps

$$\phi_i X_{jk} \sim P^{\phi}_{ijklmn}\phi_l X_{mn} + P^{A}_{ijklmn}\phi_l X_{mn} \tag{B.1}$$

Knowing that the three elements of the representation $A$ are ( $\phi_1(X_{22}-X_{33})$ , $\phi_2(X_{33}-X_{11})$ , $\phi_3(X_{11}-X_{22})$ ) we can ask "What is the form of the projector $P^{A}_{ijklmn}$ such that B.1 is consistent ?"

The answer is

$$\begin{aligned} P^{A}_{ijklmn} = {} & \delta_{i1}\delta_{l1}(\delta_{j2}\delta_{k2}-\delta_{j3}\delta_{k3})(\delta_{m2}\delta_{n2}-\delta_{m3}\delta_{n3}) \\ & \delta_{i2}\delta_{l2}(\delta_{j3}\delta_{k3}-\delta_{j1}\delta_{k1})(\delta_{m3}\delta_{n3}-\delta_{m1}\delta_{n1}) \\ & \delta_{i3}\delta_{l3}(\delta_{j1}\delta_{k1}-\delta_{j2}\delta_{k2})(\delta_{m1}\delta_{n1}-\delta_{m2}\delta_{n2}) \end{aligned} \tag{B.2}$$

which can be checked by contracting B.2 on to $\phi_l X_{mn}$. We would like to bring B.2 into a more convenient form. To do this we write the most general ansatz possible, keeping in mind that we must always obey $j=k$ and $m=n$:

$$P^{A}_{ijklmn} = a\delta_{ijklmn} + b\delta_{il}\delta_{jkmn} + c(\delta_{jk}\delta_{ilmn}+\delta_{mn}\delta_{ijkl}) + d\delta_{il}\delta_{jk}\delta_{mn} \tag{B.3}$$

comparing B.2 and B.3 we have

$$\begin{aligned} P^{A}_{122133} &= d = -1 \\ P^{A}_{122111} &= c+d = 0 \\ P^{A}_{122122} &= b+d = 1 \\ P^{A}_{111111} &= a+b+2c+d = 0 \end{aligned} \tag{B.4}$$

hence, ($a$ , $b$ , $c$ , $d$)= ($-3$ , $2$ , $1$ , $-1$) and

$$P^{A}_{ijklmn} = -3\delta_{ijklmn} + 2\delta_{il}\delta_{jkmn} + (\delta_{jk}\delta_{ilmn}+\delta_{mn}\delta_{ijkl}) - \delta_{il}\delta_{jk}\delta_{mn} \tag{B.5}$$

One can check that the generalization to any number of index values $N$ is

$$P^{A}_{ijklmn} = -\delta_{ijklmn} + \frac{N-1}{N}\delta_{il}\delta_{jkmn} + \frac{1}{N}(\delta_{jk}\delta_{ilmn} + \delta_{mn}\delta_{ijkl}) - \frac{1}{N}\delta_{il}\delta_{jk}\delta_{mn} \tag{B.6}$$

where we have divided by a factor of $N$ compared to B.5. Also, for completeness, note that $P^{\phi}_{ijklmn}$ is (for general $N$)

$$P^{\phi}_{ijklmn} = \delta_{ijklmn} - \frac{1}{N}(\delta_{jk}\delta_{ilmn} + \delta_{mn}\delta_{ijkl}) + \frac{1}{N^2}\delta_{il}\delta_{jk}\delta_{mn} \tag{B.7}$$

Remarkably these invariant tensors can by used not only for Hypercubic theories ($C_N = Z_2^N \rtimes S_N$), but for any theory with the symmetry $G' = G^N \rtimes S_N$ where $G$ is arbitrary. This is because the operator $X_{ij}$ is always a singlet of $G$. The only needed modification is the multiplication of B.6 and B.7 with $\delta_{rs}$ where $r$ and $s$ are $G$ indices (i.e. we have $\phi_i^r$ instead of $\phi_i$ when $G \neq Z_2$). An important observation is that $\delta_{rs}$ factors out, thus it does not affect the crossing equation sum rules at all.

# Appendix C

# $\phi - X$ crossing equations in generic theories

## C.1 $\langle \phi X \phi X \rangle = \langle \phi X \phi X \rangle$ and $\langle \phi \phi X X \rangle = \langle x \phi \phi X \rangle$ crossing sum rules

Note that for the 6 index projectors (B.6, B.7, 4.32, 4.33) we have the following two relations (defining $P^1 = P^S$, $P^2 = P^X$, $P^3 = P^\phi$ and $P^4 = P^A$)

$$P^3 = P^2 + \frac{1}{N} P^1 \tag{C.1}$$

$$P^4 = -P^2 + \frac{1}{N} P^1 \tag{C.2}$$

where we have left all indices implicit. Then 5.7 applied to the crossing equation $\langle \phi\phi XX \rangle = \langle X\phi\phi X \rangle$ leads to

$$\begin{aligned} 0 = \sum_O [ & \lambda_{\phi\phi O_{S+}} \lambda_{XXO_{S+}} P^1 F^{\phi\phi,XX}_{\mp,\Delta,l} + \lambda_{\phi\phi O_{X+}} \lambda_{XXO_{X+}} P^2 F^{\phi\phi,XX}_{\mp,\Delta,l} \\ & \pm (-1)^l (P^2 + \frac{1}{N} P^1) \lambda^2_{\phi X O_y} F^{X\phi,\phi X}_{\mp,\Delta,l} \\ & \pm (-1)^l (-P^2 + \frac{1}{N} P^1) \lambda^2_{\phi X O_A} F^{X\phi,\phi X}_{\mp,\Delta,l} ] \end{aligned} \tag{C.3}$$

consequently, the terms multiplying $P^1$ give one pair of sum rules, and the terms multiplying $P^2$ give another (all indices on the projectors above have been dropped since they are identical).

$$\sum_O (\lambda_{\phi\phi O_{S+}} \lambda_{XXO_{S+}} F^{\phi\phi,XX}_{\mp,\Delta,l} \pm (-1)^l \frac{1}{N} \lambda^2_{\phi X O_y} F^{X\phi,\phi X}_{\mp,\Delta,l} \pm (-1)^l \frac{1}{N} \lambda^2_{\phi X O_A} F^{X\phi,\phi X}_{\mp,\Delta,l}) = 0 \tag{C.4}$$

$$\sum_O (\lambda_{\phi\phi O_{X+}} \lambda_{XXO_{X+}} F^{\phi\phi,XX}_{\mp,\Delta,l} \pm (-1)^l \lambda^2_{\phi X O_y} F^{X\phi,\phi X}_{\mp,\Delta,l} \mp (-1)^l \lambda^2_{\phi X O_A} F^{X\phi,\phi X}_{\mp,\Delta,l}) = 0 \tag{C.5}$$

As explained in Appendix B these equations are valid for any group $G' = G^N \rtimes S_N$ with $G$ arbitrary[1]. Lastly, since $P^A_{ijklmn} = P^A_{ljkimn}$ and $P^\phi_{ijklmn} = P^\phi_{ljkimn}$ , the sum rules derived from $\langle \phi X \phi X \rangle = \langle \phi X \phi X \rangle$ are easily worked out to be

[1] Assuming that $N \geqslant 3$. Since otherwise we have less representations appearing on the right hand side of the $\phi \times X$ OPE.

$$\sum_O \lambda^2_{\phi X O_A} F^{\phi X,\phi X}_{\mp,\Delta,l} = 0 \tag{C.6}$$

and

$$\sum_O \lambda^2_{\phi X O_\phi} F^{\phi X,\phi X}_{\mp,\Delta,l} = 0 \tag{C.7}$$

In all the above "+" subscripts on operators are used to denote that the sum should be taken only over even-spin operators. Whereas if there is no subscript the sum runs both over even and odd-spin operators.

## C.2 $\langle XXXX\rangle = \langle XXXX\rangle$ crossing sum rules

As explained in Section 4.2 the operator $X$ transforms in the defining representation of $S_N$. The crossing sum rules for $Z_2 \times S_N$[2] have been worked out in [100] and [93] hence we do not repeat the calculation here and simply report the results of [100].

$$\sum_{S^+} c_O^2 \begin{pmatrix} 0 \\ F^-_{\Delta,\ell} \\ F^+_{\Delta,\ell} \\ 0 \end{pmatrix} + \sum_{X^+} c_O^2 \begin{pmatrix} 0 \\ 0 \\ -\frac{4}{N+1} F^+_{\Delta,\ell} \\ F^-_{\Delta,\ell} \end{pmatrix} + \sum_{Y^+} c_O^2 \begin{pmatrix} F^-_{\Delta,\ell} \\ \frac{2(N-1)}{N} F^-_{\Delta,\ell} \\ -\frac{(N+1)(N-2)}{N(N-1)} F^+_{\Delta,\ell} \\ -\frac{N+1}{2(N-1)} F^-_{\Delta,\ell} \end{pmatrix} + \sum_{\bar{S}^-} c_O^2 \begin{pmatrix} F^-_{\Delta,\ell} \\ 0 \\ F^+_{\Delta,\ell} \\ 0 \end{pmatrix} = \begin{pmatrix} 0 \\ 0 \\ 0 \\ 0 \end{pmatrix}. \tag{C.8}$$

### C.2.1 The case $N = 3$

The $N = 3$ $\langle XXXX\rangle$ = $\langle XXXX\rangle$ crossing equation has the same sum rules as the $O(2)$ vector model. This can be seen since $S_3$ is a subgroup of $O(2)$ and they share the same irreps on the right hand side of the OPE. Alternatively, one can derive the crossing equations using the projectors from Section 4.2. The sum rules can be found in e.g. [60].

$$\sum_{S^+} c_O^2 \begin{pmatrix} 0 \\ F^-_{\Delta,\ell} \\ F^+_{\Delta,\ell} \end{pmatrix} + \sum_{X^+} c_O^2 \begin{pmatrix} F^-_{\Delta,\ell} \\ 0 \\ -2F^+_{\Delta,\ell} \end{pmatrix} + \sum_{\bar{S}^-} c_O^2 \begin{pmatrix} F^-_{\Delta,\ell} \\ -F^-_{\Delta,\ell} \\ F^+_{\Delta,\ell} \end{pmatrix} = \begin{pmatrix} 0 \\ 0 \\ 0 \end{pmatrix}$$

From the viewpoint of invariant tensors, the sum rules are reduced from four to three in the $N = 3$ case due to 4.23.

[2] These crossing equations are the same as if we had neglected the $Z_2$ in $Z_2 \times S_N$. The only difference is that we will allow $X$ to appear in the $X \times X$ OPE. Which we could not do if we had the $Z_2$.

# Appendix D

# $O_a$-$S$ System of Correlators Sum Rules

In this appendix we write down the sum rules resulting from the crossing equations $\langle O_a O_b SS\rangle = \langle SO_b O_a S\rangle$, $\langle O_a SO_b S\rangle = \langle O_b SO_a S\rangle$ and $\langle SSSS\rangle = \langle SSSS\rangle$. Where $O_a$ should be thought of as some arbitrary scalar operator (with respect to space-time transformations) in some arbitrary representation of some arbitrary group, with its indices collectively and schematically denoted by $a$.

The relevant OPEs schematically are

$$O_a \times S \sim O_a \tag{D.1}$$

and

$$S \times S \sim S \tag{D.2}$$

where on the right hand side we have left the sum over all possible operators in a given representation and their OPE coefficients implicit. Plugging these formulas in to the aforementioned correlators we obtain (schematically)

$$\langle O_a SO_b S\rangle \sim \langle O_a O_b\rangle \sim r_{ab} \tag{D.3}$$

and

$$\langle O_a O_b SS\rangle \sim r_{ab}\langle SS\rangle \tag{D.4}$$

where $r_{ab}$ is some appropriate tensor that we do not need to write explicitly for our present purposes.

With D.3 and D.4 in hand, and using 5.7, we obtain the following sum rules

$$\sum_{S^+} \lambda^2_{SSO_S} F^{-SS,SS}_{\Delta,l} = 0 \tag{D.5}$$

$$\sum_{V^\pm} \lambda^2_{OSO_V} F^{-OS,OS}_{\Delta,l} = 0 \tag{D.6}$$

$$\sum_{S^+} \lambda_{OOO_S}\lambda_{SSO_S} F^{\mp OO,SS}_{\Delta,l} \pm \sum_{V^\pm} (-1)^l \lambda^2_{OSO_V} F^{\mp SO,OS}_{\Delta,l} = 0 \tag{D.7}$$

where $V$ in this case denotes the representation $O_a$ transforms in. The superscripts on the irreps that are summed over denote the allowed spins of the exchanged operators (even/odd).

# Appendix E

# Emergence of $O(2) \times O(n)$ symmetry in physical systems

We will show in two separate cases, namely helimagnets and stacked triangular antiferromagnets, how a $O(2) \times O(n)$ global symmetry can emerge. The global symmetry of the microscopic system, i.e. the lattice system, in both cases will be $O(n)$.

## E.1 Stacked Triangular Antiferromagnets

We will consider a lattice made up of stacked triangular sub-lattices. For example, to build one in three dimensions, we need to stack two dimensional lattices. Each of the two dimensional lattices is made up by placing particles on the vertices of equilateral triangles[1]. Thus, nearest neighbours of a given particle in the sub-lattice are positioned at angles of $\frac{2\pi}{6}$ between each other. For figures see e.g. [56]. Our starting point will be the microscopic Hamiltonian

$$H = \sum_{ij} J_{ij} \vec{S}_i \cdot \vec{S}_j + \sum_{ij} J'_{ij} \vec{S}_i \cdot \vec{S}_j \tag{E.1}$$

where the first sum runs over antiferromagnetic nearest neighbor interactions within the plane of the triangular lattice, and the second sum runs over nearest neighbors in the transverse direction[2]. As will become apparent, it is not very important what the sign of $J'$ is, as long as it is not zero. If it were zero the dimensionality of the system would reduce but the global symmetry would be unchanged[3]. We can use a Hubbard-Stratonovich transformation to exchange the fixed length spins in E.1 for unconstrained length spins, see [40] for a pedagogic review. This leads us to the following expression in wave vector space[4]

$$H = \sum_{q} (E(q) + m_0^2) \vec{S}_q \cdot \vec{S}_{-q} + g \sum_{q_1,q_2,q_3,q_4} \delta(q_1 + q_2 + q_3 + q_4) \vec{S}_{q_1} \cdot \vec{S}_{q_2} \vec{S}_{q_3} \cdot \vec{S}_{q_4} \tag{E.2}$$

the quantities $m_0^2$ and $g$ in E.2 are related to those in E.1. The only information we need is that $E(q)$ is related to the Fourrier transform of $J$ and $J'$. The couplings $J$ and $J'$, as a function of the coordinates, are by definition only non zero at the location of nearest neighbours. Thus, they may be parametrized as $J \sim \delta(r-a)\delta(z) \sum_{\theta_i} \delta(\theta - \theta_i)$ where $(r^2 = x^2 + y^2)$ and $J' \sim \delta(|z| - b)\delta(x)\delta(y)$. Where $a$ is the distance between

[1] This is a hexagonal lattice with particles also in the center of each cell.

[2] I.e. the direction in which we stack the sub-lattices.

[3] In other words the system would be described by a $D = d - 1$ dimensional field theory.

[4] By abuse of notation we use the same symbol $S$ for both the constrained and unconstrained length spin.

nearest neighbours in the $x-y$ plane, $b$ is the distance between nearest neighbours located at two different planes (i.e. they are located at different values of $z$) and $\theta_i = 2N\pi/6$ are the angles at which nearest neighbours are located. The distances $a$ and $b$ can be rescaled to unity without harm of generality. We then have

$$J(q) \sim \sum_{q_x}\sum_{q_y} e^{iq_x x} e^{iq_y y} \delta(r-1) \sum_{\theta_i} \delta(\theta - \theta_i) \tag{E.3}$$

using $x = rcos\theta$ and $y = rsin\theta$ we obtain

$$J(q) \sim cos(q_x) + 2cos(\frac{q_x}{2})cos(\frac{\sqrt{3}q_y}{2}) \tag{E.4}$$

including the contribution of the $J'$ term we obtain (for $d \geqslant 3$)

$$E(q) \sim J(q) + J'(q) \sim cos(q_x) + 2cos(\frac{q_x}{2})cos(\frac{\sqrt{3}q_y}{2}) + k(cos(q_3) + ... + cos(q_d)) \tag{E.5}$$

where $k$ is proportional to the ratio of the two couplings in E.1. Also, $q_3 = q_z$ etc. The present author became aware of E.5 from [55].

One can check that E.5 has two minima

$$q_{min} = \pm Q = \pm(\frac{4\pi}{3}, 0, 0, ..., 0) \tag{E.6}$$

In order to study the theory we must expand around its minima. We have

$$\begin{aligned} S_r &= \sum_q e^{iqr} S_q \\ \Rightarrow S_r &= \sum_{q\to Q} e^{iqr} S_q + \sum_{q\to -Q} e^{iqr} S_q \\ \Rightarrow S_r &= \sum_{q\to 0} (S_{q-Q} e^{i(q-Q)r} + S_{q+Q} e^{i(q+Q)r}) \end{aligned} \tag{E.7}$$

where in the second line we have split the sum and kept only the dominant contributions, which are centered around the two minima. In the third line we redefined the variable summed over in order to collapse everything into one sum. We now define $A_q = S_{q+Q}$ and $B_q = S_{q-Q}$, thus

$$S_q^\star = S_{-q} \Rightarrow A_q^\star = B_{-q} \quad and \quad B_q^\star = A_{-q} \tag{E.8}$$

Using all the above, E.2 may be recast in the following form

$$\begin{aligned} H &= \sum_q (q^2 + m^2)(|A|^2 + |B|^2) \\ &+ g' \sum_{q_1,q_2,q_3,q_4} \delta(q_1+q_2+q_3+q_4)(\vec{A}_{q_1}\cdot\vec{A}_{q_2}\vec{B}_{q_3}\cdot\vec{B}_{q_4} + 2\vec{A}_{q_1}\cdot\vec{B}_{q_2}\vec{A}_{q_3}\cdot\vec{B}_{q_4}) \end{aligned} \tag{E.9}$$

where we have expanded in $q$ around the minima of $E(q)$. We can further define the combinations $\vec{\phi}_1 = (\vec{A} + \vec{B})/2$ and $\vec{\phi}_2 = (\vec{A} - \vec{B})/2i$, and finally Fourrier transform

back to real space to get

$$H = \frac{1}{2}\sum_a \partial_\mu \vec{\phi}_a \cdot \partial^\mu \vec{\phi}_a + \frac{u}{24}\left(\sum_a \vec{\phi}_a^2\right)^2 + \frac{v}{24}\sum_{a,b}\left((\vec{\phi}_a \cdot \vec{\phi}_b)^2 - \vec{\phi}_a^2\vec{\phi}_b^2\right) \tag{E.10}$$

which is precisely 6.2. For further details we refer to [56] and references therein. Note that terms including factors of $e^{iQr}$ have been dropped. This is what is sometimes referred to as the slowly varying approximation.

## E.2 Helimagnets

In order to study helimagnets, we will consider the case of a hypercubic lattice where all nearest neighbour interactions are ferromagnetic, but in one of the directions, e.g. the $x$ direction, we also have a next-nearest neighbour interaction that is antiferromagnetic. The Hamiltonian is

$$H = \sum_{ij} J_{ij}\vec{S}_i \cdot \vec{S}_j + \sum_{ij} J'_{ij}\vec{S}_i \cdot \vec{S}_j \tag{E.11}$$

where now the first sum runs over all nearest neighbors and the second one over the next-nearest neighbours in one of the directions. Thus, now we have (e.g. for $d = 3$)

$$J \sim (\delta(z)\delta(r-a)\sum_{\theta_i}\delta(\theta-\theta_i) + \delta(|z|-a)\delta(r)\delta(\theta)) \tag{E.12}$$

where $r^2 = x^2 + y^2$, and

$$J' \sim \delta(z)\delta(r-2a)\sum_{\bar{\theta}_i}\delta(\theta-\bar{\theta}_i) \tag{E.13}$$

where $a$ is again the lattice spacing, but this time $\theta_i$=(0, $\pi/2$, $\pi$, $3\pi/2$) and $\bar{\theta}_i$=(0, $\pi$). This leads us to

$$E(q) \sim c_1(cos(q_x) + cos(q_y) + cos(q_z)) + c_2 cos(2q_x) \tag{E.14}$$

which again has two minima for appropriate values of $c_1$ and $c_2$. Thus all steps follow through as in the previous section and we can again derive E.10.

# Appendix F

# $\phi_i$-$X_{jk}$ system of correlators in cubic theories

For completeness, in this appendix we write down the full system of crossing equations for hypercubic theories involving the operators $\phi$ and $X$ with $N = 3$ as they appeared in [62]. Note that there is a slight change of notation. The operator denoted as $\phi$ in the main text is denoted $Y^-$ here. This is due to a group theory duality specific for $N = 3$. There exists a tensor such that $\phi_i = c_{ijk} Y^-_{jk}$ ,where $c_{ijk}$ is totally symmetric and non-zero only if all its indices take different values.

$$\sum_{S^+} \begin{pmatrix} \lambda_{\phi\phi\mathcal{O}_S} & \lambda_{XX\mathcal{O}_S} \end{pmatrix} \vec{T}_{S,\Delta,\ell} \begin{pmatrix} \lambda_{\phi\phi\mathcal{O}_S} \\ \lambda_{XX\mathcal{O}_S} \end{pmatrix} + \sum_{X^+} \begin{pmatrix} \lambda_{\phi\phi\mathcal{O}_X} & \lambda_{XX\mathcal{O}_X} \end{pmatrix} \vec{T}_{X,\Delta,\ell} \begin{pmatrix} \lambda_{\phi\phi\mathcal{O}_X} \\ \lambda_{XX\mathcal{O}_X} \end{pmatrix}$$
$$+\sum_{Y^+} \lambda^2_{\phi\phi\mathcal{O}_Y} \vec{V}_{Y,\Delta,\ell} + \sum_{A^-} \lambda^2_{\phi\phi\mathcal{O}_A} \vec{V}_{A,\Delta,\ell} + \sum_{Y'^{\pm}} \lambda^2_{\phi X\mathcal{O}_{Y'}} \vec{V}_{Y',\Delta,\ell} + \sum_{A'^{\pm}} \lambda^2_{\phi X\mathcal{O}_{A'}} \vec{V}_{A',\Delta,\ell} + \sum_{\bar{S}^-} \lambda^2_{\phi\phi\mathcal{O}_{\bar{S}}} \vec{V}_{\bar{S},\Delta,\ell} = 0 \tag{F.1}$$

where $\vec{V}_{Y,\Delta,\ell}$, $\vec{V}_{A,\Delta,\ell}$, $\vec{V}_{Y',\Delta,\ell}$, $\vec{V}_{A',\Delta,\ell}$, and $\vec{V}_{\bar{S},\Delta,\ell}$ are 13 component vectors of scalar quantities, while $\vec{T}_{S,\Delta,\ell}$ and $\vec{T}_{X,\Delta,\ell}$ are 13 componentt vectors of $2 \times 2$ matrices. They are given by

$$T^1_{S,\Delta,\ell} = \begin{pmatrix} 0 & 0 \\ 0 & 0 \end{pmatrix}, \quad T^2_{S,\Delta,\ell} = \begin{pmatrix} F^{\phi\phi;\phi\phi}_{-,\Delta,\ell} & 0 \\ 0 & 0 \end{pmatrix}, \quad T^3_{S,\Delta,\ell} = \begin{pmatrix} F^{\phi\phi;\phi\phi}_{+,\Delta,\ell} & 0 \\ 0 & 0 \end{pmatrix}, \quad T^4_{S,\Delta,\ell} = \begin{pmatrix} F^{\phi\phi;\phi\phi}_{-,\Delta,\ell} & 0 \\ 0 & 0 \end{pmatrix},$$
$$T^5_{S,\Delta,\ell} = \begin{pmatrix} 0 & 0 \\ 0 & 0 \end{pmatrix}, \quad T^6_{S,\Delta,\ell} = \begin{pmatrix} 0 & 0 \\ 0 & F^{XX;XX}_{-,\Delta,\ell} \end{pmatrix}, \quad T^7_{S,\Delta,\ell} = \begin{pmatrix} 0 & 0 \\ 0 & F^{XX;XX}_{+,\Delta,\ell} \end{pmatrix},$$
$$T^8_{S,\Delta,\ell} = \begin{pmatrix} 0 & \frac{1}{2} F^{\phi\phi;XX}_{+,\Delta,\ell} \\ \frac{1}{2} F^{\phi\phi;XX}_{+,\Delta,\ell} & 0 \end{pmatrix}, \quad T^9_{S,\Delta,\ell} = \begin{pmatrix} 0 & \frac{1}{2} F^{\phi\phi;XX}_{+,\Delta,\ell} \\ \frac{1}{2} F^{\phi\phi;XX}_{+,\Delta,\ell} & 0 \end{pmatrix}, \quad T^{10\text{–}13}_{S,\Delta,\ell} = \begin{pmatrix} 0 & 0 \\ 0 & 0 \end{pmatrix}, \tag{F.2}$$

$$T^1_{X,\Delta,\ell} = \begin{pmatrix} 0 & 0 \\ 0 & 0 \end{pmatrix}, T^2_{X,\Delta,\ell} = \begin{pmatrix} -\frac{1}{3} F^{\phi\phi;\phi\phi}_{-,\Delta,\ell} & 0 \\ 0 & 0 \end{pmatrix}, T^3_{X,\Delta,\ell} = \begin{pmatrix} -\frac{1}{3} F^{\phi\phi;\phi\phi}_{+,\Delta,\ell} & 0 \\ 0 & 0 \end{pmatrix}, T^4_{X,\Delta,\ell} = \begin{pmatrix} \frac{2}{3} F^{\phi\phi;\phi\phi}_{-,\Delta,\ell} & 0 \\ 0 & 0 \end{pmatrix},$$
$$T^5_{X,\Delta,\ell} = \begin{pmatrix} 0 & 0 \\ 0 & F^{XX;XX}_{-,\Delta,\ell} \end{pmatrix}, \quad T^6_{X,\Delta,\ell} = \begin{pmatrix} 0 & 0 \\ 0 & 0 \end{pmatrix}, \quad T^7_{X,\Delta,\ell} = \begin{pmatrix} 0 & 0 \\ 0 & -2 F^{XX;XX}_{+,\Delta,\ell} \end{pmatrix},$$
$$T^8_{X,\Delta,\ell} = \tfrac{1}{3} T^{10}_{X,\Delta,\ell} = \begin{pmatrix} 0 & \frac{1}{6} F^{\phi\phi;XX}_{-,\Delta,\ell} \\ \frac{1}{6} F^{\phi\phi;XX}_{-,\Delta,\ell} & 0 \end{pmatrix}, \quad T^9_{X,\Delta,\ell} = \tfrac{1}{3} T^{11}_{X,\Delta,\ell} = \begin{pmatrix} 0 & \frac{1}{6} F^{\phi\phi;XX}_{+,\Delta,\ell} \\ \frac{1}{6} F^{\phi\phi;XX}_{+,\Delta,\ell} & 0 \end{pmatrix},$$
$$T^{12,13}_{X,\Delta,\ell} = \begin{pmatrix} 0 & 0 \\ 0 & 0 \end{pmatrix}, \tag{F.3}$$

$$V^1_{Y,\Delta,\ell} = F^{\phi\phi;\phi\phi}_{-,\Delta,\ell}, \quad V^2_{Y,\Delta,\ell} = F^{\phi\phi;\phi\phi}_{-,\Delta,\ell}, \quad V^3_{Y,\Delta,\ell} = -F^{\phi\phi;\phi\phi}_{+,\Delta,\ell}, \quad V^{4\text{–}13}_{Y,\Delta,\ell} = 0, \tag{F.4}$$

$$V^{1}_{A,\Delta,\ell} = F^{\phi\phi;\phi\phi}_{-,\Delta,\ell}\,, \quad V^{2}_{A,\Delta,\ell} = -F^{\phi\phi;\phi\phi}_{-,\Delta,\ell}\,, \quad V^{3}_{A,\Delta,\ell} = F^{\phi\phi;\phi\phi}_{+,\Delta,\ell}\,, \quad V^{4\text{–}13}_{A,\Delta,\ell} = 0\,, \tag{F.5}$$

$$V^{1\text{–}7}_{Y',\Delta,\ell} = 0\,, \quad V^{8}_{Y',\Delta,\ell} = \tfrac{2}{3}V^{10}_{Y',\Delta,\ell} = \tfrac{2}{3}(-1)^{\ell}F^{\phi X;X\phi}_{-,\Delta,\ell}\,, \quad V^{9}_{Y',\Delta,\ell} = \tfrac{2}{3}V^{11}_{Y',\Delta,\ell} = \tfrac{2}{3}(-1)^{\ell+1}F^{\phi X;X\phi}_{+,\Delta,\ell}\,,$$
$$V^{12}_{Y',\Delta,\ell} = F^{\phi X;\phi X}_{-,\Delta,\ell}\,, \quad V^{13}_{Y',\Delta,\ell} = 0\,, \tag{F.6}$$

$$V^{1\text{–}9}_{A',\Delta,\ell} = 0\,, \quad V^{10}_{A',\Delta,\ell} = (-1)^{\ell+1}F^{\phi X;X\phi}_{-,\Delta,\ell}\,, \quad V^{11}_{A',\Delta,\ell} = (-1)^{\ell}F^{\phi X;X\phi}_{+,\Delta,\ell}\,,$$
$$V^{12}_{A',\Delta,\ell} = 0\,, \quad V^{13}_{A',\Delta,\ell} = F^{\phi X;\phi X}_{+,\Delta,\ell}\,, \tag{F.7}$$

$$V^{1\text{–}4}_{\bar{S},\Delta,\ell} = 0\,, \quad V^{5}_{\bar{S},\Delta,\ell} = -V^{6}_{\bar{S},\Delta,\ell} = F^{XX;XX}_{-,\Delta,\ell}\,, \quad V^{7}_{\bar{S},\Delta,\ell} = F^{XX;XX}_{+,\Delta,\ell}\,, \quad V^{8\text{–}13}_{\bar{S},\Delta,\ell} = 0\,. \tag{F.8}$$

Where as usual

$$F^{ab,cd}_{\pm,\Delta_O,l}(u,v) \equiv v^{\frac{\Delta_c+\Delta_b}{2}} g^{\Delta_{ab},\Delta_{cd}}_{\Delta_O,l}(u,v) \pm u^{\frac{\Delta_c+\Delta_b}{2}} g^{\Delta_{ab},\Delta_{cd}}_{\Delta_O,l}(v,u) \tag{F.9}$$

# Appendix G

# One index MN notation.

In this appendix we present the one index notation for $G' = G^N \rtimes S_N$ theories in the name of completeness. We will consider the specific example of $G = O(2)$ and $N = 2$ for simplicity. The generalizations will be straightforward. Invariant tensors have been worked out in terms of the one index notation for $G = O(M)$ and $G = Z_2^2 \rtimes S_2$ in [101]. Our approach will be slightly different in that we will write the projectors only in terms of Kronecker deltas.

Take for instance the representation $I_2 = A$ which appeared in 9.11. We want to find the projector that corresponds to the appearance of $A_{ij}$ as an exchanged operator in the $\phi_i \times \phi_j$ OPE. The indices $i$ and $j$ now run over $MN = 2 * 2 = 4$ values given that we chose $G = O(2)$ and $N = 2$. We take $i = 1$ and $i = 2$ to correspond to the first copy of $O(2)$ and $i = 3$ and $i = 4$ to correspond to the second. Then $A$ has the following two elements

$$A_{12} = \phi_1\phi_2 - \phi_2\phi_1 \tag{G.1}$$
$$A_{34} = \phi_3\phi_4 - \phi_4\phi_3 \tag{G.2}$$

remembering the relation $A_{ij} = P^A_{ijkl}\phi_i\phi_j$ it is easy to write down the projector explicitly

$$\begin{aligned} P^A_{ijkl} = &\frac{1}{2}(\delta_{i1}\delta_{j2} - \delta_{i2}\delta_{j1})(\delta_{k1}\delta_{l2} - \delta_{k2}\delta_{l1}) \\ &+\frac{1}{2}(\delta_{i3}\delta_{j4} - \delta_{i4}\delta_{j3})(\delta_{k3}\delta_{l4} - \delta_{k4}\delta_{l3}) \end{aligned} \tag{G.3}$$

Given that we have written what all operators look like in the $\phi_i \times \phi_j$ OPE in Chapter 9 it is a straightforward exercise to write down all the relevant projectors, and check that they give equivalent crossing equation sum rules. An interesting irrep to comment further on is $X$. Remember that $X$ is always a singlet of $G$ and is traceless in $G'$. Thus, in our current example

$$\begin{aligned} X_{11} &= (\phi_1\phi_1 + \phi_2\phi_2) - (\phi_3\phi_3 + \phi_4\phi_4) \\ X_{22} &= (\phi_1\phi_1 + \phi_2\phi_2) - (\phi_3\phi_3 + \phi_4\phi_4) \\ X_{33} &= (\phi_3\phi_3 + \phi_4\phi_4) - (\phi_1\phi_1 + \phi_2\phi_2) \\ X_{44} &= (\phi_3\phi_3 + \phi_4\phi_4) - (\phi_1\phi_1 + \phi_2\phi_2) \end{aligned} \tag{G.4}$$

which leads to

$$P^X_{ijkl} = \frac{1}{4}(\delta_{i1}\delta_{j1} + \delta_{i2}\delta_{j2} - \delta_{i3}\delta_{j3} - \delta_{i4}\delta_{j4})(\delta_{k1}\delta_{l1} + \delta_{k2}\delta_{l2} - \delta_{k3}\delta_{l3} - \delta_{k4}\delta_{l4}) \tag{G.5}$$

which could of course be generalized for any $G$ and $N$ if we wished. What we want to point out, though, is that all the elements of $X$ for a given copy of $G$ are the same i.e. $X_{11} = X_{22}$ and $X_{33} = X_{44}$. This is equivalent to the fact that in the two index notation $X$ has only $a$ and $b$ indices but not $i$ and $j$ indices. If we define $X_{11} = X_{22} = \tilde{X}_1$ and $X_{33} = X_{44} = \tilde{X}_2$, we have

$$X_{ij} = \sum_{m=1}^{2} (\delta_{i,2m-1}\delta_{j,2m-1} + \delta_{i,2m}\delta_{j,2m})\tilde{X}_m \tag{G.6}$$

the generalization to arbitrary group $G$ and arbitrary number of copies $N$ is

$$X_{ij} = \sum_{m=1}^{N} (\delta_{i,Mm-(M-1)}\delta_{j,Mm-(M-1)} + ... + \delta_{i,Mm-1}\delta_{j,Mm-1} + \delta_{i,Mm}\delta_{j,Mm})\tilde{X}_m \tag{G.7}$$

where $M$ depends on what $G$ is, e.g. for $G = O(20)$ we have $M = 20$. This equation is simply a generalization of 4.9. Thus all possible $\langle XXXX \rangle$ = $\langle XXXX \rangle$ crossing equation sum rules are known automatically, and are written down in C.8 and C.2.1.

# Bibliography


[1] L. Ts. Adzhemyan et al. "Six-loop $\varepsilon$ expansion study of three-dimensional $n$-vector model with cubic anisotropy". In: *Nucl. Phys. B* 940 (2019), pp. 332–350. DOI: 10.1016/j.nuclphysb.2019.02.001. arXiv: 1901.02754 [cond-mat.stat-mech].

[2] Amnon Aharony. "Critical Behavior of Anisotropic Cubic Systems in the Limit of Infinite Spin Dimensionality". In: *Phys. Rev. Lett.* 31 (25 1973), pp. 1494–1497. DOI: 10.1103/PhysRevLett.31.1494. URL: https://link.aps.org/doi/10.1103/PhysRevLett.31.1494.

[3] Amnon Aharony and Alastair D. Bruce. "Polycritical Points and Floplike Displacive Transitions in Perovskites". In: *Phys. Rev. Lett.* 33 (7 1974), pp. 427–430. DOI: 10.1103/PhysRevLett.33.427. URL: https://link.aps.org/doi/10.1103/PhysRevLett.33.427.

[4] Luis F. Alday, Johan Henriksson, and Mark van Loon. "An alternative to diagrams for the critical O(N) model: dimensions and structure constants to order $1/N^2$". In: *JHEP* 01 (2020), p. 063. DOI: 10.1007/JHEP01(2020)063. arXiv: 1907.02445 [hep-th].

[5] Luis F. Alday, Johan Henriksson, and Mark van Loon. "Taming the $\epsilon$-expansion with large spin perturbation theory". In: *JHEP* 07 (2018), p. 131. DOI: 10.1007/JHEP07(2018)131. arXiv: 1712.02314 [hep-th].

[6] Oleg Antipin and Jahmall Bersini. "Spectrum of anomalous dimensions in hypercubic theories". In: *Phys. Rev. D* 100.6 (2019), p. 065008. DOI: 10.1103/PhysRevD.100.065008. arXiv: 1903.04950 [hep-th].

[7] P. Bak and D. Mukamel. "Physical realizations of $n \geqslant 4$-component vector models. III. Phase transitions in Cr, Eu, $MnS_2$, Ho, Dy, and Tb". In: *Phys. Rev. B* 13 (11 1976), pp. 5086–5094. DOI: 10.1103/PhysRevB.13.5086. URL: https://link.aps.org/doi/10.1103/PhysRevB.13.5086.

[8] Connor Behan. "Bootstrapping the long-range Ising model in three dimensions". In: *J. Phys. A* 52.7 (2019), p. 075401. DOI: 10.1088/1751-8121/aafd1b. arXiv: 1810.07199 [hep-th].

[9] Connor Behan. "PyCFTBoot: A flexible interface for the conformal bootstrap". In: *Commun. Comput. Phys.* 22.1 (2017), pp. 1–38. DOI: 10.4208/cicp.OA-2016-0107. arXiv: 1602.02810 [hep-th].

[10] Riccardo Ben Alì Zinati, Alessandro Codello, and Omar Zanusso. "Multicritical hypercubic models". In: (Apr. 2021). arXiv: 2104.03118 [hep-th].

[11] Amel Ben Hassine et al. "Critical behaviors near the paramagnetic-ferromagnetic phase transitions of La0.47Eu0.2Pb0.33MnO3 and La0.47Y0.2Pb0.33MnO3 perovskites". In: *Journal of Molecular Structure* 1142 (2017), pp. 102–109. ISSN: 0022-2860. DOI: https://doi.org/10.1016/j.molstruc.2017.04.051. URL: https://www.sciencedirect.com/science/article/pii/S0022286017304933.

[12] Dario Benedetti, Razvan Gurau, and Sabine Harribey. "Trifundamental quartic model". In: *Phys. Rev. D* 103.4 (2021), p. 046018. DOI: 10.1103/PhysRevD.103.046018. arXiv: 2011.11276 [hep-th].

[13] Dario Benedetti et al. "Long-range multi-scalar models at three loops". In: *J. Phys. A* 53.44 (2020), p. 445008. DOI: 10.1088/1751-8121/abb6ae. arXiv: 2007.04603 [hep-th].

[14] Damon J. Binder. "The Cubic Fixed Point at Large $N$". In: (June 2021). arXiv: 2106.03493 [hep-th].

[15] Alastair D. Bruce. "Structural phase transitions. II. Static critical behaviour". In: *Advances in Physics* 29.1 (1980), pp. 111–217. DOI: 10.1080/00018738000101356. eprint: https://doi.org/10.1080/00018738000101356. URL: https://doi.org/10.1080/00018738000101356.

[16] Pasquale Calabrese, Andrea Pelissetto, and Ettore Vicari. "Multicritical behavior in frustrated spin systems with noncollinear order". In: *Nucl. Phys.* B709 (2005), pp. 550–577. DOI: 10.1016/j.nuclphysb.2004.12.006. arXiv: cond-mat/0408130.

[17] Pasquale Calabrese et al. "Critical behavior of O(2) x O(N) symmetric models". In: *Phys. Rev. B* 70 (2004), p. 174439. DOI: 10.1103/PhysRevB.70.174439. arXiv: cond-mat/0405667.

[18] John L. Cardy. *Scaling and renormalization in statistical physics*. 1996.

[19] Alejandro Castedo Echeverri, Benedict von Harling, and Marco Serone. "The Effective Bootstrap". In: *JHEP* 09 (2016), p. 097. DOI: 10.1007/JHEP09(2016)097. arXiv: 1606.02771 [hep-th].

[20] Shai M. Chester. "Weizmann Lectures on the Numerical Conformal Bootstrap". In: (July 2019). arXiv: 1907.05147 [hep-th].

[21] Shai M. Chester et al. "Bootstrapping Heisenberg Magnets and their Cubic Instability". In: (Nov. 2020). arXiv: 2011.14647 [hep-th].

[22] Shai M. Chester et al. "Carving out OPE space and precise $O(2)$ model critical exponents". In: *JHEP* 06 (2020), p. 142. DOI: 10.1007/JHEP06(2020)142. arXiv: 1912.03324 [hep-th].

[23] A. Codello et al. "Critical models with $N \leqslant 4$ scalars in $d = 4 - \epsilon$". In: *Phys. Rev. D* 102.6 (2020), p. 065017. DOI: 10.1103/PhysRevD.102.065017. arXiv: 2008.04077 [hep-th].

[24] R.A. Cowley. "Structural phase transitions I. Landau theory". In: *Advances in Physics* 29.1 (1980), pp. 1–110. DOI: 10.1080/00018738000101346. eprint: https://doi.org/10.1080/00018738000101346. URL: https://doi.org/10.1080/00018738000101346.

[25] Martino De Prato, Andrea Pelissetto, and Ettore Vicari. "The Normal to planar superfluid transition in He-3". In: *Phys. Rev. B* 70 (2004), p. 214519. DOI: 10.1103/PhysRevB.70.214519. arXiv: cond-mat/0312362.

[26] Delamotte et al. "Analysis of the 3d massive renormalization group perturbative expansions: a delicate case". In: *Condensed Matter Physics* 13.4 (2010), p. 43703. ISSN: 1607-324X. DOI: 10.5488/cmp.13.43703. URL: http://dx.doi.org/10.5488/CMP.13.43703.

[27] B. Delamotte, D. Mouhanna, and M. Tissier. "Nonperturbative renormalization group approach to frustrated magnets". In: *Phys. Rev. B* 69 (2004), p. 134413. DOI: 10.1103/PhysRevB.69.134413. arXiv: cond-mat/0309101.

[28] B. Delamotte et al. "About the relevance of the fixed dimension perturbative approach to frustrated magnets in two and three dimensions". In: *Phys. Rev. B* 82 (2010), p. 104432. DOI: 10.1103/PhysRevB.82.104432. arXiv: 1009.1492 [cond-mat.stat-mech].

[29] B Delamotte et al. "Fixed points in frustrated magnets revisited". In: *Journal of Statistical Mechanics: Theory and Experiment* 2008.03 (2008), P03014. ISSN: 1742-5468. DOI: 10.1088/1742-5468/2008/03/p03014. URL: http://dx.doi.org/10.1088/1742-5468/2008/03/P03014.

[30] B. Delamotte et al. "Functional renormalization group approach to noncollinear magnets". In: *Physical Review B* 93.6 (2016). ISSN: 2469-9969. DOI: 10.1103/physrevb.93.064405. URL: http://dx.doi.org/10.1103/PhysRevB.93.064405.

[31] Parijat Dey, Apratim Kaviraj, and Kallol Sen. "More on analytic bootstrap for O(N) models". In: *JHEP* 06 (2016), p. 136. DOI: 10.1007/JHEP06(2016)136. arXiv: 1602.04928 [hep-th].

[32] Parijat Dey, Apratim Kaviraj, and Aninda Sinha. "Mellin space bootstrap for global symmetry". In: *JHEP* 07 (2017), p. 019. DOI: 10.1007/JHEP07(2017)019. arXiv: 1612.05032 [hep-th].

[33] P. Di Francesco, P. Mathieu, and D. Senechal. *Conformal Field Theory*. Graduate Texts in Contemporary Physics. New York: Springer-Verlag, 1997. ISBN: 978-0-387-94785-3, 978-1-4612-7475-9. DOI: 10.1007/978-1-4612-2256-9.

[34] F. A. Dolan and H. Osborn. "Conformal four point functions and the operator product expansion". In: *Nucl. Phys. B* 599 (2001), pp. 459–496. DOI: 10.1016/S0550-3213(01)00013-X. arXiv: hep-th/0011040.

[35] F. A. Dolan and H. Osborn. "Conformal partial waves and the operator product expansion". In: *Nucl. Phys. B* 678 (2004), pp. 491–507. DOI: 10.1016/j.nuclphysb.2003.11.016. arXiv: hep-th/0309180.

[36] Matthew T. Dowens and Chris A. Hooley. "$O(15) \otimes O(3)$ critical theories in $d = 3$: a multi-correlator conformal bootstrap study". In: (Apr. 2020). arXiv: 2004.14978 [hep-th].

[37] Sheer El-Showk and Miguel F. Paulos. "Bootstrapping Conformal Field Theories with the Extremal Functional Method". In: *Phys. Rev. Lett.* 111.24 (2013), p. 241601. DOI: 10.1103/PhysRevLett.111.241601. arXiv: 1211.2810 [hep-th].

[38] Sheer El-Showk and Miguel F. Paulos. "Extremal bootstrapping: go with the flow". In: *JHEP* 03 (2018), p. 148. DOI: 10.1007/JHEP03(2018)148. arXiv: 1605.08087 [hep-th].

[39] Rajeev S. Erramilli et al. "blocks_3d: Software for general 3d conformal blocks". In: (Nov. 2020). arXiv: 2011.01959 [hep-th].

[40] Michael E. Fisher. "Scaling, universality and renormalization group theory". In: *Critical Phenomena, Proceedings of the Summer School Held at the University of Stellenbosch, South Africa January 18–29, 1982*. Ed. by F.J.W. Hahne. Springer, 1983.

[41] Mocho Go. "An Automated Generation of Bootstrap Equations for Numerical Study of Critical Phenomena". In: (June 2020). arXiv: 2006.04173 [hep-th].

[42] Mocho Go and Yuji Tachikawa. "autoboot: A generator of bootstrap equations with global symmetry". In: *JHEP* 06 (2019), p. 084. DOI: 10.1007/JHEP06(2019)084. arXiv: 1903.10522 [hep-th].

[43] J. A. Gracey. "Chiral exponents in O(N) x O(m) spin models at O(1 / N**2)". In: *Phys. Rev. B* 66 (2002), p. 134402. DOI: 10.1103/PhysRevB.66.134402. arXiv: cond-mat/0208309.

[44] J. A. Gracey. "Critical exponent omega at O(1/N) in O(N) x O(m) spin models". In: *Nucl. Phys. B* 644 (2002), pp. 433–450. DOI: 10.1016/S0550-3213(02)00818-0. arXiv: hep-th/0209053.

[45] Martin Hasenbusch. "Monte Carlo study of an improved clock model in three dimensions". In: *Physical Review B* 100.22 (2019). ISSN: 2469-9969. DOI: 10.1103/physrevb.100.224517. URL: http://dx.doi.org/10.1103/PhysRevB.100.224517.

[46] Martin Hasenbusch and Ettore Vicari. "Anisotropic perturbations in three-dimensional O(N)-symmetric vector models". In: *Physical Review B* 84.12 (2011). ISSN: 1550-235X. DOI: 10.1103/physrevb.84.125136. URL: http://dx.doi.org/10.1103/PhysRevB.84.125136.

[47] Johan Henriksson, Stefanos Robert Kousvos, and Andreas Stergiou. "Analytic and Numerical Bootstrap of CFTs with $O(m) \times O(n)$ Global Symmetry in 3D". In: *SciPost Phys.* 9.3 (2020), p. 035. DOI: 10.21468/SciPostPhys.9.3.035. arXiv: 2004.14388 [hep-th].

[48] Johan Henriksson and Andreas Stergiou. "Perturbative and Nonperturbative Studies of CFTs with MN Global Symmetry". In: (Jan. 2021). arXiv: 2101.08788 [hep-th].

[49] Johan Henriksson and Mark Van Loon. "Critical O(N) model to order $\epsilon^4$ from analytic bootstrap". In: *J. Phys. A* 52.2 (2019), p. 025401. DOI: 10.1088/1751-8121/aaf1e2. arXiv: 1801.03512 [hep-th].

[50] Matthijs Hogervorst, Miguel Paulos, and Alessandro Vichi. "The ABC (in any D) of Logarithmic CFT". In: *JHEP* 10 (2017), p. 201. DOI: 10.1007/JHEP10(2017)201. arXiv: 1605.03959 [hep-th].

[51] Matthijs Hogervorst and Chiara Toldo. "Bounds on multiscalar CFTs in the $\epsilon$ expansion". In: *JHEP* 04 (2021), p. 068. DOI: 10.1007/JHEP04(2021)068. arXiv: 2010.16222 [hep-th].

[52] Christian B. Jepsen and Fedor K. Popov. "Homoclinic RG flows, or when relevant operators become irrelevant". In: (May 2021). arXiv: 2105.01625 [hep-th].

[53] Hikaru Kawamura. "Generalized Chiral Universality". In: *Journal of the Physical Society of Japan* 59.7 (1990), pp. 2305–2308. DOI: 10.1143/JPSJ.59.2305. eprint: https://doi.org/10.1143/JPSJ.59.2305. URL: https://doi.org/10.1143/JPSJ.59.2305.

[54] Hikaru Kawamura. "Renormalization-group analysis of chiral transitions". In: *Phys. Rev. B* 38 (7 1988), pp. 4916–4928. DOI: 10.1103/PhysRevB.38.4916. URL: https://link.aps.org/doi/10.1103/PhysRevB.38.4916.

[55] Hikaru Kawamura. "Renormalization-Group Approach to the Frustrated Heisenberg Antiferromagnet on the Layered-Triangular Lattice". In: *Journal of the Physical Society of Japan* 55.7 (July 1986), p. 2157. DOI: 10.1143/JPSJ.55.2157.

[56] Hikaru Kawamura. "Universality of phase transitions of frustrated antiferromagnets". In: *Journal of Physics: Condensed Matter* 10.22 (1998), pp. 4707–4754. DOI: 10.1088/0953-8984/10/22/004.

[57] Zohar Komargodski and David Simmons-Duffin. "The Random-Bond Ising Model in 2.01 and 3 Dimensions". In: *J. Phys. A* 50.15 (2017), p. 154001. DOI: 10.1088/1751-8121/aa6087. arXiv: 1603.04444 [hep-th].

[58] M. V. Kompaniets, A. Kudlis, and A. I. Sokolov. "Six-loop $\epsilon$ expansion study of three-dimensional $O(n) \times O(m)$ spin models". In: *Nucl. Phys. B* 950 (2020), p. 114874. DOI: 10.1016/j.nuclphysb.2019.114874. arXiv: 1911.01091 [cond-mat.stat-mech].

[59] Filip Kos, David Poland, and David Simmons-Duffin. "Bootstrapping Mixed Correlators in the 3D Ising Model". In: *JHEP* 11 (2014), p. 109. DOI: 10.1007/JHEP11(2014)109. arXiv: 1406.4858 [hep-th].

[60] Filip Kos, David Poland, and David Simmons-Duffin. "Bootstrapping the $O(N)$ vector models". In: *JHEP* 06 (2014), p. 091. DOI: 10.1007/JHEP06(2014)091. arXiv: 1307.6856 [hep-th].

[61] Filip Kos et al. "Precision Islands in the Ising and $O(N)$ Models". In: *JHEP* 08 (2016), p. 036. DOI: 10.1007/JHEP08(2016)036. arXiv: 1603.04436 [hep-th].

[62] Stefanos R. Kousvos and Andreas Stergiou. "Bootstrapping Mixed Correlators in Three-Dimensional Cubic Theories". In: *SciPost Phys.* 6.3 (2019), p. 035. DOI: 10.21468/SciPostPhys.6.3.035. arXiv: 1810.10015 [hep-th].

[63] Stefanos R. Kousvos and Andreas Stergiou. "Bootstrapping Mixed Correlators in Three-Dimensional Cubic Theories II". In: *SciPost Phys.* 8.6 (2020), p. 085. DOI: 10.21468/SciPostPhys.8.6.085. arXiv: 1911.00522 [hep-th].

[64] Stefanos R. Kousvos and Andreas Stergiou. "Work In Progress". In: ().

[65] Walter Landry and David Simmons-Duffin. "Scaling the semidefinite program solver SDPB". In: (Sept. 2019). arXiv: 1909.09745 [hep-th].

[66] Zhijin Li. "Symmetries of conformal correlation functions". In: (June 2020). arXiv: 2006.05119 [hep-th].

[67] Zhijin Li and David Poland. "Searching for gauge theories with the conformal bootstrap". In: (May 2020). arXiv: 2005.01721 [hep-th].

[68] Zhijin Li and Ning Su. "Bootstrapping Mixed Correlators in the Five Dimensional Critical O(N) Models". In: *JHEP* 04 (2017), p. 098. DOI: 10.1007/JHEP04(2017)098. arXiv: 1607.07077 [hep-th].

[69] J. A. Lipa et al. "Specific heat of liquid helium in zero gravity very near the lambda point". In: *Phys. Rev. B* 68 (17 2003), p. 174518. DOI: 10.1103/PhysRevB.68.174518. URL: https://link.aps.org/doi/10.1103/PhysRevB.68.174518.

[70] A. I. Mudrov and K. B. Varnashev. "Critical behavior of certain antiferromagnets with complicated ordering: Four-loop $\varepsilon$-expansion analysis". In: *Physical Review B* 64.21 (2001). ISSN: 1095-3795. DOI: 10.1103/physrevb.64.214423. URL: http://dx.doi.org/10.1103/PhysRevB.64.214423.

[71] D. Mukamel and S. Krinsky. "Physical realizations of $n \geqslant 4$-component vector models. I. Derivation of the Landau-Ginzburg-Wilson Hamiltonians". In: *Phys. Rev. B* 13 (11 1976), pp. 5065–5077. DOI: 10.1103/PhysRevB.13.5065. URL: https://link.aps.org/doi/10.1103/PhysRevB.13.5065.

[72] D. Mukamel and S. Krinsky. "Physical realizations of $n \geqslant 4$-component vector models. II. $\epsilon$-expansion analysis of the critical behavior". In: *Phys. Rev. B* 13 (11 1976), pp. 5078–5085. DOI: 10.1103/PhysRevB.13.5078. URL: https://link.aps.org/doi/10.1103/PhysRevB.13.5078.

[73] David Mukamel. "Physical Realizations of $n > 4$ Vector Models". In: *Phys. Rev. Lett.* 34 (8 1975), pp. 481–485. DOI: 10.1103/PhysRevLett.34.481. URL: https://link.aps.org/doi/10.1103/PhysRevLett.34.481.

[74] K. A. Müller and W. Berlinger. "Static Critical Exponents at Structural Phase Transitions". In: *Phys. Rev. Lett.* 26 (1 1971), pp. 13–16. DOI: 10.1103/PhysRevLett.26.13. URL: https://link.aps.org/doi/10.1103/PhysRevLett.26.13.

[75] Yoshihiro Nagano, Kazuki Uematsu, and Hikaru Kawamura. "Monte Carlo study of the critical properties of noncollinear Heisenberg magnets: O(3)×O(2) universality class". In: *Physical Review B* 100.22 (2019). ISSN: 2469-9969. DOI: 10.1103/physrevb.100.224430. URL: http://dx.doi.org/10.1103/PhysRevB.100.224430.

[76] Yu Nakayama and Tomoki Ohtsuki. "Approaching the conformal window of $O(n) \times O(m)$ symmetric Landau-Ginzburg models using the conformal bootstrap". In: *Phys. Rev. D* 89.12 (2014), p. 126009. DOI: 10.1103/PhysRevD.89.126009. arXiv: 1404.0489 [hep-th].

[77] Yu Nakayama and Tomoki Ohtsuki. "Bootstrapping phase transitions in QCD and frustrated spin systems". In: *Phys. Rev. D* 91.2 (2015), p. 021901. DOI: 10.1103/PhysRevD.91.021901. arXiv: 1407.6195 [hep-th].

[78] Hugh Osborn and Andreas Stergiou. "Heavy Handed Quest for Fixed Points in Multiple Coupling Scalar Theories in the $\epsilon$ Expansion". In: *JHEP* 04 (2021), p. 128. arXiv: 2010.15915 [hep-th].

[79] Hugh Osborn and Andreas Stergiou. "Seeking fixed points in multiple coupling scalar theories in the $\epsilon$ expansion". In: *JHEP* 05 (2018), p. 051. DOI: 10.1007/JHEP05(2018)051. arXiv: 1707.06165 [hep-th].

[80] A.J. Paterson. "Coleman-Weinberg symmetry breaking in the chiral SU(n) × SU(n) linear $\sigma$ model". In: *Nuclear Physics B* 190.1 (1981). Volume B190 [FS3] No.2 To Follow in Approximately Two Months, pp. 188–204. ISSN: 0550-3213. DOI: https://doi.org/10.1016/0550-3213(81)90489-2. URL: https://www.sciencedirect.com/science/article/pii/0550321381904892.

[81] Andrea Pelissetto, Paolo Rossi, and Ettore Vicari. "Large n critical behavior of O(n) x O(m) spin models". In: *Nucl. Phys. B* 607 (2001), pp. 605–634. DOI: 10.1016/S0550-3213(01)00223-1. arXiv: hep-th/0104024.

[82] Andrea Pelissetto, Paolo Rossi, and Ettore Vicari. "The Critical behavior of frustrated spin models with noncollinear order". In: *Phys. Rev. B* 63 (2001), p. 140414. DOI: 10.1103/PhysRevB.63.140414. arXiv: cond-mat/0007389.

[83] Andrea Pelissetto, Antonio Tripodo, and Ettore Vicari. "Criticality of O(N) symmetric models in the presence of discrete gauge symmetries". In: *Phys. Rev. E* 97.1 (2018), p. 012123. DOI: 10.1103/PhysRevE.97.012123. arXiv: 1711.04567 [cond-mat.stat-mech].

[84] Andrea Pelissetto and Ettore Vicari. "Critical phenomena and renormalization group theory". In: *Phys. Rept.* 368 (2002), pp. 549–727. DOI: 10.1016/S0370-1573(02)00219-3. arXiv: cond-mat/0012164.

[85] João Penedones, Emilio Trevisani, and Masahito Yamazaki. "Recursion relations for conformal blocks". In: *Journal of High Energy Physics* 2016.9, 70 (Sept. 2016), p. 70. DOI: 10.1007/JHEP09(2016)070. arXiv: 1509.00428 [hep-th].

[86] R. D. Pisarski and D. L. Stein. "Critical behavior of linear $\Phi^4$ models with $G \times G'$ symmetry". In: *Phys. Rev. B* 23 (7 1981), pp. 3549–3552. DOI: 10.1103/PhysRevB.23.3549. URL: https://link.aps.org/doi/10.1103/PhysRevB.23.3549.

[87] David Poland, Slava Rychkov, and Alessandro Vichi. "The Conformal Bootstrap: Theory, Numerical Techniques, and Applications". In: *Rev. Mod. Phys.* 91 (2019), p. 015002. DOI: 10.1103/RevModPhys.91.015002. arXiv: 1805.04405 [hep-th].

[88] Alexander M. Polyakov. "Conformal symmetry of critical fluctuations". In: *JETP Lett.* 12 (1970), pp. 381–383.

[89] Joshua D. Qualls. "Lectures on Conformal Field Theory". In: (Nov. 2015). arXiv: 1511.04074 [hep-th].

[90] Riccardo Rattazzi et al. "Bounding scalar operator dimensions in 4D CFT". In: *JHEP* 12 (2008), p. 031. DOI: 10.1088/1126-6708/2008/12/031. arXiv: 0807.0004 [hep-th].

[91] Marten Reehorst, Maria Refinetti, and Alessandro Vichi. "Bootstrapping traceless symmetric $O(N)$ scalars". In: (Dec. 2020). arXiv: 2012.08533 [hep-th].

[92] Marten Reehorst et al. "Navigator Function for the Conformal Bootstrap". In: (Apr. 2021). arXiv: 2104.09518 [hep-th].

[93] Junchen Rong and Ning Su. "Scalar CFTs and Their Large N Limits". In: *JHEP* 09 (2018), p. 103. DOI: 10.1007/JHEP09(2018)103. arXiv: 1712.00985 [hep-th].

[94] Slava Rychkov. *EPFL Lectures on Conformal Field Theory in D>= 3 Dimensions*. SpringerBriefs in Physics. Jan. 2016. ISBN: 978-3-319-43625-8, 978-3-319-43626-5. DOI: 10.1007/978-3-319-43626-5. arXiv: 1601.05000 [hep-th].

[95] Slava Rychkov and Andreas Stergiou. "General Properties of Multiscalar RG Flows in $d = 4 - \varepsilon$". In: *SciPost Phys.* 6.1 (2019), p. 008. DOI: 10.21468/SciPostPhys.6.1.008. arXiv: 1810.10541 [hep-th].

[96] Mahmoud Safari, Gian Paolo Vacca, and Omar Zanusso. "Crossover exponents, fractal dimensions and logarithms in Landau–Potts field theories". In: *Eur. Phys. J. C* 80.12 (2020), p. 1127. DOI: 10.1140/epjc/s10052-020-08687-0. arXiv: 2009.02589 [cond-mat.stat-mech].

[97] David Simmons-Duffin. "A Semidefinite Program Solver for the Conformal Bootstrap". In: *JHEP* 06 (2015), p. 174. DOI: 10.1007/JHEP06(2015)174. arXiv: 1502.02033 [hep-th].

[98] David Simmons-Duffin. "The Lightcone Bootstrap and the Spectrum of the 3d Ising CFT". In: *JHEP* 03 (2017), p. 086. DOI: 10.1007/JHEP03(2017)086. arXiv: 1612.08471 [hep-th].

[99] A. O. Sorokin. "First-order and pseudo-first-order transition in the high dimensional $O(N) \otimes O(M)$ model". In: (Apr. 2021). arXiv: 2105.00072 [cond-mat.str-el].

[100] Andreas Stergiou. "Bootstrapping hypercubic and hypertetrahedral theories in three dimensions". In: *JHEP* 05 (2018), p. 035. DOI: 10.1007/JHEP05(2018)035. arXiv: 1801.07127 [hep-th].

[101] Andreas Stergiou. "Bootstrapping MN and Tetragonal CFTs in Three Dimensions". In: *SciPost Phys.* 7 (2019), p. 010. DOI: 10.21468/SciPostPhys.7.1.010. arXiv: 1904.00017 [hep-th].

[102] M. Tissier, B. Delamotte, and D. Mouhanna. "Heisenberg frustrated magnets: A Nonperturbative approach". In: *Phys. Rev. Lett.* 84 (2000), pp. 5208–5211. DOI: 10.1103/PhysRevLett.84.5208. arXiv: cond-mat/0001350.

[103] M. Tissier, B. Delamotte, and D. Mouhanna. "XY frustrated systems: Continuous exponents in discontinuous phase transitions". In: *Phys. Rev. B* 67 (2003), p. 134422. DOI: 10.1103/PhysRevB.67.134422. arXiv: cond-mat/0107183.

[104] J C Tolédano and P Tolédano. *The Landau Theory of Phase Transitions*. WORLD SCIENTIFIC, 1987. DOI: 10.1142/0215. eprint: https://www.worldscientific.com/doi/pdf/10.1142/0215. URL: https://www.worldscientific.com/doi/abs/10.1142/0215.

[105] Th. von Waldkirch et al. "Fluctuations and Correlations in $SrTiO_3$ for $T \geqslant T_c$". In: *Phys. Rev. Lett.* 28 (8 1972), pp. 503–506. DOI: 10.1103/PhysRevLett.28.503. URL: https://link.aps.org/doi/10.1103/PhysRevLett.28.503.

[106] K. G. Wilson and John B. Kogut. "The Renormalization group and the epsilon expansion". In: *Phys. Rept.* 12 (1974), pp. 75–199. DOI: 10.1016/0370-1573(74)90023-4.

[107] Kenneth G. Wilson and Michael E. Fisher. "Critical exponents in 3.99 dimensions". In: *Phys. Rev. Lett.* 28 (1972), pp. 240–243. DOI: 10.1103/PhysRevLett.28.240.

[108] Al. B. Zamolodchikov. "Conformal symmetry in two-dimensional space: Recursion representation of conformal block". In: *Theoretical and Mathematical Physics* 73.1 (Oct. 1987), pp. 1088–1093. DOI: 10.1007/BF01022967.

[109] Al. B. Zamolodchikov. "Conformal symmetry in two dimensions: an explicit recurrence formula for the conformal partial wave amplitude". In: *Communications in Mathematical Physics* 96.3 (1984), pp. 419 –422. DOI: cmp/1103941860. URL: https://doi.org/.

[110] Jean Zinn-Justin. *Phase transitions and renormalization group*. 2007.